DEFINING A METHOD TO PREDICT MOUTH MORPHOLOGY IN EDENTULOUS SKULLS

By

Luke-John Daniels

Thesis presented in fulfilment of the requirements for the degree of Master of Science in the Faculty of Medicine and Health Science at Stellenbosch University

The financial assistance of the National Research Foundation (NRF) towards this research is hereby acknowledged. Opinions expressed and conclusions arrived at, are those of the author and are not necessarily to be attributed to the NRF.

Supervisor: Dr Amanda Alblas

Co-Supervisor: Dr Kathryn Smith

Co-Supervisor: Prof. Tina Roberts

April 2022

DECLARATION

By submitting this thesis electronically, I declare that the entirety of the work contained therein is my own, original work, that I am the sole author thereof (save to the extent explicitly otherwise stated), that reproduction and publication thereof by Stellenbosch University will not infringe any third party rights and that I have not previously in its entirety or in part submitted it for obtaining any qualification.

April 2022

ABSTRACT

Forensic facial depiction (FFD) is the process whereby a face is modelled to depict a face from an unknown deceased individual's skull to assist with human identification. The field of FFD that has not been researched extensively, is the edentulous mouth, where edentulism refers to the condition of not having teeth. Therefore, this study attempted to establish whether a method could be produced to predict edentulous mouth morphology for FFD practice. To achieve this, Pearson's correlation analysis was used and the relationship between the individual's soft tissue measurements (somatometry) and skull measurements (osteometry) were analysed. Dentate patients, those with teeth, were also included in the study to understand the morphometric difference between the mouths of dentate and edentulous patients.

Cone Beam Computer Tomography (CBCT) scans of n=63 patients were retrieved. This included 40 dentate patients (n=24 males and n=16 females) and 23 edentulous patients (n=7 males and n=16 females). The patients' CBCT scans were retrieved from the Oral Health Centre of the University of the Western Cape's Picture Archiving and Communication System. The morphometrics software, Stratovan Checkpoint™, was used to perform osteometry and somatometry on these scans. The somatometry of all patients included measuring soft tissue thicknesses (STTs) of the upper mouth as well as the patients' lip height (LH) and philtrum length (PL). For the edentulous patients, the STTs included the mid-philtrum (H), and mid-upper lip margin (I). For the dentate patients, the STTs measured were the H, I, the upper incisor (II) and lateral supra-labiale (F). For osteometry, all patients' skulls were measured to retrieve the following skull lengths: the bizygomatic breadth, basion-prosthion length, basion-gnathion length, maxillo-alveolar breadth, maxillo-alveolar length, nasion-prosthion, and the cranial base length. These lengths were then used to calculate the maxilla-alveolar (MAI), upper facial, subnasal gnathic (SGI), and gnathic indices.

A Shapiro-Wilk test was performed, and it was found that all osteometry and somatometry were normally distributed. Therefore, the correlation analysis could be applied. For the edentulous patients, the correlation analysis was only applied to the female patients since the male group was below the suggested sample size for correlation analysis ($n<10$). The results found that no significant correlations exist between female edentulous mouth somatometry and osteometry. For the dentate males, significant correlations were identified in: the MAI, and II-right and II-left; GI and H; and SGI and LH. For the dentate females: SGI, and II-left, F-left, and LH. Based on this study, it cannot be concluded that osteometry is a good predictor of edentulous mouth morphology. Other factors may play a role in the results of this research such as the sample size and certain edentulous anomalies, for example, residual ridge resorption (RRR). In the dentate group, significant correlations were found since RRR did not affect these patients. Therefore, for future studies, it is suggested that a larger sample is retrieved that is strictly controlled for edentulous anomalies.

ABSTRAK

Forensiese beelding van die gesig (FFD) is die proses waardeur ń onbekende persoon wat oorlede is se gesig gemodelleer word vanaf die persoon se skedel, vir die doel van om die persoon te identifiseer. Een deel van FFD wat nog nie omvattend nagevors is nie, is edentulisme, wat verwys na ń toestand van tandeloosheid. Die studie het dus ten doel gehad om ń metode daar te stel waarmee mondmorfologie weens edentulisme voorspel kan word. Dus, was Pearson se korrelasie-analise gebruik om die verhouding tussen die individu se sagteweefselafmetings (somatometrie) en skedelafmetings (osteometrie) te analiseer. Pasiënte met tande is ook by die studie ingesluit om die morfometriese verskille tussen die monde van pasiënte met tande, en edentuleuse pasiënte te verstaan.

ń Studiepopulasie van n=63 pasiënte is ingesluit. Dit het 40 pasiënte met tande (n=24 mans en n=16 vrouens), en 23 edentuleuse pasiënte (n=7 mans en n=16 vrouens) ingesluit. Die pasiënte is met behulp van keëlstraal-rekenaartomografiese skanderings wat vanaf die Beeldings Argief- en Kommunikasiestelsel van die Tand- en Mondheelkunde hospitaal van die Universiteit van die Wes-Kaap verkry is, geanaliseer. Stratovan Checkpoint^{TM} sagteware is gebruik om die afmetings op hierdie skanderings te doen. Alle pasiënte se somatometriese afmetings het sagteweefseldeursnit (STTs), sowel as liphoogte (LH) en filtrumlengte (PL) ingesluit. Vir edentuleuse pasiënte het STTs die mid-filtrum (H) en mid-bolip-grens (I) ingesluit. Vir pasiënte met tande het STT afmetings die H en I, en afmetings van die boonste snytande (II) en laterale supra-labiale (F) area, ingesluit. Osteometriese afmetings van alle pasiënte se skedels is gedoen om die volgende te bepaal: bisigomatiese breedte, basion-prostion lengte, basion-gnation lengte, maksillo-alveolêre breedte, maksillo-alveolêre lengte, nasion-prostion hoogte, en die kraniale basislengte. Hierdie afmetings is gebruik om die maksillo-alveolêre- (MAI), boonste gesigs-, subnasale gnatiese- (SGI) en gnatiese indekse te bereken.

ń Shapiro-Wilk toets het bepaal dat al die osteometrie en somatometrie normaal versprei is. Korrelasie analise kon dus toegepas word. Vir edentuleuse pasiënte is die korrelasie analise slegs toegepas op die vroulike pasiënte omdat die manlike groep minder as die voorgestelde steekproef grootte vir korrelasie analise (n<10), is. Uit dié resultate is gevind dat daar nie ń betekenisvolle korrelasie bestaan tussen die somatometrie en osteometrie vir vroulike edentuleuse monde nie. In manlike patiente met tande is betekenisvolle korrelasies identifiseer in die volgende: die MAI, en II-regs en II-links; GI en H; en SGI en LH. In vrouens met tande is betekenisvolle korrelasies identifiseer in die volgende: SGI, en II-links, F-links, en LH. Uit die studie kan die afleiding gemaak word dat osteometrie nie ń goeie metode is om die edentuleuse mond se morfologie te voorspel nie. Ander faktore kon ń rol speel in die resultate, soos die grootte van die populasie, en sekere anomalieë wat met edentulisme assosieer word, byvoorbeeld, residuele absorpsie van die alveolêre rand (RRR). In die groep met tande is ń betekenisvolle korrelasie gevind omdat RRR nie die pasiënte in die groep affekteer nie. Dus, vir toekomstige studies word voorgestel dat ń groter studiepopulasie gebruik word, met streng kontrole oor anomalieë wat met edentulisme geassosieer word.

ACKNOWLEDGEMENTS

I would like to acknowledge my father, mother, and family members. Thank you for pushing me to do my best and wanting me to take my studies further. Thank you for always being willing to support me in my academic career even without a bursary. However, thankfully, through the National Research Foundation, I was able to receive funding for my master's degree. Therefore, to the NRF, thank you for granting me this remarkable opportunity.

My gratitude also goes to my Pastors of Encounter Church Cape Town, Pastors Stephan and Jackie Botha, who were able to teach me the truth of The Gospel. They guided me into shaping my character and allowed me to remain steadfast in The Word. By showing me what God wants for my life and how much He loves me, made it so much easier to fulfil my academic tasks and balance it with my servitude to The Church. I want to honour and thank my Pastors for answering The Call and moving down to Cape Town to help usher in the Revival that will soon take place.

Thank you to my supervisors, Dr Amanda Alblas, Dr Kathryn Smith, and Prof. Tina Roberts. Dr Alblas, even with an inundated schedule, would always be available for her students. She cares for us and always encourages us in academia. I look forward to more research and forensic adventures with you, Dr Alblas. Thank you, Dr Smith, for introducing me to the art behind anatomy and forensic science, I cannot wait to see what the future of forensic art holds in South Africa. Prof. Roberts and the University of the Western Cape's Oral Health Centre, thank you for welcoming me and assisting me with the clinical area of my research. Human dentition was a topic foreign to me, and you were able to assist greatly.

Finally, thank you Chantelle Marais for taking time from your research to assist me in being the second observer for the interobserver error analysis. It is greatly appreciated. I wish you the very best with completing your masters.

CONTENT

LIST OF FIGURES

ADDENDUM B: BLAND-ALTMAN PLOTS TO SHOW THE INTRA- AND INTEROBSERVER ANALYSIS

LIST OF TABLES

ADDENDUM A: TABLE FOR DATA COLLECTION

LIST OF EQUATIONS

ABBREVIATIONS

3D	Three dimensions
ASTD	Average soft tissue depth
BMD	Bone mineral density
BMREC	Biomedical Research Ethics Committee
BNL	Cranial base length
BPL	Basion prosthion length
CBCT	Cone Beam Computer Tomography
CFR	Craniofacial reconstruction
Ch	Chelion
CT	Computer tomography
DNA	Deoxyribonucleic acid
FA	Forensic anthropology
FFD	Forensic facial depiction
FFR	Forensic facial reconstruction
FOV	Field of view
GI	Gnathic index
GM	Geometric morphometrics
HREC	Health research ethics committee
LH	Lip height
M1	First molar
M2	Second molar
M3	Third molar

MAB	Maxillo-alveolar breadth
MAI	Maxillo-alveolar Index
MLR	Multiple linear regression
NHRD	National Health Research Database
NLB	Nasal breadth
NLH	Nasal height
NPH	Nasion prosthion height
OHC	Oral Health Centre
OP	Osteoporosis
PACS	Picture Archiving and Communication System
PD	Periodontitis
PI	Principal investigator
PL	Philtrum length
RRR	Residual ridge resorption
SA	South African
SGI	Subnasal gnathic index
STT	Soft-tissue thickness
TBH	Tygerberg Hospital
TFI	Total facial index
UFI	Upper facial index
UWC	University of the Western Cape
ZYB	Bizygomatic breadth

CHAPTER 1: INTRODUCTION

Reconstruction, approximation, and depiction are terms which are used to refer to methodologies and principles of interpreting a living face from human remains. Although they speak to different processes, they are used interchangeably and as such, these terms have been contested within the practice. Therefore, practitioners and professional associations are attempting define their meaning (Smith 2020). In practical terms, "reconstruction" prioritises using individual facial and head anatomy, with reference to average soft tissue thickness (STTs) as guidelines, to interpret face and feature shape, whereas "approximation" prioritises the average STTs and facial feature approximation to estimate face and feature shape. After the approximation/reconstruction process, textures such as wrinkles, skin texture, and other interpretable details will be added to the face in an attempt to produce a recognisable face, resulting in a forensic facial *depiction*, or FFD (Smith 2020). The process of FFD can be performed digitally (using appropriate software) or using a modelling mastic (such as clay or modelling wax) to depict a face from an unknown deceased individual's skull to assist with identification. The process requires expertise and ability in art and science, specifically craniofacial morphology and anatomy (Wilkinson 2004).

Facial depiction is only required in cases where the deceased is beyond visual recognition (i.e. skeletonised, or where the face is no longer identifiable) and when the individual has no form of identification such as an identity card, fingerprints and/or DNA (Vermeulen 2012). In these instances, the South African Police Services will request an FFD to generate leads towards identification. To perform the reconstruction as successfully and objectively as possible, the forensic artist will consult various literature and forensic standards to proceed with the depiction (Iscan & Steyn 2013).

In cases where the skull presents with antemortem or healed trauma and pathology, the practitioner will have to carefully interpret the most likely antemortem appearance of the soft tissue in those parts of the face affected by these anomalies. One of these anomalies may refer to tooth loss, known as edentulism. The reason tooth loss may pose a problem in reconstruction is due to the changes it brings to the mandible and/or maxilla. After tooth loss, the alveolar sockets will close and the alveolar ridge will begin resorbing (Reich, Huber, Lippnig, Ulm, Watzek & Tangl 2011). Subsequently, the individual's mouth and lips are affected over time, giving the mouth a sunken-in appearance (Pietrokovski, Starinsky, Arensburg & Kaffe 2007).

Currently, there is some research available for FFD of the mouth and lips; however, it is limited to certain population groups or geographical regions and usually, edentulous patients are placed as an exclusion criterion. The reason for the exclusion of edentulous patients in research is due to the edentulous mouth being a challenge to study morphologically. The edentulous alveolar ridge, or rather known as the residual ridge (Figure 1), undergoes bone resorption, influencing the morphology of the mouth. The shape of the mouth also depends on how much bone resorption has taken place; and when teeth are extracted at different times, it leads to an uneven residual ridge as seen in Figure 2. In Figure 2A the maxillary teeth were all extracted during a single procedure, whereas the patient in Figure 2B had their teeth extracted at different times as seen by the uneven residual ridge (Cavanagh & Steyn 2011; Briers, Briers, Becker & Steyn 2015).

Due to the given evidence that edentulism alters mouth and alveolar ridge morphology and the lack of morphological research in edentulism for FFD, this study focused on how edentulism affects the dimensions of the mouth. To understand this morphological or metric change, dentate patients (patients with teeth) were being used as a basis to compare dentate and edentulous morphology. In so doing, the metric changes taking place in an edentulous mouth could be further understood.

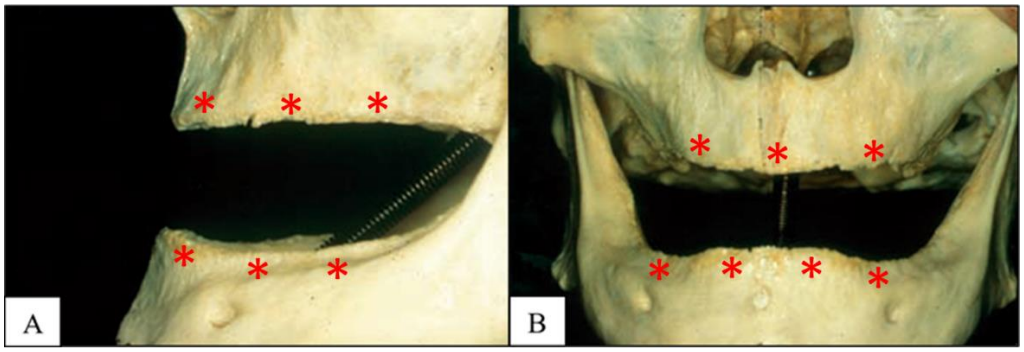

(Pietrokovski *et al.* 2007)

Figure 1: The residual ridge (red). Lateral view (A) and anterior view (B).

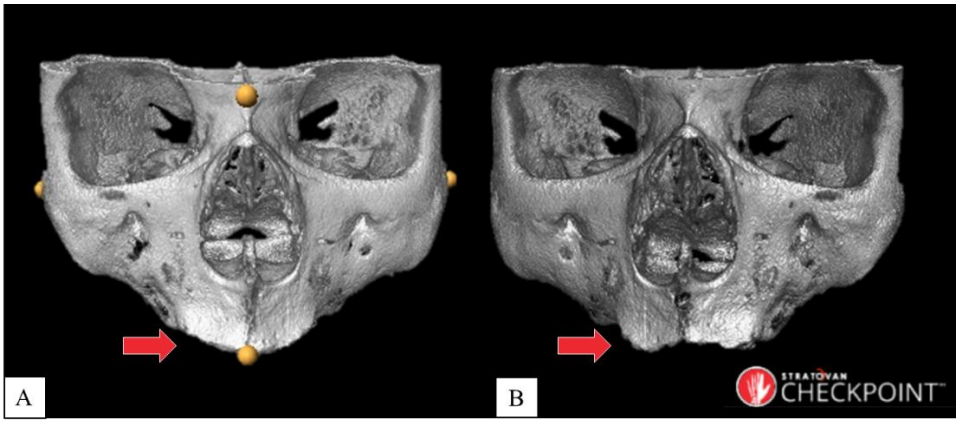

(Stratovan Checkpoint^{TM})

Figure 2: Cone Beam Computer Tomography scan of edentulous patients showing the comparison between an even and uneven resorbed residual ridge (red arrow): A - even maxillary residual ridge, B - uneven maxillary residual ridge.

1.1 PROBLEM STATEMENT

The process that causes the residual ridge of the jaw to resorb is known as residual ridge resorption (RRR). This anomaly causes mouth morphological changes that have not been metrically studied. Coupled with the diversity in mouth and lip morphology of the Western Cape population, it further enhances the need for research in this area for FFD.

In many instances, edentulous patients wear dentures, and if the dentures accompany human remains, the face of the skull can be depicted by the forensic artist using facial reconstruction standards of dentate individuals (Taylor 2000). However, if dentures are absent from human remains, the artist has to interpret mouth shape with less reliable techniques to guide the process. Taylor (2000) suggested a method to achieve a reasonable resting mouth pose for edentulous skulls (i.e., placing a pencil between the mandible and cranium when articulating the mandibular condyles within the temporomandibular joint), which some artists follow as a basis to reconstruct the edentulous individual's face. However, there is no somatometric information for edentulous FFD at present.

In this study, somatometry, which refers to soft tissue measurements of a living individual, was gathered of the upper lip, the area of the mouth above the lip, as well as the philtrum (Figure 3). The area of the mouth to be studied in this research is shown in Figure 3 and shall be referred to as the "upper mouth". The reason for only focusing on the upper mouth in this research was due to the patient's chin and mandible being distorted in the patient sample. These distortions will be further discussed in the latter chapters. Osteometry (skeletal measurements) was also performed on the skull in both edentulous and dentate patients to determine how the absence of teeth affects the mouth and whether a method can be produced to better predict and define the morphology of the mouth.

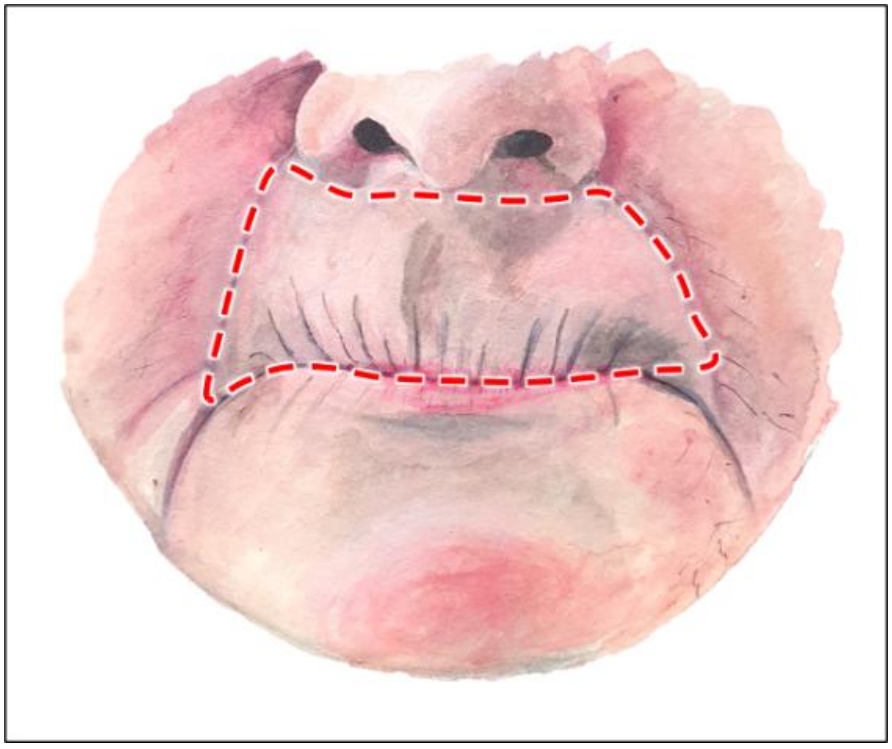

(Illustration by L. Daniels)

Figure 3: The red outline depicts the area of the mouth to be studied for this research, i.e. the "upper mouth".

1.2 SIGNIFICANCE OF PROJECT

This research attempted to investigate a method to predict the morphology of the mouth in edentulous patients. This research may be significant in its novelty but also since it uses Cone Beam Computer Tomography (CBCT) scans to gather anthropometric data of the skull and mouth. Where "anthropometry" refers to the measurement of the body and includes both somatometry and osteometry (Heymsfield, Bourgeois, Sommer & Shepherd 2018).

Computer Tomography (CT) measurements prove more precise than physically measuring tissue and bone (Stull, Tise & Fowler 2014; Ismail, Abdullah, Noor, Lai, Shafie & Nor 2019). The methodology for measurements for facial research of the past has always been done either on cadavers, radiographs, and CT slices, and this data is still being used today to reconstruct faces (Cavanagh & Steyn 2011; Briers *et al.* 2015).

Somatometry of deceased individuals and radiographs could prove inaccurate due to cadavers possibly presenting with tissue deformations and postmortem facial changes, and radiographs not portraying spatial awareness or objects in three dimensions (3D) (Wilkinson 2004; Wilkinson, Rynn, Peters, Taister, Kau & Richmond 2006; Stull, Tise & Fowler 2014). By utilising CBCT scans, it allows the investigator to thoroughly examine the skull and tissue in 3D, while also viewing the superimposed version of the skull and facial tissues (Ridel, Demeter, Liebenberg, L'Abbé, Vandermeulen & Oettlé 2018). This will ensure that when measurements are performed, they will be done perpendicularly to the skull as suggested by Cavanagh & Steyn (2011).

Some of the somatometry, such as with soft tissue depths, was correlated to the proportions of the skull. No facial study has done this on the mouth before, however, Ridel *et al.* (2018) has performed this on the nose. Regardless of the results of our study, FFD practice could consider the use of skull proportions in addition to the ancestral information to reconstruct faces. The reason for this is due to current methods, to predict ancestry in biological anthropology, varying in accuracy which cannot precisely predict an individual's ancestral background.

1.2.1 Research question

Can the somatometry of an edentulous individual's mouth be predicted from the osteometry of their skull?

1.3 AIM

Using the morphometrics software, Stratovan Checkpoint™, and Pearson's correlation analysis, this study aimed to determine whether there is a strong significant correlation coefficient between skull osteometry and somatometry of the upper mouth in edentulous and dentate patients.

1.4 OBJECTIVES

The objectives of this study were as follows:

- To calculate skull indices by digitally measuring distances between standard skull landmarks on CBCT scans.
- To determine somatometry of mouth morphology by digitally placing landmarks on the skull and soft tissue.
- To use Pearson's correlation analysis to investigate whether somatometry of the upper mouth can be determined from skull indices.

CHAPTER 2: LITERATURE REVIEW

The skull sets the foundation for the face, and its bony features give unique characteristics to every individual (Wilkinson *et al.* 2003). In the field of FFD, the morphological and anthropometric relationship between the skull and face has been increasingly better understood over the years (Gerasimov 1971; Wilkinson 2004; Langley, Jantz, Ousley, Jantz & Milner 2016, Ridel *et al.* 2018). However, the mouth and its relation to the jaw has not thoroughly been researched. While several studies have successfully attempted to understand the mandible and maxilla, and its morphological relation to the mouth, additional anthropometric information is required.

Studies conducted by Gerasimov (1971) mention how teeth size and occlusion can determine the shape of the lips, whereas Wilkinson, Motwani, and Chiang (2003) refer to the interlimbus distance and its relation to the width of the mouth, where the "interlimbus distance" refers to the distance between the medial borders of the irises. These studies provide meticulous guidance in determining the shape of a dentate mouth, but it cannot be extrapolated to individuals without teeth. Therefore, for edentulous individuals, Taylor (2000) introduced an informal method that lends the jawbones a resting pose to commence FFD; this is further discussed in 2.3.2.

Edentulism leads to various morphological changes of the mouth since the teeth are not present to hold the lips in their typical position. Therefore, the lips sink into the mouth, giving the individual a distinct edentulous appearance. This sunken-in appearance progresses over time since the severity of RRR also increases as the individual ages (Figure 4) (Pietrokovski *et al.* 2007).

Since significant changes occur in the residual ridge which affects the morphology of the mouth, and currently, since there is no anthropometric research for this condition, it provides the opportunity to collect data for FFD practice. Our current era of technological advancement calls for the use of CBCT to retrieve metric information from edentulous individuals. Using geometrics morphometrics alongside this technology for data collection may provide this research with results that could be reliable, considering the vulnerability of the results due to landmark placement and scanning errors (Ridel *et al.* 2018; Stull *et al.* 2014).

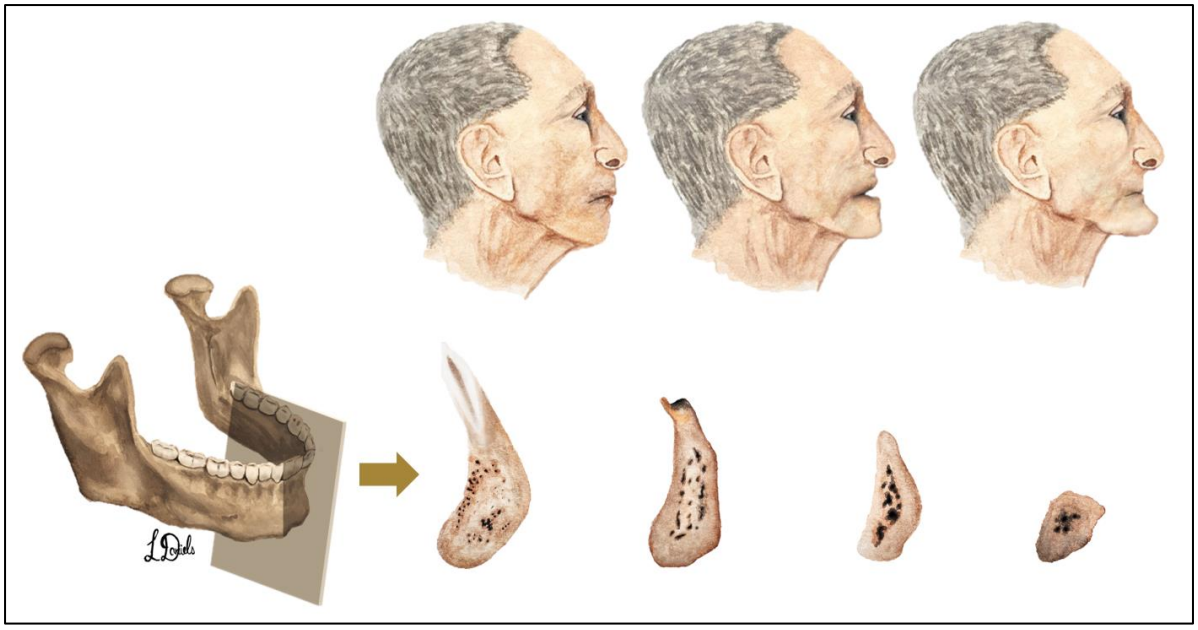

(Illustration by L. Daniels)

Figure 4: The progression of residual ridge resorption shown in the saggital section of the mandibular alveolar ridge, and the consequential changes to mouth morphology seen in a lateral view.

2.1 RESIDUAL RIDGE RESORPTION

Teeth are attached to their sockets in the alveolar ridge or process via the periodontal ligament (Figure 5 & Figure 6) (Mark 2019). After teeth have been extracted from their sockets, the alveolar ridge becomes the residual ridge (Figure 1) and undergoes resorption and remodelling for the rest of an individual's lifetime (Figure 4) (Hummel, Wilson, Marker & Nunn 2002). The aetiology around RRR is not well understood, however, some authors have discussed various theories over the years (Carlsson 2004). Pietrokovski *et al.* (2007) mention that RRR is initiated during the healing process and that it continues after the socket is healed due to the lack of normal vertical stresses on the bone. According to Pisulkar, Agrawal, Belkhode, Nimonkar, Borle and Godbole (2019), when the bone is disused, it undergoes its inevitable "disuse atrophy" as it no longer experiences biomechanical activity.

The cause of RRR may not be well understood, but the process and physiology thereof are known extensively. During the first six months after teeth have been extracted, RRR occurs rapidly. Thereafter it continues throughout the individual's lifetime at a much slower rate until the alveolar ridge is severely resorbed (Figure 4). The rate at which RRR occurs is also dependent on bone densities and it is for this reason, the edentulous mandibles and maxillae experience different rates of bone resorption. This is due to the maxilla being more cancellous than the mandible and therefore, the mandible's RRR rate is faster than the maxilla's (Gupta, Singh & Arya, 2019; El Maroush, Benhamida, Elgendy & Elsaltani 2019).

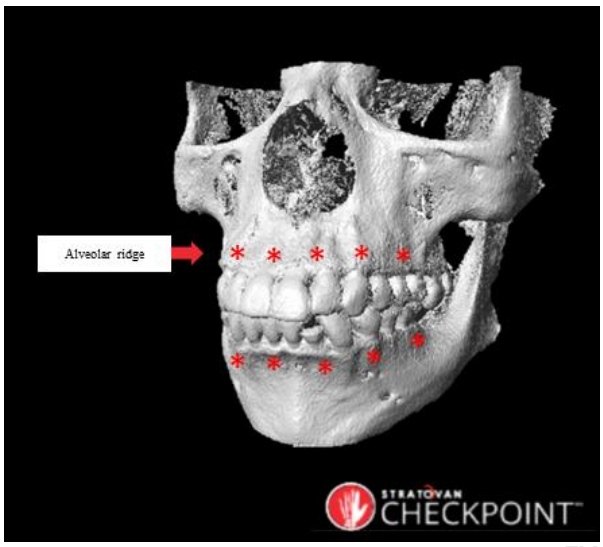

(Stratovan Checkpoint™)

Figure 5: The alveolar ridge of the jaw indicated in red.

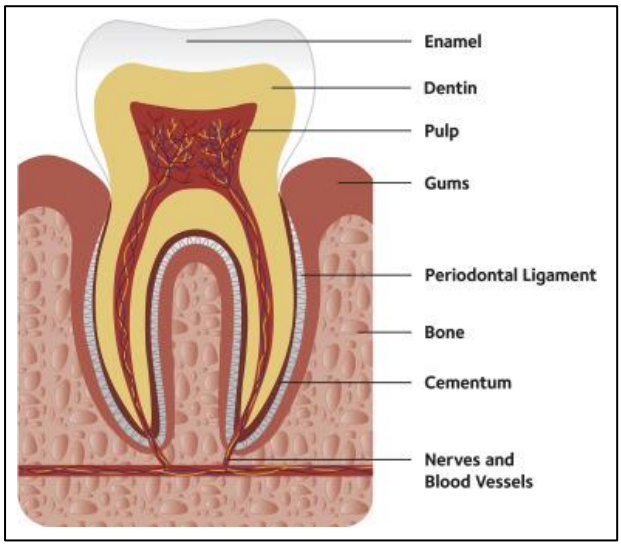

(Mark 2019)

Figure 6: The tooth structure to show the various parts of the tooth.

2.1.1 How does the residual ridge form and when is RRR initiated?

After tooth extraction or tooth avulsion (if the tooth is lost through trauma) a series of phases take place to heal the socket. As reviewed by Trombelli, Farina, Marzola, Bozzi, Liljenberg and Lindhe (2008), Reich *et al.* (2011), and Mezzomo, Shinkai, Mardas and Donos (2011), the inflammatory phase begins first where the blood vessels within the socket haemorrhage and blood clot formation commence. Inflammatory cells migrate to the wound and clear out necrotic cells. Granulation tissue forms and is progressively replaced with a tissue matrix rich in collagen fibres. During this process, bundle bone, or the bone surrounding the tooth is rapidly resorbed. New bone begins to form around and inside extraction socket, and the tooth socket will be filled with two-thirds of bone after five weeks (Amler, Johnson & Salman 1960). After RRR of the bundle bone takes place, bone resorption will continue in the alveolar bone (Pagni, Pellegrini, Giannobile & Rasperini 2012).

Shiroma, Terrado-Naguinlin and Zuerlein (2019) reviewed various skeletal case representations of the socket's healing and bundle bone resorption (Figure 7). Figure 7A represents a tooth that has been lost or removed peri-/post-mortem. The alveolar socket is smooth and intact, and no resorption occurs. After one to two months, the bundle bone is resorbed partially (Figure 7B & C). This coincides with the first phase of socket healing where osteoclastic activity takes precedent in the destruction of the original socket (Devlin & Sloan 2002). At three or four months (Figure 7D) the sockets start showing evidence of bone-filling. In Figure 7E to H, the final stages of healing are displayed after seven, eight, and nine months, and one year respectively. The bundle bone has been resorbed completely and only two-thirds of the socket will be filled with bone. This bone will eventually continue resorbing, progressively (Pagni *et al.* 2012).

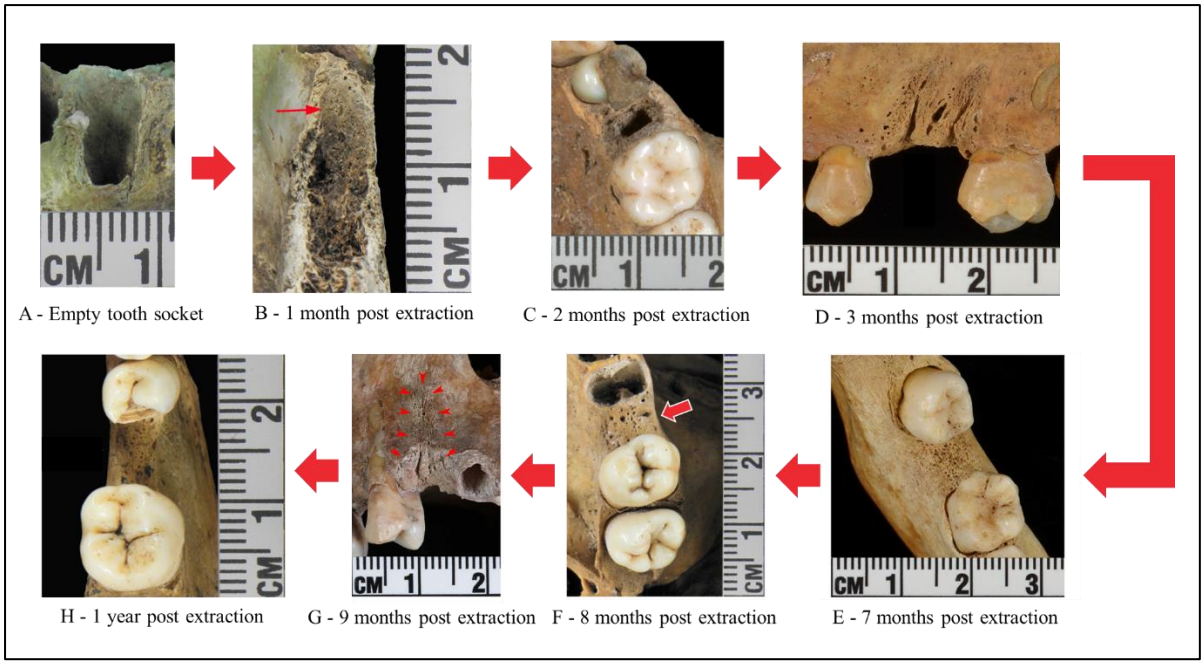

(Adapted from Shiroma *et al.* 2019)

Figure 7: Skeletal case representations of the healing socket after tooth loss. Cases A to E are all of different individuals' human remains.

2.1.2 Classifying RRR severity

Various classification systems for the extent of RRR is used since the process of RRR does not halt and continues with age (Kaur, Kumar, Jindal & Badalia 2017). In order to provide a method of describing the extent and pathology of RRR, a system of six residual ridges have been described by Cawood and Howel (1988), and Atwood (1958) (Figure 8 & Figure 9).

The reduction of the residual ridge leads to five different ridge forms after the tooth is extracted. Class I is classified as "dentate" where the tooth is still in its socket. Class II is post-extraction, where the socket will start undergoing healing (Figure 7A). Class III confirms the resorption of the bundle bone. Class IV to VI occurs as the alveolar bone continues to start resorbing (Figure 8 & Figure 9; Table 1) (Cawood & Howell 1988).

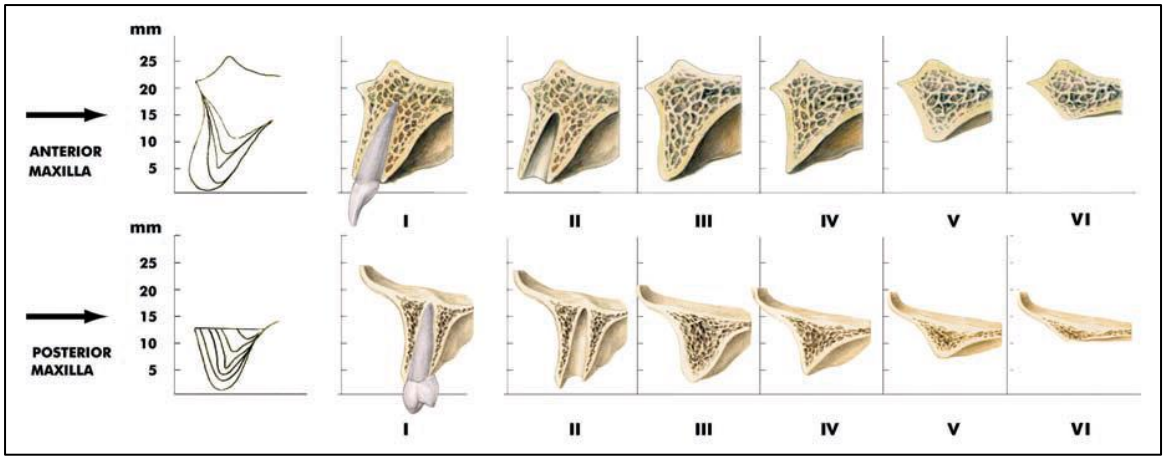

(Cawood & Howell 1988)

Figure 8: Visual representation of the classification system of RRR classes of the posterior and anterior maxillary alveolar ridge.

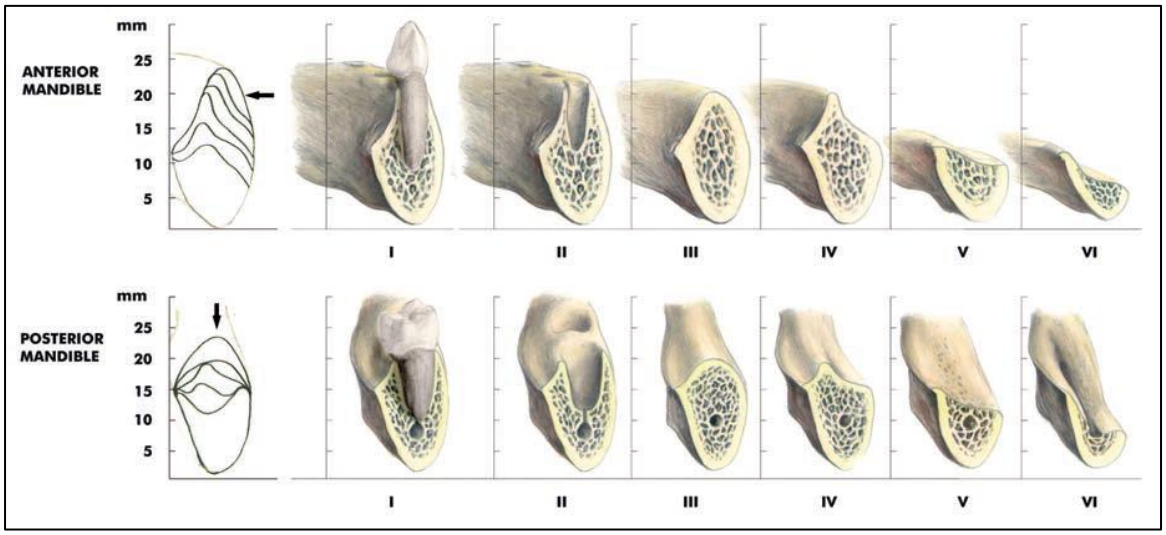

(Cawood & Howell 1988)

Figure 9: Visual representation of the classification system of RRR classes of the posterior and anterior mandible.

Table 1: Cawood and Howell's descriptive classification of the changes of the shape of the alveolar processes of the edentulous jaws Class Description.

Class	**Description**
Class I	Dentate
Class II	Immediately post extraction
Class III	Well-rounded ridge form, adequate in height and width
Class IV	Knife-edged ridge form, adequate in height and inadequate in width
Class V	Flat ridge form, inadequate in height and width
Class VI	Depressed ridge form, with some basilar loss evident

(Cawood & Howell 1988)

2.1.3 Factors which influence tooth socket healing and RRR

Residual ridge resorption has been described as a progressive, chronic, and cumulative multifactorial disease (Pagni *et al.* 2012). The interindividual variation in the rate of RRR and its aetiology is not well understood. However, the factors which influence RRR has been reviewed extensively by many authors (Carlsson 2004; Pietrokovski *et al.* 2007; Guiglia, Di-Fede, Lo-Russo, Sprini, Rini & Campisi 2013).

2.1.3.1 Osteoporosis

A systemic factor such as osteoporosis (OP) can affect any part of the body, although the bones in the spine, hip and wrist are mostly affected. Research suggests that there is a link between OP and RRR. The link is that OP influences and increases the rate of RRR due to the consequential reduction in bone mass and skeletal fragility (Poštić 2000; Rosenquist, Baylink, & Berger).

A reduction in bone mass also affects the jaw since cortical bone porosity of the maxilla increases with age. A variation of the thickness of cortical bone is also found in the mandible, however, males present with higher cortical bone values than females. Additionally, mandibular bone mineral content increases slightly in males but decreases in females. This all occurs due to hormonal factors experienced post menopause (Guiglia *et al.* 2013). Since the bone turnover rate of the alveolar processes of the jaws is greater than in long bones, bone loss could manifest earlier at the alveolar ridge than at other skeletal sites and therefore, this could be an early indicator of OP (von Wowern & Kollerup 1992).

However, research on the topic of OP and RRR is still quite contradictory. Many studies suggest that OP does not significantly affect RRR (Von Wowern & Kollerup 1992), but some studies insist that it does. Klemetti and Vainio (1993), and White and Rudolph (1999), found statistically significant correlations between RRR and OP. Another study found that metabolic bone loss and systemic osteoporosis are directly responsible for the appearance of the pronounced reduction in the alveolar regions of the jaw (Bras, Van Ooij & Van den Akker 1985). A more recent study conducted by Poštić 2000 concluded that systemic osteoporosis causes a decrease in jawbone density and induces RRR.

The reason behind the association of OP and RRR are scant in research, however, some explanations have come forth. Rosenquist *et al.* (1978) and Poštić (2000) mention how reduced blood flow to the jaw is associated with systemic osteoporosis. This is due to carotid artery calcifications and atherosclerosis of the alveolar arteries which are not specific to OP but rather are consequences of ageing (Bradley 1975; Dewake, Ishioka, Uchida, Taguchi, Higashi, Yoshida & Yoshinari 2020). Therefore, with all this contradictory information, a thorough conclusion cannot be made regarding whether OP affects RRR. However, with all the given research, it would perhaps be beneficial to consider OP when performing edentulous research (Dewake *et al.* 2020).

2.1.3.2 Pressure

Another systemic factor researchers are unsure about is the relationship between the pressure inflicted on the residual ridge and RRR. There are many ways pressure can be inflicted on the residual ridge. For example, dentures put pressure on the residual ridge and studies show that individuals wearing dentures lose more bone than those who do not (Campbell 1960; Carlsson *et al.* 1969). The theory is that the less dentures are worn, the rate of RRR will decrease (Carlsson & Persson 1967). However, Bergman and Carlsson (1985), and Kalk and de Baat (1989) state the opposite. This may be due to the variation of the rate of bone loss of the alveolar ridge observed in these studies as well as the difference in cortical thickness between the mandible and maxilla.

Further supporting research by Pietrokovski *et al.* (2007) found larger edentulous arches and ridges in non-denture users compared to denture wearers. Other studies have similar conclusions (Campbell 1960; Józefowicz 1970; Carlsson 1967; Pietrokovski, Azuelos, Tau & Mostavoy 1995). The clinical findings of the aforementioned research state that bone resorption is enhanced in denture use when there is occlusal loading on the underlying denture bearing tissues. Therefore, the pressure exerted by dentures and the effect it brings to the residual ridge could also be dependent on the type of dentures prescribed for the patient (Pietrokovski *et al.* 2007).

A particular syndrome, known as “combination syndrome”, is claimed to influence RRR significantly. Combination syndrome occurs when a patient with reduced mandibular dentition with only the anterior teeth present, and who wears complete maxillary dentures, or has a mandibular overdenture on the anterior permanent teeth or implants; these factors together increase RRR in the maxillary anterior ridge (Figure 10) (Jyoti, Shah & Karthik 2010). There is a lack of evidence to support this theory, however, a definition has been published in *The Glossary of Prosthodontic Terms* (Ferro, Morgano, Driscoll, Freilich, Guckes, Knoernschild, McGarry & Twain 2017).

(Jyoti *et al.* 2010)

Figure 10: Combination syndrome morphology.

2.1.3.3 Periodontitis

A disease which influences RRR is Periodontitis (PD) since it also degrades the structure of the jaw. In advanced forms, PD also causes the loss of soft tissue and leads to tooth detachment (Poštić 2000). The body’s immune system and bacteria break down the alveolar bone and its connective tissue. Alongside RRR, it aggravates the resorption rate leaving the individual with remodelled alveolar ridge with a progressive reduction in its height (Figure 11) (Zmysłowska, Ledzion & Jędrzejewski, 2007).

(Fujita 2012)

Figure 11: Archaeological case representation of periodontal disease.

2.1.3.4 Tobacco and alcohol use

Tobacco and alcohol primarily affect socket healing, which subsequently affects the rate of RRR. Nicotine in tobacco is known to have harmful effects in tissue healing where it affects angiogenesis, osteogenesis, and cellular healing such as with the inhibition of fibroblast proliferation and adhesion, and collagen synthesis (Pinto, Bosco, Okamoto, Guerra & Piza 2002).

In a study performed by Pinto *et al.* (2002) on male Wistar rats, it was reported that the healing of the alveolar sockets was delayed significantly after the rats received a dose of nicotine hemisulphate. The research further mentions that the delay in socket healing may be due to the inhibition of epithelisation indirectly caused by the nicotine

Tobacco use also affects osteoclast and osteoblast activity, resulting in poor bone health. This is due to nicotine's inhibitory effect on osteogenesis where nicotine will bind to nicotinic receptors in osteoblasts. At low levels, this binding to receptors increases cell proliferation, however, at high levels it inhibits osteoblast production resulting in cell death, subsequently slowing down the healing rate of the tooth socket (Al-Bashaireh, Haddad, Weaver, Chengguo, Kelly & Yoon 2018)

Alcohol on the other hand is a contributing factor to osteoporosis and bone loss (Sampson, Perks, Champney & DeFee 1996). Alcohol use may depress new bone formation with more negligible effect on bone resorption. This leads to negative bone balance and progressive bone loss (Lindholm, Steiniche, Rasmussen, Thamsborg, Nielsen, Brockstedt-rasmussen, Storm, Hyldstrup & Schou 1991).

2.2 FORENSIC FACIAL DEPICTION

Many of these systemic factors mentioned in 2.1.3 could influence a FFD if the human skull is severely affected by these factors. If these systemic factors are shown to influence the human remains, the forensic artist will depict it on the reconstructed face using existing scientific standards that are of a metric and morphoscopic nature (Wilkinson 2004; Vermeulen 2012; Briers *et al.* 2015).

Extensive data is available for FFD since it is such a vast field of research. Average soft tissue depths (ASTD) are some of the data available, and as the name implies, ASTDs are the averaged measurements of the tissue thickness at a specific tissue depth landmark on the skull for specific cohorts, as depicted in Figure 12 and Table 2. In FFD, these measurements are used to create average tissue depth markers with lengths that correlate to ASTDs.

In Figure 13, ASTDs and their landmarks are seen used in two different FFD methods, the Manchester and American method. With the Machester method, the tissue depth markers are set at defined craniofacial landmarks; muscles and facial organs are modelled and eventually, the tissue will be built around the markers until the face is complete (Wilkinson & Neave 2003). This can be done manually using a modelling mastic and digitally using relevant software (Figure 14). In the American method, facial anatomy is considered but not actively applied as in the Manchester method. In the American Method, the artist also places tissue depth markers on the skull, and the tissue is built up around the markers and the individual's facial features are reconstructed (Figure 13) (Gatliff & Snow 1979; Vermeulen 2012).

Anatomical information, age, sex, and occasionally ancestry of human remains, can lend objectivity to an FFD, however, the need for subjective interpretation is heavily increased when a skull presents with pathology or trauma. The practitioner would then need to suggest what effect these anomalies may have had on the individual's face (Wilkinson 2004). With a focus on edentulism, not much data exists for individuals without teeth, hence conducting this study. The more teeth that are missing, the more noticeable edentulism becomes as it affects the shape of the mouth. It makes the mouth appear "sunken-in" due to RRR and remodelling of the alveolar ridge (Reich *et al.* 2011). A skull with edentulism and RRR requires much understanding of the morphological changes that takes place to reconstruct the mouth as accurately as possible (Taylor 2000).

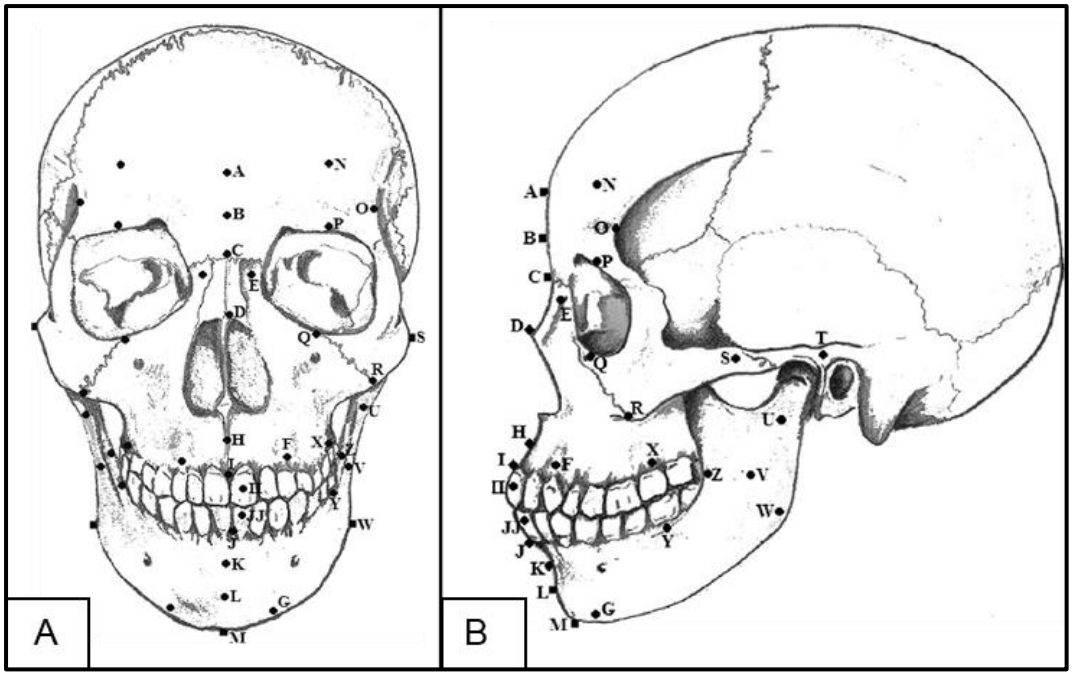

(Cavanagh & Steyn 2011)

Figure 12: Frontal view (A) and lateral view (B) of tissue depth landmarks.

Table 2: Landmarks for measurements and location of tissue depth markers. Landmarks A–M (except F and G) are midline landmarks, but landmarks N–Z are bilateral.

Hard Tissue Landmark		**Definition**
A[a]	Supra-glabella	Above the glabella.
B[a]	Glabella	Most prominent point between supra-orbital ridges in mid-sagittal plane.
C[a]	Nasion	Midpoint of the suture between the frontal and the two nasal bones.
D[a]	Endofnasals (Rhinion)	Anterior tip of the nasal bones on the inter nasal suture.
E[c]	Lateral nasal	A point on the side of the bridge of the nose in line with the endocanthion, or inner corner of the eye.
F[b]	Lateralsupra-labiale (Supracanine)	A point on the maximum bulge of the maxillary/uppercanine eminence.
G[b]	Mental tubercle	Most prominent point on the lateral bulge of the chin mound.
H[a]	Mid-philtrum (Subspinale)	Midline of the maxilla, placed as high as possible before the curvature of the anterior nasal spine begins.
I[a]	Mid upper lip margin (Supradentale alveolare)	Between the maxillary (upper) central incisors at the level of the cementum–enamel junction.
II[c]	Upper incisor	Halfway down the height of the enamel of the upper central incisors.
J[a]	Mid lower lip margin (Infradentale)	Centered between the mandibular (lower) central incisors at the level of the cementum–enamel junction.
JJ[c]	Lower incisor	Halfway down the height of the enamel of the lower central incisors.
K[a]	Supra-mentale (chin–lip fold or mid labiomentale)	The deepest midline point of indentation on the mandible between the teeth and the chin protrusion.
L[a]	Mental eminence (pogonion or anterior symphyseal)	The most anterior projecting point in the midline on the chin.
M[a]	Menton	The lowest point on the mandible.
N[a]	Frontal eminence	A point on the projections at both sides of the forehead.
O[b]	Fronto-temporale	The most medial point on the curve of the temporal ridge, on the frontal bones, above the zygomatico frontal suture.
P[a]	Supra-orbital	Above the orbit, centred on the uppermost margin of the orbit.

Q[a]	Sub-orbital	Below the orbit, centred on the lowermost margin of the orbit.
R[b]	Zygomaxillare	Lowest point on the suture between the zygomatic and maxillary bones.
S[b]	Lateral zygomatic arch (zygion)	A point on the maximum lateral outer curvature of the zygoma.
T[a]	supra-glenoid	Above, and slightly forward of the external auditory meatus.
U[c]	Area of the parotid	A midline point between the external auditory meatus and point V (mid-masseteric).
V[b]	Mid masseteric	A point at the centre of an area bounded by the lower borders of the zygomatic arch and mandible, anterior fibres of the masseter muscle and posterior border of the ascending ramus of the mandible.
W[a]	Gonion	The most lateral point on the mandibular angle.
X[a]	Supra M2	Above the second maxillary molar.
Y[a]	Sub M2	Below the second mandibular molar.
Z[a]	Occlusal line	On anterior margin of the ramus of the mandible, in alignment with the line where the teeth occlude or ‘‘bite’’.

(Cavanagh & Steyn 2011)

[a]Landmarks defined by Rhine and Campbell (1980) for measurements or location of tissue depth markers.

[b]Landmarks defined by Aulsebrook *et al.* (1995) for measurements or location of tissue depth markers.

[c]Landmarks newly defined by the authors for measurements or location of tissue depth markers.

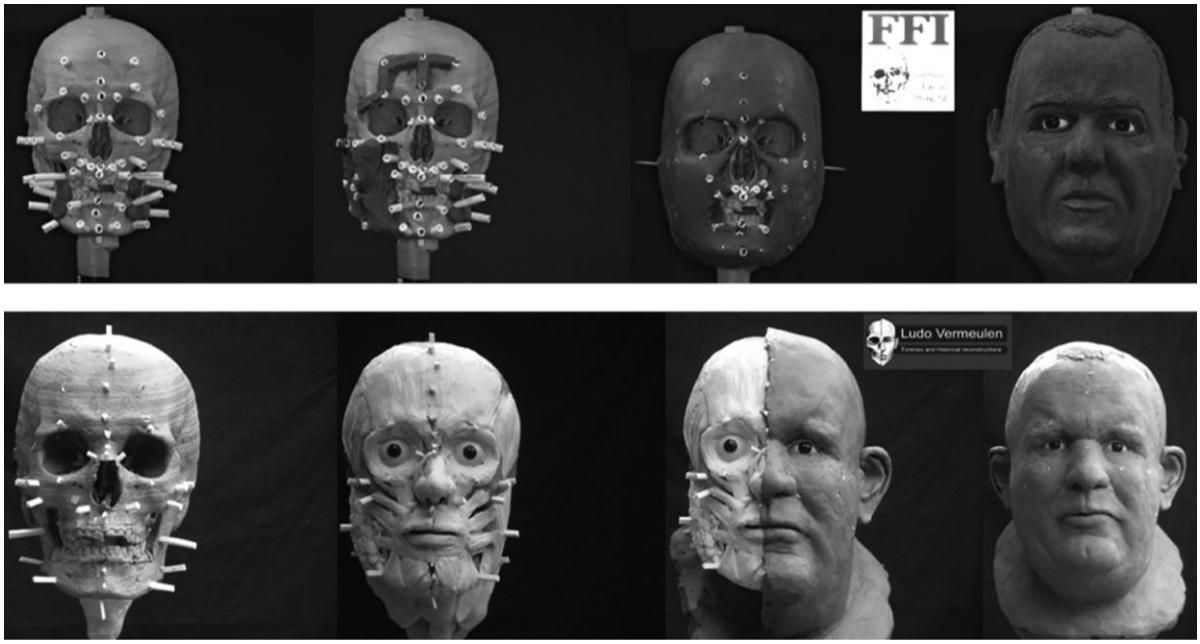

(Vermeulen 2012)

Figure 13: American Method of facial reconstruction (top row) which rely only on ASTDs, and the Manchester Method (bottom row) which rely on ASTDs and facial anatomy.

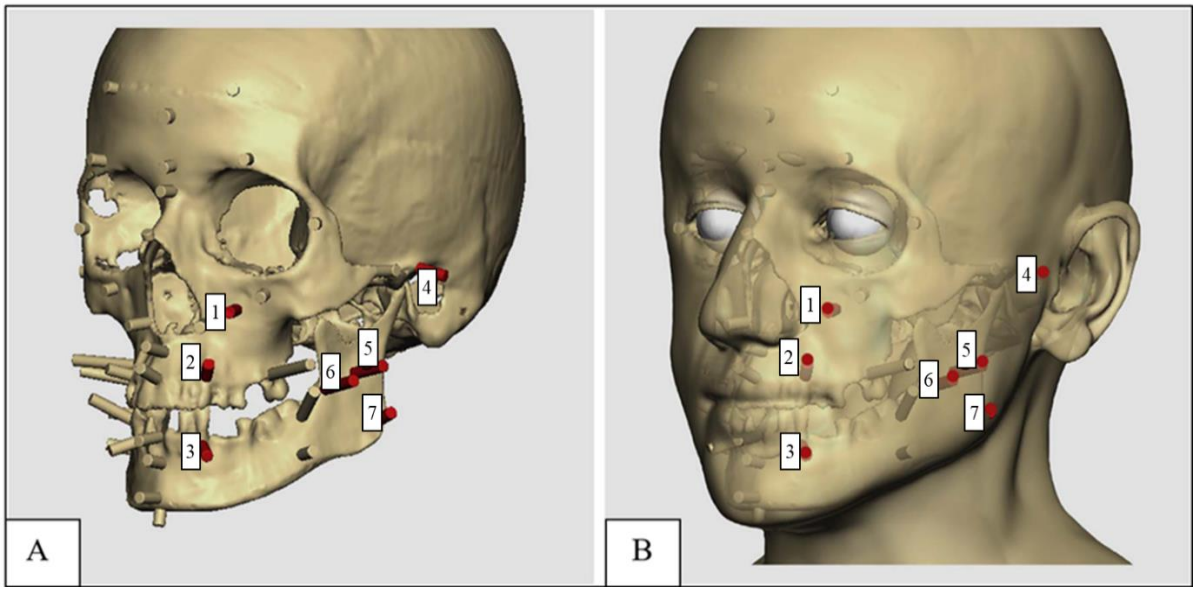

(Bulut, Liu, Koca & Wilkinson 2017)

Figure 14 : Digital facial reconstruction showing a skull with tissue depth markers (A) and B, showing the skull superimposed with a reconstructed face. 1: inferior malar; 2: supra canina, 3: sub canina, 4: supraglenoid, 5: mid masseter, 6: occlusal line; 7: gonion.

2.3 TEETH AND THEIR ROLE IN DETERMINING MOUTH SHAPE

As seen in Figure 12, Figure 13, and Figure 14, there are tissue depth markers placed on the teeth, the mandible, and maxilla. Therefore, in edentulism, ASTDs of the mouth will be affected due to the edentulous morphology (Rynn, Balueva & Veselovskaya 2012).

2.3.1 Depiction of the mouth if teeth are present.

In FFD, the teeth are used to determine the morphology of the lips and mouth. This has been proven by various researchers over the years as these authors have successfully produced methods to predict the shape of the mouth using the mandible, maxilla, and teeth (Vermeulen 2012).

Angel's (1978) research discovered that the lower edge of the bottom lip is above the middle of the bottom incisor crowns (Figure 15). The corners of the oral aperture, also known as the chelions, are demarcated at the first upper premolar-canine junction (Figure 15). Currently, the most accurate placement of chelions is using the interlimbus distance (Figure 16) (Wilkinson *et al.* 2003). Wilkinson *et al* (2003) further found that there is a positive correlation between the height of the maxillary teeth and upper lip thickness; mandibular teeth height and lower lip thickness; and the total teeth height and total lip thickness.

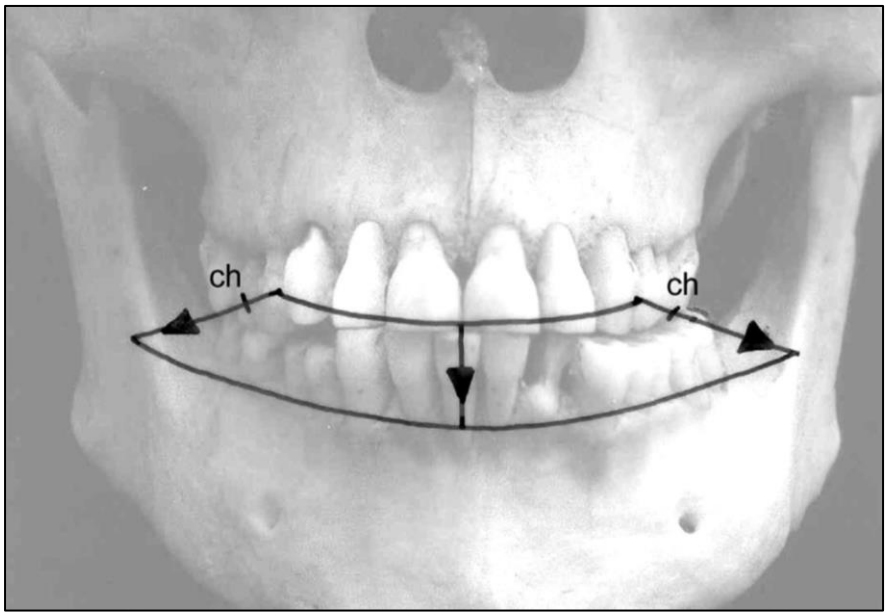

(Wilkinson 2004)

Figure 15: Predicting the shape and size of the bottom lip. Corners of the mouth = Chelion (ch).

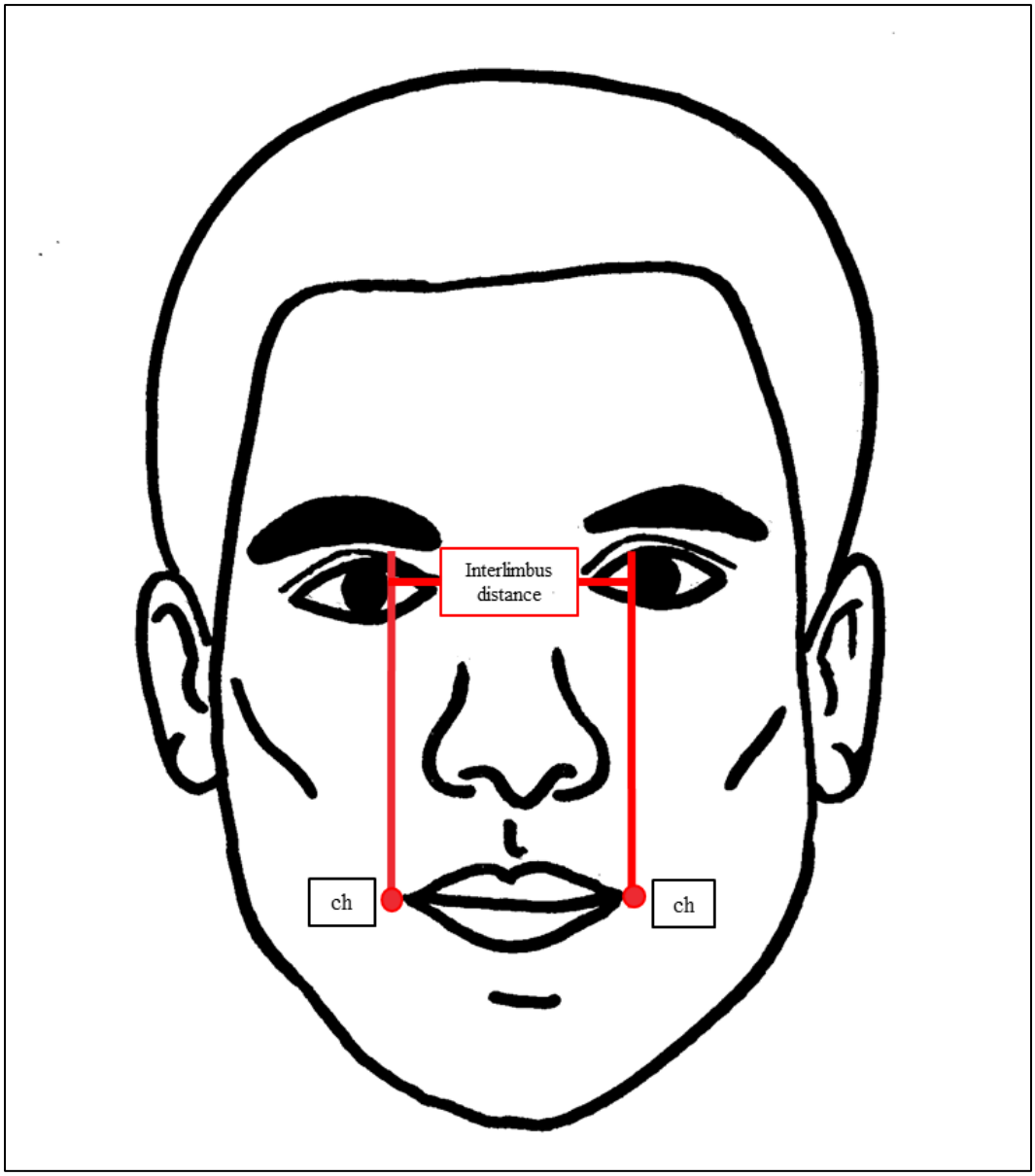

(Illustration by L. Daniels; adapted from Ray & Mathews 1957)

Figure 16: Illustration to demonstrate that the interlimbus distance is able to determine the chelions (ch) of the mouth according to Wilkinson *et al.* (2003).

According to Gerasimov (1971), lip shape and size are dependent on the prognacy of the teeth, where "prognacy" refers to the state of incisor projection and is also dependent on the alveolar processes of the maxilla and mandible (Wilkinson *et al.* 2003). Gerasimov's research uses additional terms to describe the projection of an individual's teeth, such as "orthognathism" and "prognathism". Where orthognathism refers to the teeth and alveolar processes that are not protruding, and prognathism refers to the teeth and alveolar processes that are protruding (Wilkinson 2004).

Orthognathic skulls with small teeth (Figure 17A) would usually present with thin lips whereas prognathic skulls would present with fuller lips (Figure 17C). A skull showing prognathism in the maxilla, known as an "overbite", should have the upper lip projecting further than the lower (Figure 17C & D); the same then applies to the mandible and lower lip (Figure 17E) (Fedosyutkin & Nainys 1993).

In some cases, the shape and size of the lips do not abide by prognacy. Factors such as age, ancestry, sex, and edentulism play significant roles in mouth-shape (Wilkinson 2004). This coincides with additional findings of Gerasimov, stating that prognathism in a skull does not necessarily denote fuller lips or macrocheilia. To clarify, an individual could present with prognathism and have smaller lips, leaving the individual with a puckered appearance. Where "puckered", in this case, refers to a mouth closed tightly over the teeth.

Since there is evidence that teeth play a significant role in determining the morphology of the mouth, it shows how important teeth are to the FFD practitioner. Therefore, edentulism undoubtedly alters the morphology of the mouth (Pietrokovski *et al.* 2007).

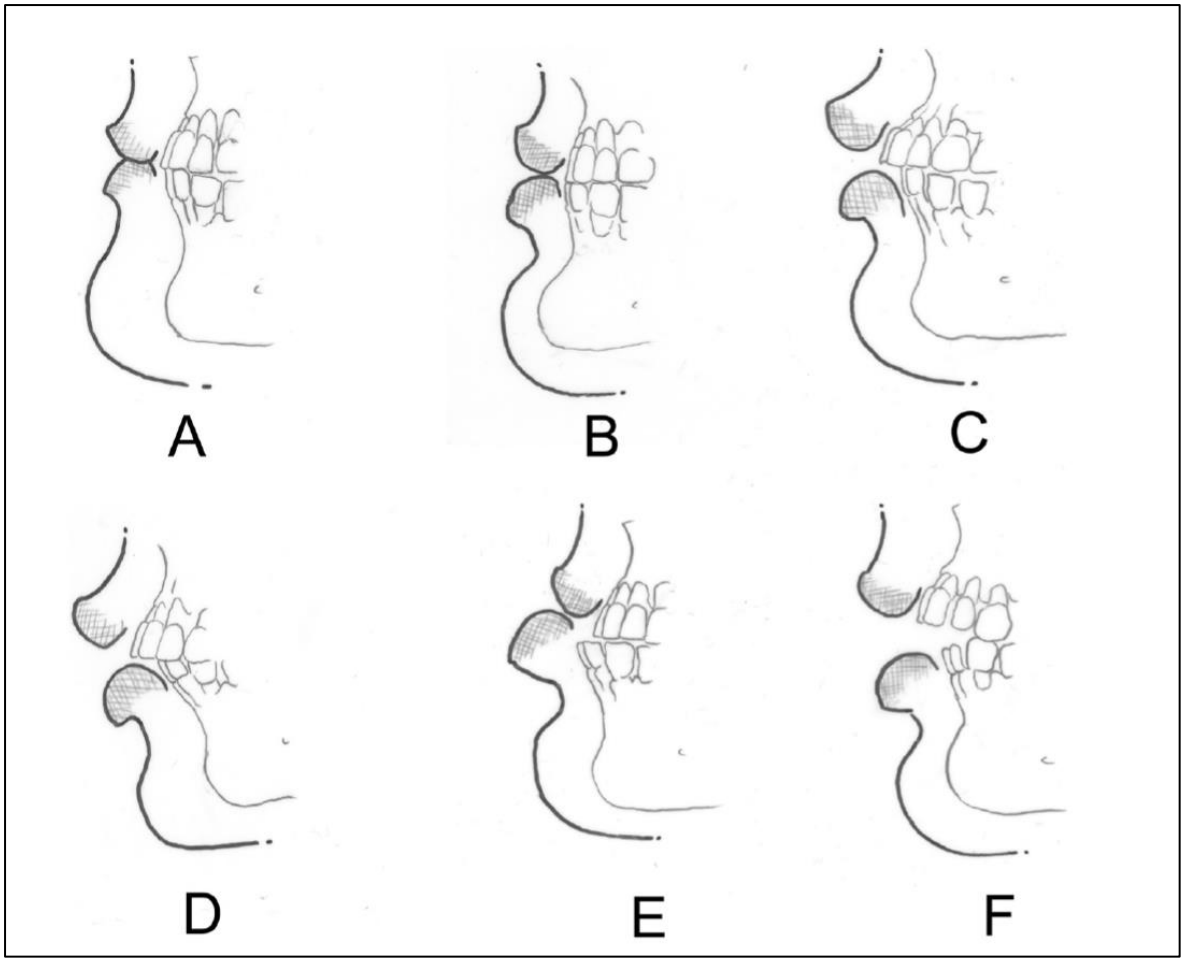

(Wilkinson 2004)

Figure 17: The basic mouth forms. A=step, B=pincer-like, C=scissor-like, D=roof-like, E=cornice-like, F=open occlusion. Modified from Gerasimov (1971).

2.3.2 Depiction of the mouth in the absence of teeth

In the absence of teeth during a forensic facial interpretation, forensic artists need to rely on other rudimentary methods to complete the reconstruction. A particular method by Taylor (2000) introduced a technique to predict the resting pose of an edentulous individual's skull. Taylor (2000) suggests that a dowel or pencil is placed through the mandibular notches behind the pterygoid bones (Figure 18). This will estimate an occlusal space when the mandible is appropriately placed in relation to the cranium. The artist will then continue depicting the face, giving the individual an edentulous appearance. The artist will continue the FFD subjectively, as the research for edentulous morphology is scant and studies only morphologically describe the "edentulous appearance".

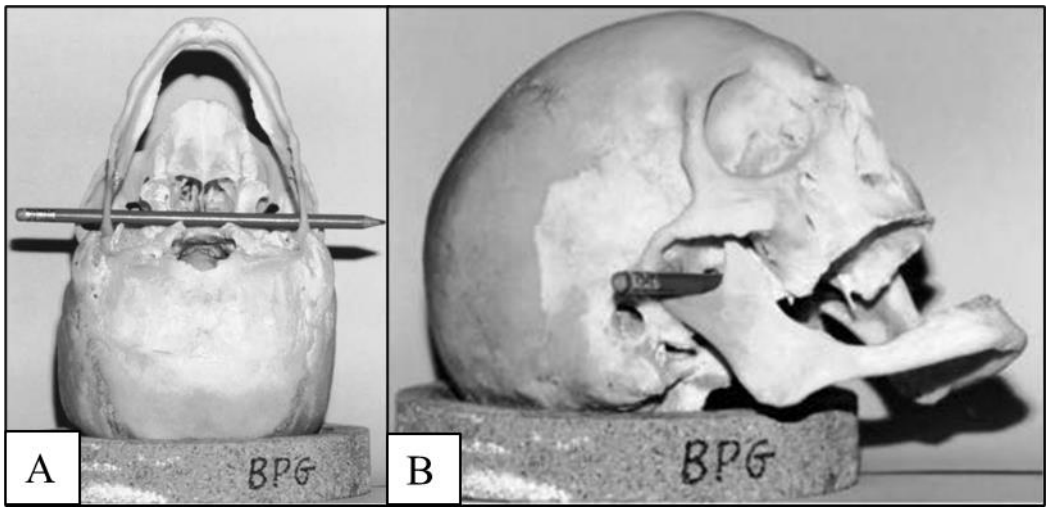

(Taylor 2000)

Figure 18: A method to achieve the edentulous resting pose. The figure shows the view from the skull base (A) and the lateral view (B).

2.3.3 Edentulous morphology

The sunken-in appearance of the mouth occurs because the teeth are no longer present to hold the lips in their original position (Kaur *et al.* 2017; Gerasimov 1971) (Figure 19). As RRR progresses, the lips gradually sink into the mouth, more than at the initial stages of RRR (Figure 4 & Figure 19). This process decreases the visibility of the lips at the resting mouth pose and eventually, the lips will sink into the mouth completely (Wilkinson *et al.* 2003).

If the patient did not initially present with a nasiolabial fold, it would begin to develop due to RRR. For those with an existing nasiolabial fold, the fold will become more prominent as RRR develops (Figure 20). In Figure 21A, the patient has a mild form of RRR, the nasolabial fold is present, and the lips are still visible in their lateral pose, however, Figure 21B shows a severe form of RRR which has been progressing for many years (Pietrokovski *et al.* 2007; Kaur *et al.* 2014). The longer RRR progresses, the shorter the patient's face becomes. In Figure 21B, the patient's overall face height is significantly decreased. These features should be considered when performing edentulous FFD (Taylor 2000, Kaur *et al.* 2014). Furthermore, the severity of RRR should be assessed as well in order to estimate how far the lips may have sunken into the mouth (Cawood & Howell 1988).

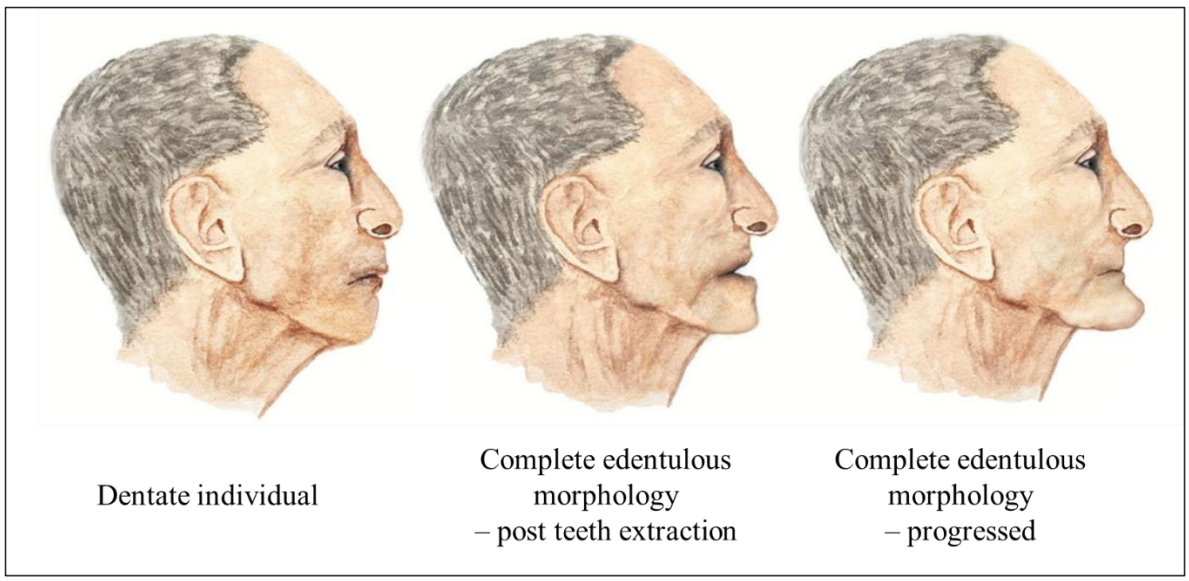

(Illustration by L. Daniels)

Figure 19: The progression of edentulous mouth morphology over time.

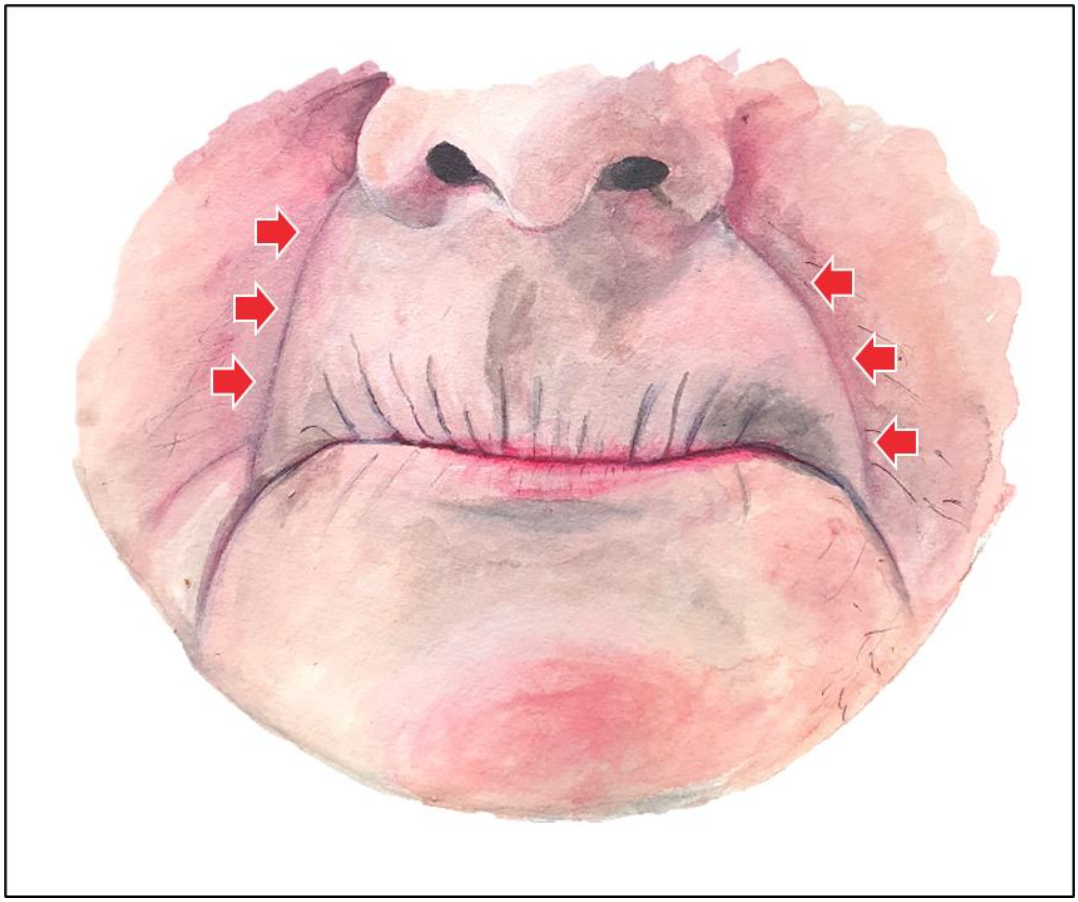

(Illustration by L. Daniels)

Figure 20: Edentulous morphology displaying nasolabial fold (red arrows).

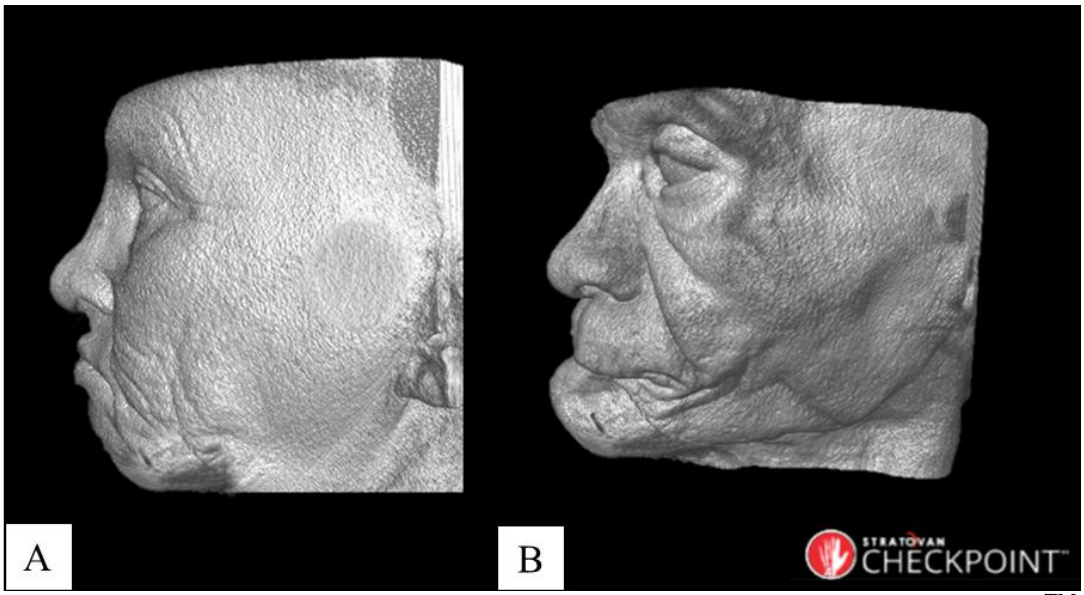

(Stratovan Checkpoint™)

Figure 21: Comparing the morphological differences between mild and severe RRR.

2.4 TRADITIONAL ANTHROPOMETRY

Anthropometric methods for data collection have always been the basis for much FFD research. For the skull, osteometry is performed using skull landmarks. Skull or skeletal landmarks (Figure 22 & Table 3) are loci that can be unambiguously defined and repeatedly located, given that they can be identified with better accuracy and precision (Richtsmeier, Paik, Elfert, Cole, & Dahlman 1995; Langley *et al.* 2016). Skeletal landmarks are also used to measure curves, angles, and coordinates, and they are vital in bone shape analysis (Wärmländer, Garvin, Guyomarc'h, Petaros & Sholts 2019). However, a noteworthy statement made by Bookstein (1991) mentioned that all skeletal landmarks are not created equal.

Therefore, in 1990 and 1991, Bookstein created a classification system where landmarks are categorised as Types 1, 2 or 3. These “Types” are based on the landmarks structural location and how informative the landmarks may be in terms of their biological processes (Wärmländer *et al.* 2019). This is not to say that a type 1 landmark is more valid to include in research; the categorisation of these landmarks is not based on how accurate they are, but rather how easily the landmark can be identified on the skeleton.

Type 1 landmarks are described by Bookstein (1991) as a point where three structures meet such as suture intersections. It could also be the centre of a small intersections or inclusions of extended curves with planes of symmetry. Examples of type 1 landmarks of the skull include the lambda and bregma.

Type 2 landmarks are the maxima of curvature points which can occur on invaginations or extrusions. For example, a type 2 landmark can be assigned to the tip of a tooth. In 1991, Bookstein classified the basion, opisthion, the middle of the basisphenoid/basioccipital synchondrosis, and the anterior nasal spine as type 2 landmarks.

Type 3 landmarks are points taken farther from other points. It also includes endpoints of diameters, intersections, centroids, and interlandmark segments. Some examples of Type 3 landmarks include the orbitale, glabella, gonion, and gnathion.

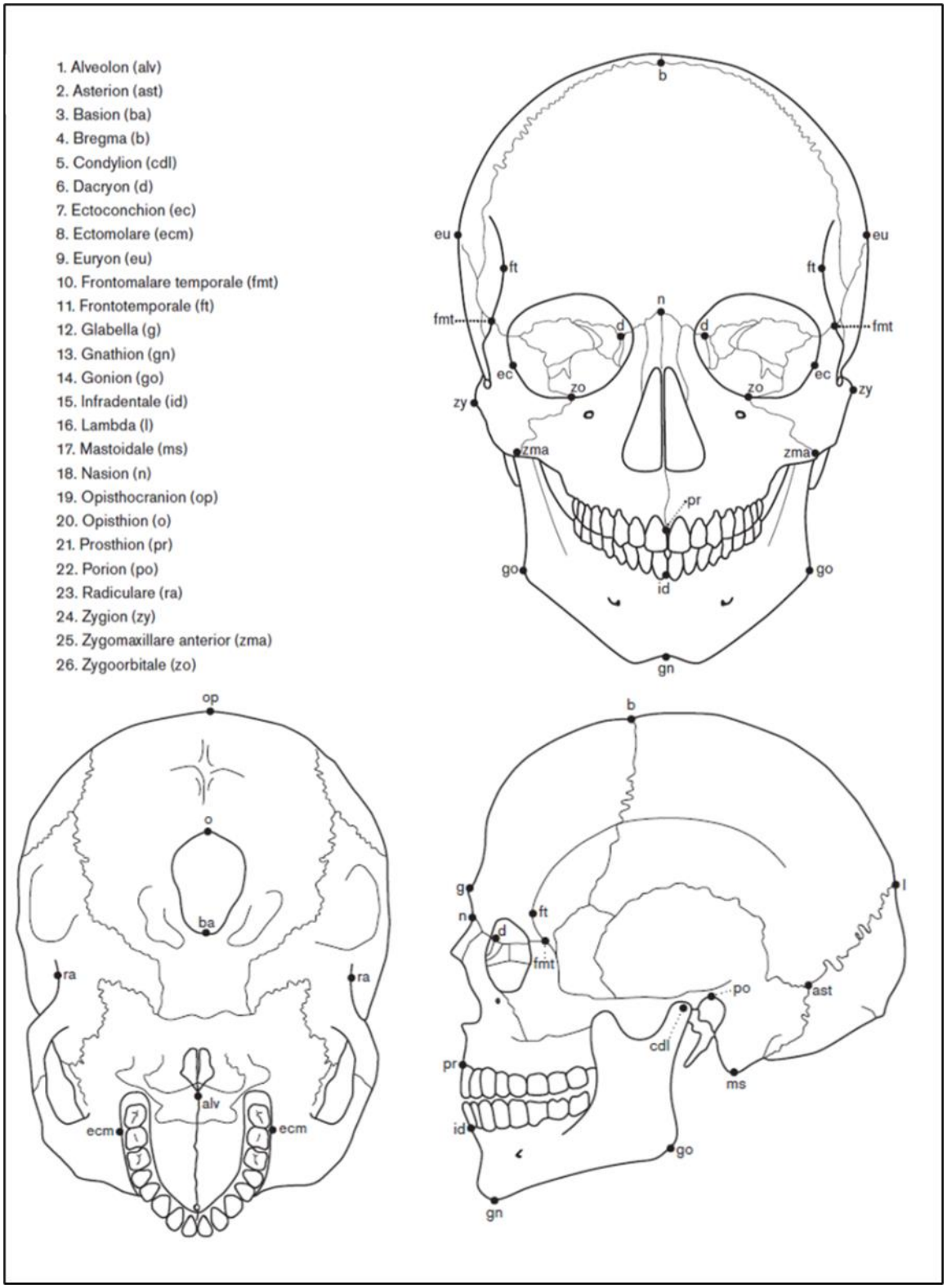

(Langley *et al.* 2016)

Figure 22: Skull landmarks for osteometry.

Table 3: Skull landmarks and their definition.

Skull Landmark		**definition**
alv	Alveolon	The point where the mid-sagittal plane of the palate is intersected by a line connecting the posterior borders of the alveolar crests.
ast	Asterion	The point where the temporal, parietal, and occipital bones meet.
ba	Basion	The point at which the anterior border of the foramen magnum is intersected by the mid-sagittal plane opposite nasion.
b	Bregma	The posterior border of the frontal bone in the mid-sagittal plane.
cdl	Condylion	The most lateral points of the mandibular condyles.
d	Dacryon	Dacryon is located on the frontal bone. When the lacrimomaxillary suture is easily found, dacryon is the point on the frontal bone where the frontal, lacrimal and maxillary sutures meet.
ec	Ectoconchion	The intersection of the most anterior edge of the lateral orbital border and a line parallel to the superior orbital border that bisects the orbit into two equal halves.
ecm	Ectomolare	The most lateral point on the buccal surface of the alveolar margin
eu	Euryon	The most laterally positioned point on the side of the braincase
fmt	Frontomalare temporale	The most laterally positioned point on the fronto-malar suture.
		A point located generally forward and inward on the superior temporal line directly above the zygomatic process of the frontal bone.
g	Glabella	The most anteriorly projecting point in the mid-sagittal plane at the lower margin of the frontal bone, which lies above the nasal root and between the superciliary arches.
gn	Gnathion	The lowest point on the inferior margin of the mandibular body in the mid-sagittal plane.
go	Gonion	The point on the mandible where the inferior margin of the mandibular corpus and the posterior margin of the ramus meet, i.e. the point on the mandibular angle which is directed most inferiorly, posteriorly, and laterally.
id	lnfradentale	The point between the lower incisor teeth where the anterior margins of the alveolar processes are intersected by the mid-sagittal plane.
l	Lambda	The apex of the occipital bone at its junction with the parietals, in the midline.
ms	Mastoidale	The most inferior point on the tip of the mastoid process.
n	Nasion	The point of intersection of the naso-frontal suture and the mid-sagittal plane.
op	Opisthocranion	The most distant point posteriorly from glabella on the occipital bone, located in the mid-sagittal plane.

o	Opisthion	The point on the inner border of the posterior margin of the foramen magnum in the mid-sagittal plane.
po	Porion	The most superior point along the upper margin of the external acoustic meatus.
pr	Prosthion	The most anterior point on the alveolar border of the maxilla between the central incisors in the mid-sagittal plane.
ra	Radiculare	The point on the lateral aspect of the root of the zygomatic process at the deepest incurvature.
zy	Zygion	The most laterally positioned point on the zygomatic arches.
zma	Zygomaxillare anterior	The intersection of the zygomaxillary suture and the limit of the attachment of the masseter muscle, on the facial surface.
zo	Zygoorbitale	The intersection of the orbital margin and the zygomaxillary suture.

(Langley *et al.* 2016)

2.5 DIGITAL ANTHROPOMETRY: GEOMETRICS MORPHOMETRICS

When performing osteometry digitally using CT, CT scan image quality is vital when identifying landmarks for digital landmark placement. Bookstein's classification of landmarks can be extrapolated to digital images since there is research to corroborate these claims. According to research performed for 3D digitisers, type 1 landmarks present the most precision while type 3 present with the least (Slice 2007; von Cramon-Taubadel, Frazier & Lahr 2007; Ross & Williams 2008; Guyomarc'h & Bruzek 2010). Ross and Williams (2008) found that inter-landmark distances between type 3 landmarks were more accurate when measured with osteometric instruments. However, when these bones were measured after digitisation, a moderate degree of intra- and interobserver error occurred in type 3 landmark locations.

If landmarks are to be placed on skulls using CT technology or any bone imaging technology, geometric morphometrics (GM) will be used to perform anthropometry on the specimens. Geometric morphometrics analysis involves the application of multivariate statistical procedures to measure distances, angles and define distance ratios (Slice 2007). The main goal of GM is to study how shapes vary. Traditionally GM was used to measure linear distances such as lengths, widths, and height, and multivariate statistical tools were used to describe the pattern of shape variation.

Studies using GM strive to use landmarks that are easily identified between skeletal material (Langley *et al.* 2016). It is recommended for landmarks to be visible between all individuals under investigation. The landmarks chosen should represent the morphology of the bony region of interest, and the placement of landmarks should be repeatable and reliable (Zelditch, Lundrigan & Garland 2004).

2.5.1 Measuring distances on the skull

Some examples of cranial lengths are shown in Figure 23 and Table 4 that can be used to perform osteometry on the skull. This can be done digitally on CT scans using various morphometric software.

Firstly, a landmark will be placed on the skull using the investigator's chosen software based on Figure 22. The morphometrics software will then measure the distance between the selected skull landmarks (Colman, De Boer, Dobbe, Liberton, Stull, Van Eijnatten, Streekstra, Oostra, Van Rijn & Van der Merwe 2019).

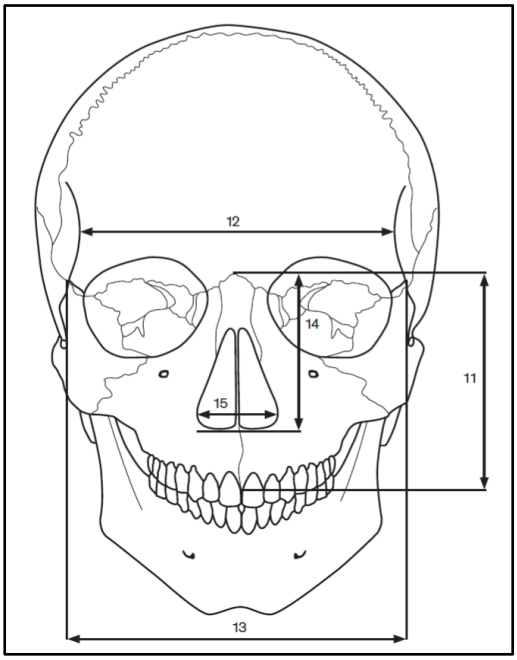

(Langley *et al.* 2016)

Figure 23: Example of some cranial lengths.

Table 4: Example of cranial lengths based on Figure 26.

Cranial length		**Definition**
11. n-pr, NPH:	Nasion-Prosthion Height	The distance from nasion (n) to prosthion (pr)
12. ft-ft	Minimum Frontal Breadth	The distance between the right and left frontotemporale
13. fmt-fmt	Upper Facial Breadth	The distance between the right and left frontomalare temporale
14. NLH	Nasal Height	The average height from nasion (n) to the lowest point on the border of the nasal aperture on either side
15. NLB	Nasal Breadth:	The maximum breadth of the nasal aperture

(Langley *et al.* 2016)

2.5.2 Calculating skull indices using cranial lengths

In anthropometry, an "index" is the ratio of two skull lengths, multiplied by 100. It is used to quantitatively represent the proportion of a specific area of the skull. These indices are used to describe the shape of the skull, cranium, nasal bones, orbits, maxilla, hard-palate, as well as prognathism (de Villiers 1979; Bass 2005; Liebenberg, Stull, L'Abbé & Botha 2015).

Skull indices are known to differ between population groups and are used in forensic anthropology (FA) to determine an individual's ancestry (Bass 2005). However, it should be noted that skull indices do not fully define an individual's ancestral background since the remains can present with more than one affinity for a population, meaning that the skull may present with various ancestral traits (Cavanagh & Steyn 2011).

An example of using an index to quantitatively define the shape of the skull is the total facial index (TFI), and it can be used to define the craniofacial shape of the skull. The TFI utilises cranial lengths of the nasion and gnathion (n-gn), and zygions (zy-zy), to calculate the index (Figure 24). These lengths will be placed into Equation 1 and the percentage calculated will indicate the TFI's value which will define the skull as either euryprosopy (broad face), mesoprosopy (average/medium face), or leptoprosopy (slender/narrow face) (Figure 24). The corresponding TFI values are seen in Table 5.

Skull indices can also be used to describe the level of prognathism or how far the maxillary teeth and alveolar ridge protrude past the nasion or gnathion. There are two ways of calculating the gnathic index. The first is the subnasal gnathic index (SGI), used by Lesciotto, Cabo, and Garvin (2016). This uses the cranial base length, or ba-n, and the basion-prosthion length (ba-pr) (Figure 25; Table 6). The gnathic index also uses the ba-pr, but the basion-gnathion length (ba-gn) as well. The SGI will quantitively present how far the maxilla protrudes past the nasion, and the GI will present how far the maxilla protrudes past the gnathion. According to Lesciotto *et al.* (2016), the SGI will determine whether the skull is orthognathic, mesognathic, or prognathic (Figure 17).

$$Total\ Facial\ Index = \frac{n - gn}{zy - zy} \times 100$$

(Bass 2005)

Equation 1: Total facial index.

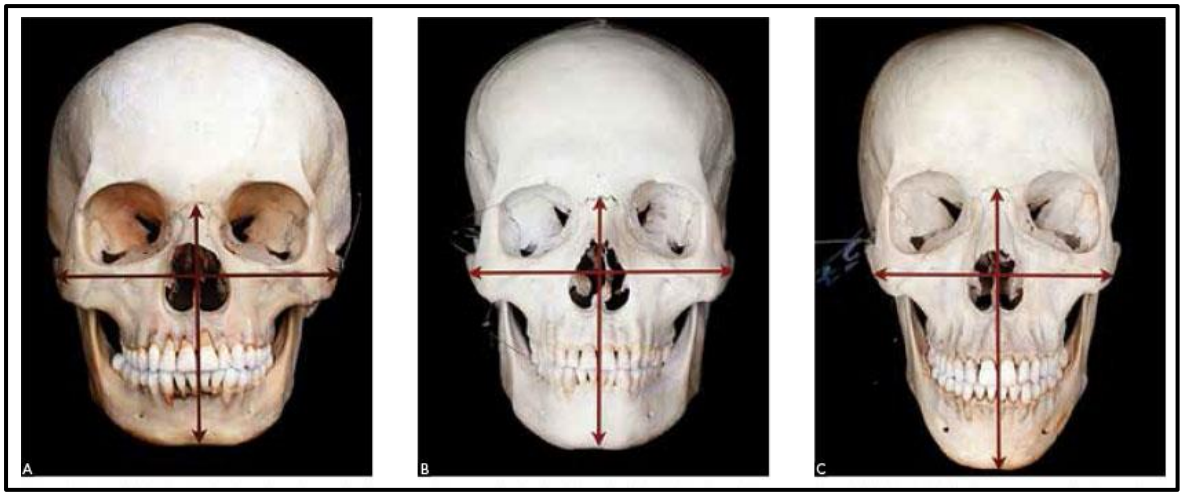

(Franco, Araujo, Vogel & Quintão 2013)

Figure 24: Various skull shapes; A -euryprosopy, B-mesoprosopy, C-leptoprosopy

Table 5: Craniofacial shape according to total facial index values.

Craniofacial shape	**Total facial index**
Euryprosopy (broad face)	80.00 - 84.99
Mesoprosopy (average/medium)	85.00 - 89.99
Leptoprosopy (slender/narrow face)	90.00 - 94.99

(Franco, Araujo, Vogel & Quintão 2013)

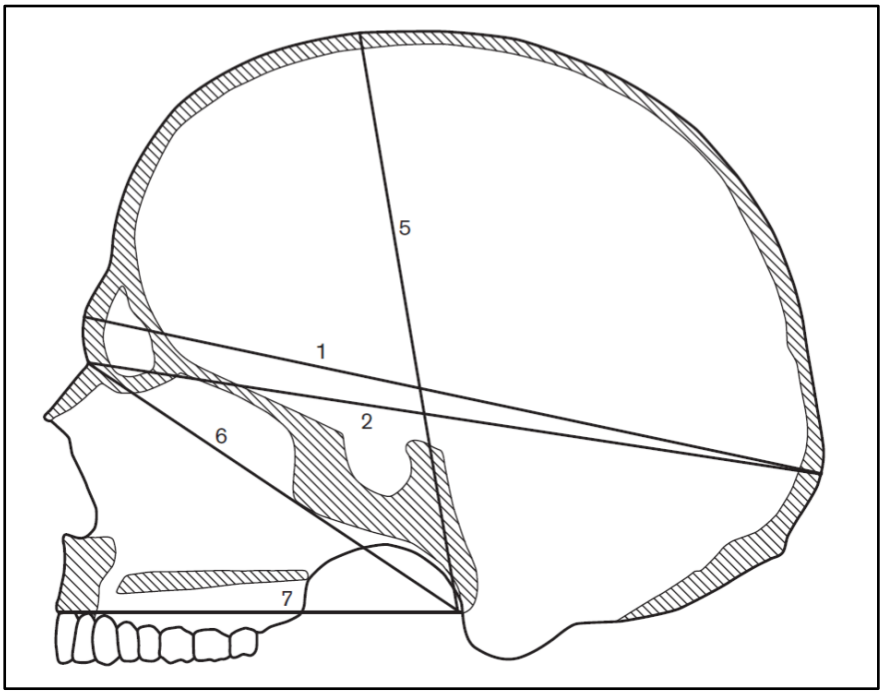

(Langley *et al.* 2016)

Figure 25: Cranial measurements in the mid-sagittal plane.

Table 6: Cranial lengths for Figure 25.

Length		**definition**
1. g-op, GOL	Maximum Cranial Length	The straight-line distance from glabella (g) to opisthocranion (op) in the midsagittal plane
2. NOL	Nasio-Occipital length	Maximum length in the midsagittal plane, measured from nasion (n)
5. ba-b, BBH	Basion-Bregma Height	The distance from basion (ba) to bregma (b)
6. ba-n, BNL	Cranial Base Length	The distance from nasion (n) to basion (ba)
7. ba-pr, BPL	Basion-Prosthion Length	The distance from basion (ba) to prosthion (pr)

(Langley *et al.* 2016)

2.5.3 Tissue depths

Using CBCTs to measure tissue depths requires perpendicular measurements to the skull. Cavanagh and Steyn (2011) did this on CT scans using ImageTool of the Centricity program to draw a tangential line on the outer surface of a bony landmark. A line was then drawn perpendicularly to the tangent and extended outward to reach the skin's surface. The length of the line from the bone to the skin surface was regarded as the soft tissue thickness (STT).

It is important that tissue depth data is collected perpendicularly from the skull, as it prevents ambiguity and significant measurement errors between investigators (Cavanagh and Steyn 2011). Using the STT landmarks as seen in Figure 12 and Table 2, the tangent line is placed on the STT landmark and the perpendicular is drawn to the skin's surface (Cavanagh & Steyn 2011). These STTs are known to differ between biological sexes, age groups, and population groups. Generally, males present with thicker STTs than females, older individuals generally present with thicker STTs than juveniles; however, as the adult continues ageing, the STT's lengths start decreasing. Various population groups present with different STT thicknesses as well and it can further vary within population groups (Wilkinson 2004). Therefore, when analysing and assigning tissue depths to skulls, age, sex, and ancestry have to be established to assign a specific set of STTs to the skull (Briers *et al.* 2015).

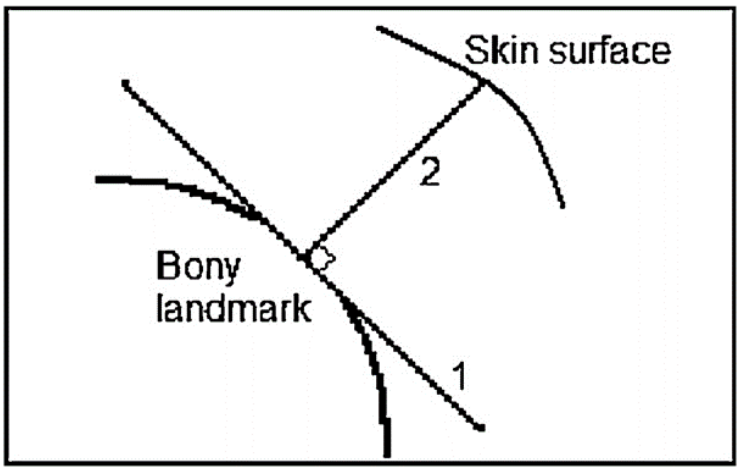

(Cavanagh & Steyn 2011)

Figure 26: Diagrammatic representation of determining tissue thickness measurements; 1-Tangent, 2-The perpendicular.

2.5.4 Measurement errors in GM

Biological anthropologists have strived to improve the current standards under which GM is used to analyse skeletal material and to perform anthropometry. The attempted improvements to GM standards are to overcome a range of methodological issues pertaining to measurement errors in research (Liebenberg & Krüger 2020).

In FA, a measurement error of 2 mm is deemed acceptable as endorsed by many authors (Verhoff, Ramsthaler, Krähahn, Deml, Gille, Grabherr, Thali, Kreutz 2008; Colman *et al.* 2019; Stull *et al.* 2014). When conducting research pertaining to quantitative factors such as with osteometry, the variance or standard deviation would then be used to quantify the extent of variation between sexes, ages, and ancestral groups. Due to measurement errors, the calculated variance may never be representative of the actual variance calculated from the measurements gathered by the investigator (Goto & Mascie-Taylor 2007).

It is known from various research that significant differences also exist between CT scan measurements and physical measurements (Oka, Murase, Moritomo, Goto, Sugamoto & Yoshikawa 2009; Stull *et al.* 2014; Ismail *et al.* 2019). These differences could arise due to investigator errors, the resolution of the scans, radiation dose, and the presence and absence of soft tissue. Voxel size and slice thickness are additional factors that affect osteometry collected from CT scans (Ford & Decker 2016). Radiation dose will also affect the quality of the images produced; however, it does not significantly affect the borders of the bone on the scans or alter its measurements as proven by Oka *et al.* in 2009.

Frequently, digital measurement errors arise when utilising CT for scanning bones *ex-situ*, otherwise known as dry bone, since it is not covered with tissue or within the body. However, this error exists due to both CT technology and human measurement error. There is not a constant indication of where the error lies. In studies performed by Colman et al (2019), it was found that in frequent cases, CT scan measurements are larger than the physical measurements performed on post cranial bones (Oka *et al.* 2009; Stull 2014; Ismail 2019). By reviewing the literature, Ismail (2019) found the largest significant difference to be 5 mm between digital and physical measurements of the maximum diameter of the femoral head. These large measurement differences and errors are one of the factors to consider when performing digital anthropometry.

2.6 CONE BEAM COMPUTER TOMOGRAPHY SCANS

Computed tomography produces scans through sectioned multidirectional X-ray images, also known as tomography. These images are then computer-processed to produce cross-sectional scans of the specimen. This allows the specimen to be viewed in 2D or as a stack of cross-sectional images in 3D (Franklin, Swift & Flavel 2016).

Studies in the FFD field make use of CBCT scans for anthropometry. Studies in the past used cadavers for anthropometry, and the data from these studies may not always be as accurate since tissue deformities and tissue desiccation occur during and after the cadaver's embalming process (Ridel *et al.* 2018; Colman *et al.* 2019). Therefore, it is crucial that research be conducted from "living patient" CT scans so that the data collected can be used for human identification (Vermeulen 2012).

The reason CBCT technology is the preferred modality for anthropometric FFD research is due to the individual being in a resting and upright position during the CBCT scan. This is important since patients in normal CT scans are supine, and the patients' facial tissues migrate from a ventral to a dorsal placement due to gravity, thereby manipulating the tissue for somatometry (Ridel *et al.* 2018).

In CBCT scans, the patient sits in a vertical position. The x-ray source and detector rotate around the patient's head and multiple sequential planar projections images of the field of view (FOV) are retrieved in a complete or partial arc using a cone-shaped X-ray beam. The FOV is defined as the dimensions of the anatomic region included in a scan (Ortega, Pedrosa, Heyde, Tong. & D'hooge 2017). This differs from traditional medical CT which acquires multiple image slices of the FOV and then stacks the slices, known as tomography, to obtain a volumetric or 3D representation of the scan. With CBCTs, there is also a lower radiation dose and higher spatial resolution (0.1 mm - 0.4 mm) for the placement of 3D landmarks which could lessen the number of measurement errors made in facial anthropometric research (Ridel *et al.* 2018; Scarfe & Farman 2008)

CHAPTER 3: METHODS AND MATERIALS

The aim of this study was to determine, using morphometrics software and Pearson's correlation analysis, whether there is a strong correlation between skull indices and somatometry of the mouth in dentate and edentulous patients. To achieve this aim, anthropometry of patients was performed on CBCT scans. The scans were collected from IQ-WEB, a Picture Archiving and Communication System (PACS) of the Oral Health Centre (OHC) of the University of the Western Cape (UWC). The patients on these scans were scanned using a CBCT scanner (NewTom VGi EVO 3D CBCT Imaging) with the following properties: 75-110 kV, 1-32 mA, standard voxel size of 200 - 300 µm, high-resolution voxel size of 100 - 150 µm and a maximum field of view of 24 x 19 cm (Figure 27).

After accessing 962 CBCT scans from the PACS, the scans underwent a selection criterion. A total of n=63 scans were retrieved that met the selection criteria. For dentate patients, a total of n=40 (24 males; 16 females) scans were retrieved. For edentulous patients, a total of n=23 (16 males; 7 females) scans were retrieved. The edentulous patient group had an age range of 38 to 81 years (Mean age: 60,13; SD:11,79). The dentate group's age range was between 22 and 78 years (Mean age: 35,68 SD: 13,17)

(New Tom VGi evo EXPANDED.VISION 2021:4)

Figure 27: NewTom VGi EVO 3D CBCT scanner.

3.1 ORIGIN OF THE SCANS

The patient scans present in the UWC, Faculty of Dentistry, OHC's PACS are mainly individuals of the Western Cape, South African (SA) Population. These individuals received and/or were referred for a CBCT scan at the OHC between 1 January 2015 and 4 August 2021.

Patients are usually recommended for a CBCT scan for an array of reasons. These reasons include facial trauma, dental implant planning, carious teeth, bone loss, periodontal disease, benign or malignant pathologies, temporomandibular joint irregularities, and endodontic or orthodontic treatments (Alamri, Sadrameli, Alshalhoob & Alshehri 2012). A CBCT scan will give the clinician or radiographer sufficient detail of the skull and its neurovascular canals and foramina, however, it gives minimal detail of soft tissues. Patients undergoing dental implants, the patients are also scanned during the treatment planning phase to ensure successful implant procedures (Correa, Spin-Neto, Stavropoulos, Schropp, da Silveira, & Wenzel 2014). The implant planning scans frequently showed edentulism and/or teeth that are severely fractured. These scans included pre-, intra-, and post-scanning for implant or orthodontic treatment.

3.2 ETHICS CONSIDERATION

The patients in the CBCT scans collected for this research could not grant consent for this research project since the scans were retrieved from the OHC's PACS. Since the PACS was used for data collection, the patients were not scanned exclusively for this research project. Therefore, ethical approval was sought from the University of Stellenbosch's Health Research Ethics Committee (HREC), the National Health Research Database (NHRD), and the Biomedical Research Ethics Committee (BMREC) of the UWC.

The University of Stellenbosch's HREC approved the research project on 04/09/2020 (Reference no: S20/07/157). The NHRD application of this project was given Reference number: WC_202009_015 and approval by the NHRD was retrieved on 09/03/2021. The BMREC of the UWC also granted ethical approval for this research project since data collection occurred within the OHC's facilities.

The potential risk of loss of confidentiality was acknowledged. Therefore, when patient information was accessed from the PACS for data collection, no identifiable data was accessed and only sex and age were recorded. No other patient information was imported to a desktop or disseminated electronically or in hardcopy. For publication, the patients' identity such as the patients' name will be protected, and only the patient's age and biological sex will be mentioned in publication. Since the research consists of CBCT scans, the patients' faces in the volumetric view of the scan are not recognisable as they lack skin colour and texture (Wilkinson 2010; Smith 2020)

3.3 SCAN SELECTION

Patients selected for this study were all scanned by the same imaging modality (NewTom VGi EVO 3D CBCT Imaging) since it is known for measurement errors to exist between various CT modalities as discussed in the literature (Ismail *et al* 2019; Stull *et al.* 2014).

To select the scans for dentate patients, the diagnoses for these patients assisted with retrieving scans. Many dentate patients were scanned for carious teeth, orthodontic and endodontic treatments, and bone trauma. Edentulous patients were mostly scanned for dental implants or those in the process of the treatment plan for dentures or dental implants.

The scan selection occurred for the patients using an inclusion and exclusion criteria. The selection criteria is seen in Table 7 and Table 8, and further discussed in the rest of this section.

Table 7: Summary for the inclusion and exclusion criteria for edentulous patient scan selection.

Inclusion Criteria	**Exclusion Criteria**
Patients of known age (older than 21 years) (Tuteja *et al.* 2012)	Periodontal diseases (Zmysłowska *et al.* 2007)
Patients of known biological sex (Wilkinson 2004).	Patients with fractured teeth present in the socket
Patients with complete edentulism	The presence of wiring or metal in the jaw
Patients scanned for dental implants during the treatment planning phase for dentures or dental implants.	Fractures, pathologies, or anomalies present on the maxilla, foramen magnum, zygomatic bones, nasal bones, and soft tissue of the mouth
The entire mouth, jaw and soft tissue around the jaw should be present in the scan.	Scans with the chinrest and bite plate distorting the upper lip/mouth
Patients with completely healed/closed alveolar sockets (Shiroma *et al.* 2019).	Patients showing facial expressions

Table 8: Summary for the inclusion and exclusion criteria for dentate patient scan selection

Inclusion Criteria	**Exclusion Criteria**
Patients of known age (older than 21 years).	Periodontal diseases (Zmysłowska *et al.* 2007)
Patients of known biological sex (Wilkinson 2004).	The presence of wiring or metal in the jaw and amalgam tooth fillings.
Complete dentate patients	Fractures, pathologies, traumas, and/or anomalies present on the incisors, canines, maxilla, foramen magnum, zygomatic bones, nasal bones, and soft tissue of the mouth.
Patients scanned for carious teeth, orthodontic and endodontic treatments, trauma on areas of the skull other than the maxilla, foramen magnum, nasal bones, and zygomatic bones.	Absent first and second molars
The entire mouth, jaw and soft tissue around the jaw should be present in the scan.	Edentulous patients
	Scans with the chinrest and bite plate distorting the upper lip/mouth
	Patients showing facial expressions

3.3.1 The condition of the patient's mouth, mandible, and maxilla

Both dentate and edentulous patients had to have no anomalies of the soft tissue of the mouth, hard tissue of the mandible and maxilla, zygomatic bone, foramen magnum, or nasal bones, as these bones were used for anthropometry. In addition, the soft tissue of mandible and maxilla could not be compromised such as the lips and philtrum, as these were the areas for anthropometry.

With the CBCT modality used for this research's scans, the patient was scanned using a "chinrest" and "bite plate" which held the patients head and jaw in position for the scan (Figure 24). The chinrest and bite plate distorted many of the patients' lips, however, in some scans it did not. The morphological anomalies caused by the chinrest and bite plate is further discussed in 3.4.1. Additional anomalies the edentulous and dentate patients could not show included facial expressions, as facial expressions distort the natural pose of the face and mouth which would hinder anthropometry.

If tissue distortions, trauma, or pathologies were present on other parts of the skull and face, the scans were still selected if the anomalies did not influence the aforementioned anatomical structures.

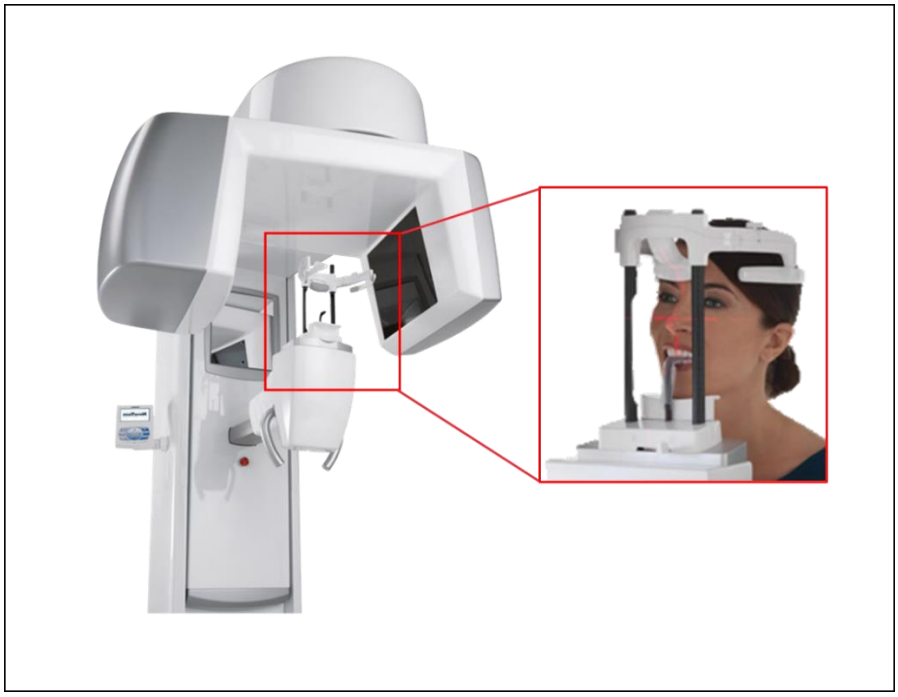

(Adapted from VGi evo EXPANDED.VISION 2021:19)

Figure 28: Demonstrating the use of the bite plate and chinrest in the CBCT scanner.

3.3.2 Dentition

In the dentate patient group, the patient had to have all teeth present and erupted. The edentulous patients were required to have no teeth at all.

3.3.2.1 Dentate patients

Dentate patients had to be older than 21 years of age since this is frequently the age of third-molar eruption. In some individuals, third molar eruption has also been reported to begin at the age of 17, however, this was not met in the research sample (Tuteja, Bahirwani & Balaji 2012; Priyadharshini, Idiculla, Sivapathasundaram, Mohanbabu, Augustine & Patil 2015).

Erupted or unerupted third molars (M3) influence the dimensions of the alveolar ridge (Langley *et al.* 2016). Therefore, it was preferred for the dentate sample to have erupted M3s even if it had been extracted. Patients with extracted M3s may have undergone “wisdom tooth extractions” due to tooth impaction (failed tooth eruption), infection, or other M3 pathologies (Flygare & Öhman 2008). The additional molars, first (M1) and second molars (M2), were also required to be present in the dentate sample. The reason being is that the alveolar process at M2 is frequently at its widest at the buccal surface of the maxilla; this is where the width of the maxillary alveolar ridge was measured (Langley *et al.* 2016).

It was acceptable for the patients to present with caries and tooth fractures on the molars and pre-molars as long as it did not affect the alveolar ridge, since osteometry was mainly performed on the maxillary medial incisors, canines, and alveolar ridge.

3.3.2.2 Edentulous patients

The edentulous group was required to be older than 21 years of age with no evidence of teeth within the alveolar ridge. The edentulous patient's teeth must have been removed completely without impacted tooth remnants and the residual ridge must have undergone healing. If a patient's jaw morphology seemed edentulous, but on further inspection, the patient had some fractured or carious teeth at the root, the patient was then not classified as completely edentulous.

Figure 29 shows an example of teeth that are carious at the root, and Figure 30 shows a fractured tooth. The alveolar ridge of fractured or carious teeth will not undergo RRR in the same way as the residual ridge with empty sockets (Shiroma *et al.* 2019). Depending on where this occurs, it could affect the dimensions of the alveolar ridge.

In Figure 31, the dentate and edentulous maxillary alveolar ridge is seen on an axial slice of a CBCT scan, and the dimensions are clearly different. This is owed to the absence or presence of teeth. An edentulous jaw will undergo RRR which decreases the amount of bone at the level of the maxillary alveolar ridge (Figure 31) (Pagni *et al.* 2012).

(Bhayat & Madiba 2017)

Figure 29: Clinical case showing a child with carious maxillary teeth which include the incisors, canines, premolars and first molars.

(Krastl, Filippi, Zitzmann, Walter & Weiger 2011)

Figure 30: Crown-root fracture of the right lateral incisor.

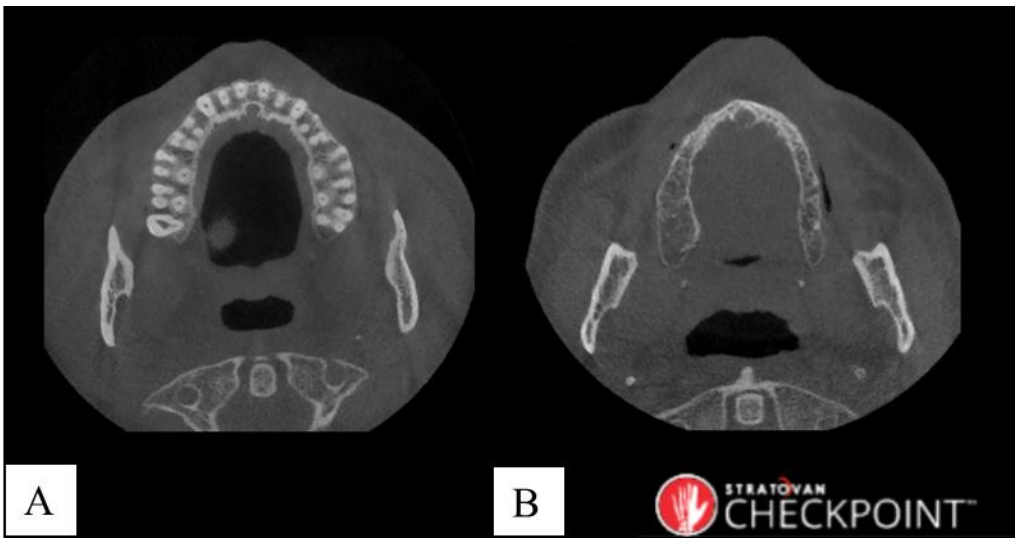

(Stratovan Checkpoint™)

Figure 31: The difference between the dentate (A) and edentulous (B) maxillary alveolar ridge as shown on an axial volume slice of two different patients.

3.3.3 The presence of metal

In both edentulous and dentate groups, the patients could not have any amalgam tooth-fillings, braces, wires or metal present in the mandible or maxilla. This causes streak artefacts in CBCT scans (Baer & Kachelrieß 2012; Baer, Hammer, Knaup, Schmidt, Christoph & Kachelrieß 2012). This artefact prevented a clear view of the alveolar ridge and therefore, landmark placement could not take place in these cases. These artefacts are seen in a volume slice (Figure 32) and a volumetric scan (Figure 33).

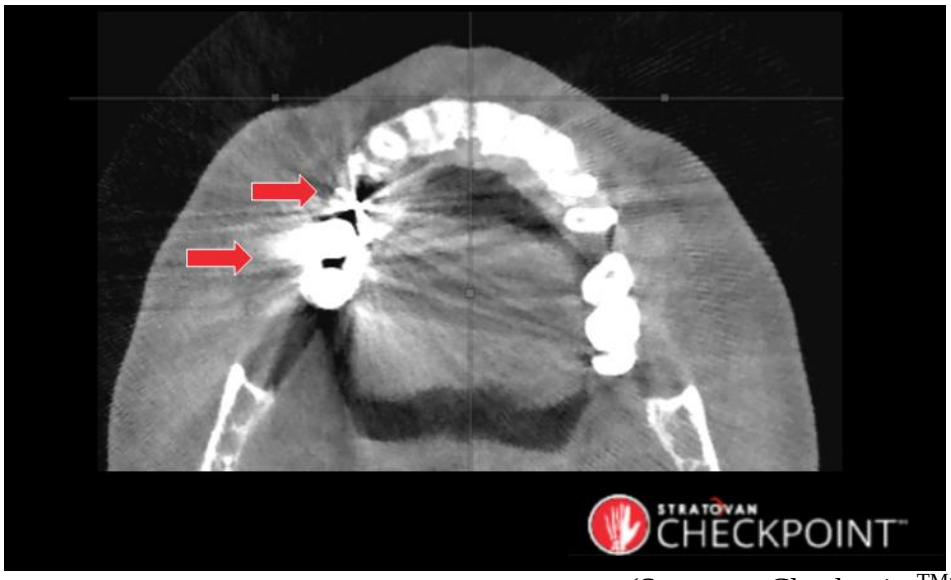

(Startovan Checkpoint™)

Figure 32: Axial scan of CBCT scan to show the artefacts caused by amalgam tooth fillings.

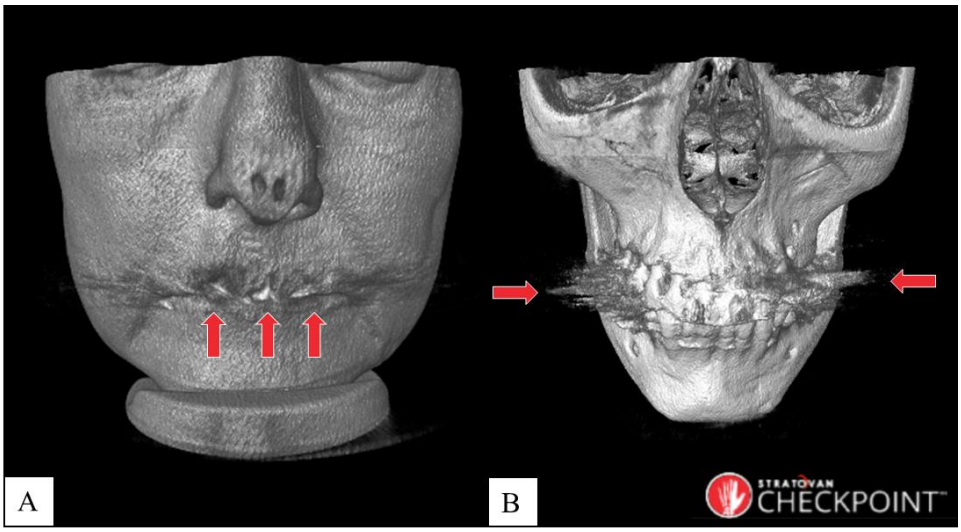

(Stratovan Checkpoint™)

Figure 33: Example of artefacts caused by amalgam tooth fillings as shown on the soft- (A) and hard-tissue (B) of a CBCT scan, indicated by the red arrows.

3.3.4 Total scans analysed and collected

A total of 962 scans were analysed using the inclusion and exclusion criteria seen in tables Table 7 and Table 8. A total of 384 scans matched these selection criteria and after further analysis in Stratovan Checkpoint™, these scans presented with various scan artefacts and patient mouth movements, which is further discussed in 3.4.1. The reason this was not noted in the PACS, was since the patient scans could only be viewed in its CBCT sagittal, axial, or coronal slices (Figure 34), its panorex (radiograph) (Figure 35), or its "scout" (radiograph) (Figure 36) views using IQ-WEB (Nazir., Benamore & Gleeson 2013). To note, the scans in Figure 34 are shown as an example using Stratovan Checkpoint™; in PACS, the scans were in this view using IQ-WEB. Stratovan Checkpoint™ is an integrated software package for geometric morphometrics that enables the investigator to collect, manipulate, and analyse landmarks and semi-landmark points in 3D. Stratovan Checkpoint™ was the chosen software for this research (Kuzminsky & Gardiner 2012). After further analysing the scans using Stratovan Checkpoint™ and using the selection criteria (Table 7 & Table 8), 63 CBCT scans were retrieved that met the selection criteria.

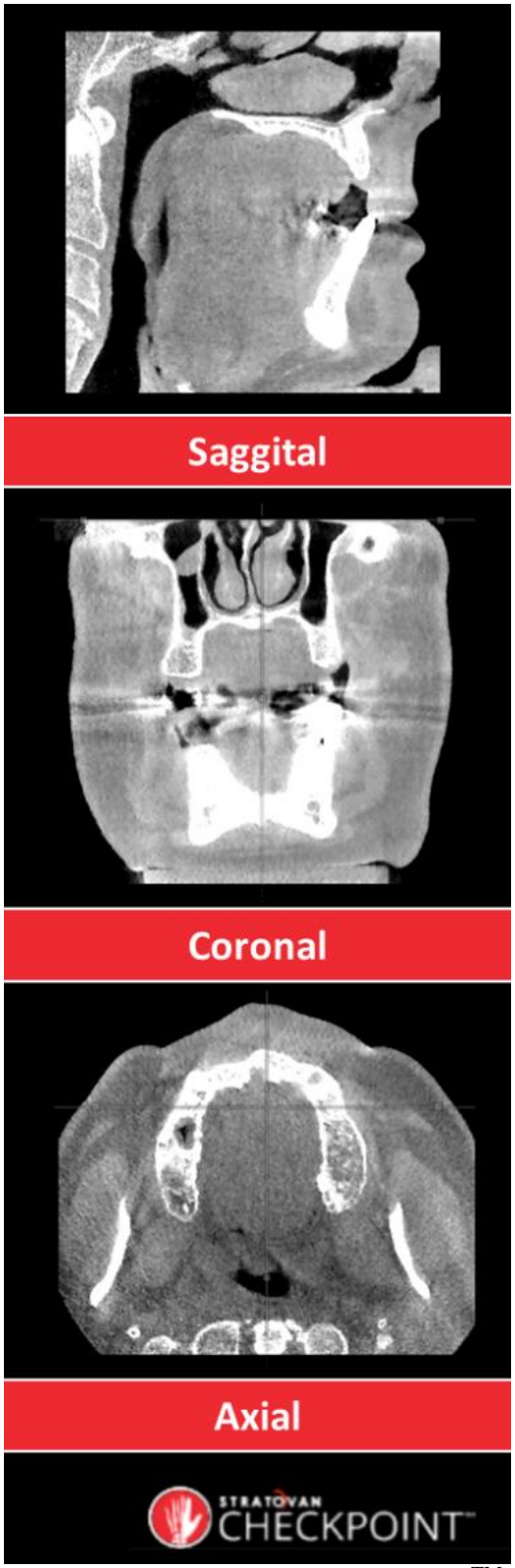

(Stratovan Checkpoint™)

Figure 34: Sagittal, coronal, and axial volume slices of a CBCT scan.

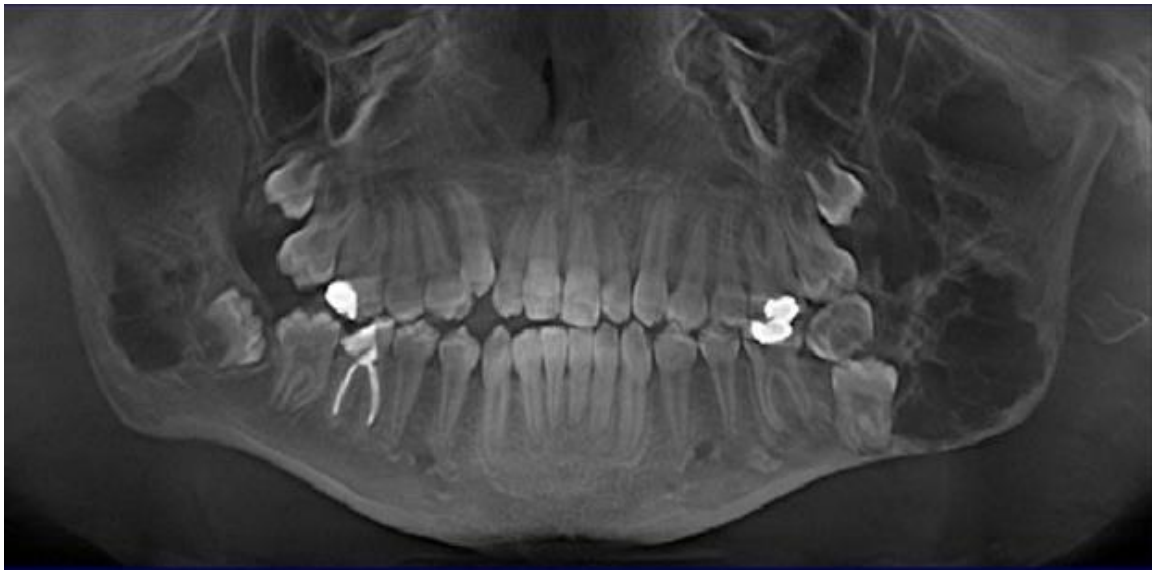

(Kau, Souccar, English, Kamel & Wong 2012)

Figure 35: Projected panorex showing bilateral pathologies in the areas of the ramus of the mandible and the second quadrant of the maxilla.

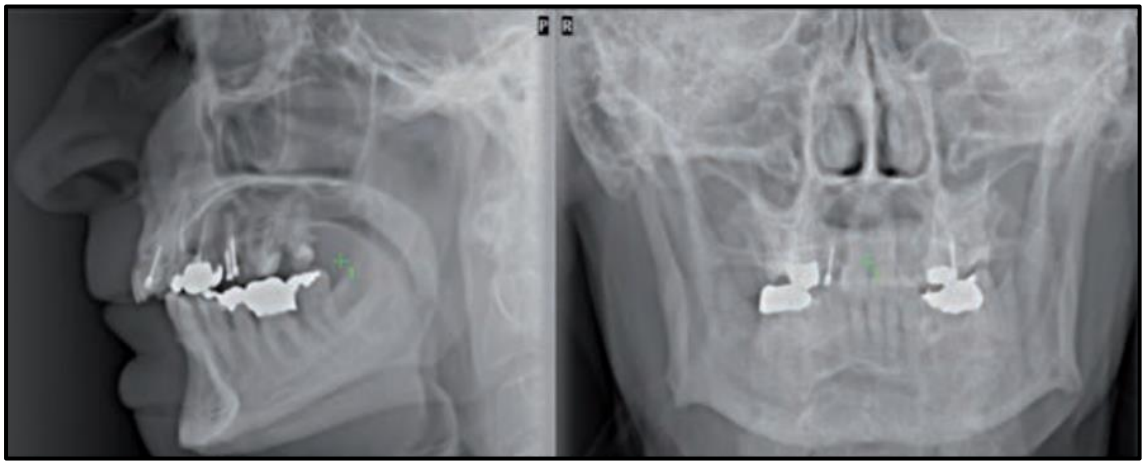

(Pauwels, Jacobs, Bosmans, Schulze 2012)

Figure 36: Lateral and frontal scout images of a CBCT scan.

3.4 LIMITATIONS OF THE STUDY MATERIAL

The sample size was greatly affected for this research since the PACS had a limited number of scans that met the selection criteria set out for this study. The reason for this was since the PACS for the OHC housed CBCT scans of patients for diagnostic purposes and for various dental treatments. Despite these limitations, it was also the only dataset accessible with the ethical approval granted.

3.4.1 Scan artefacts

In PACS, the scans that were performed for diagnostic or treatment planning purposes, the anomaly was usually present on the hard tissue or teeth alone. Therefore, the patient's soft tissue was not required for diagnosis, and the scan's FOV was adjusted to only include the tissue required for diagnosis (Ortega *et al.* 2017). Therefore, some patients were not "fully scanned", and some of the soft tissue was absent. These scans could not be used for anthropometry (Figure 37).

Soft tissue was also distorted in the CBCT scanner, such as with the lips and chin. This is due to the bite plate and chinrest of the scanner (Figure 28 & Figure 38), or due to gauze or cotton placed in the patient's mouth (Figure 39). However, the bite plate did not affect certain patients' upper mouth (Figure 40), and some patients were scanned without a bite plate (Figure 41); these were the scans selected for this research. In some cases, the tissue was distorted due to facial expressions, as seen by the smile and the nasolabial folds being stretched to the back in Figure 42, therefore these patients did not meet the selection criteria.

It was hoped for this study to also investigate anthropometry of the mandible, however, distortions caused by the chinrest compressed soft tissue of the chin. The use of the chinrest is seen in Figure 28, Figure 38, and Figure 42. Therefore, this study does not include research of the mandible and its surrounding tissue.

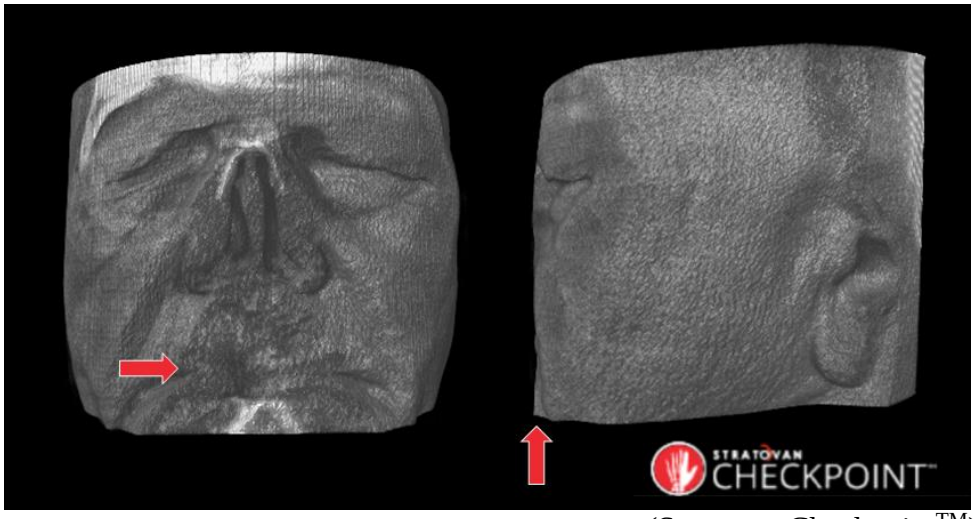

(Stratovan Checkpoint™)

Figure 37: The mouth and nose not included in CBCT scan's field of view indicated by the red arrow.

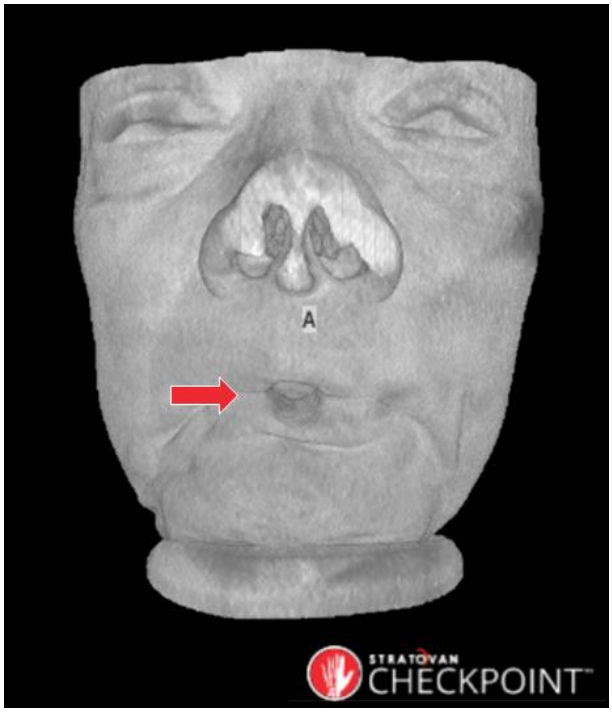

(Stratovan Checkpoint™)

Figure 38: The mouth distortion caused by the CBCT scanner’s bite plate shown by the red arrow.

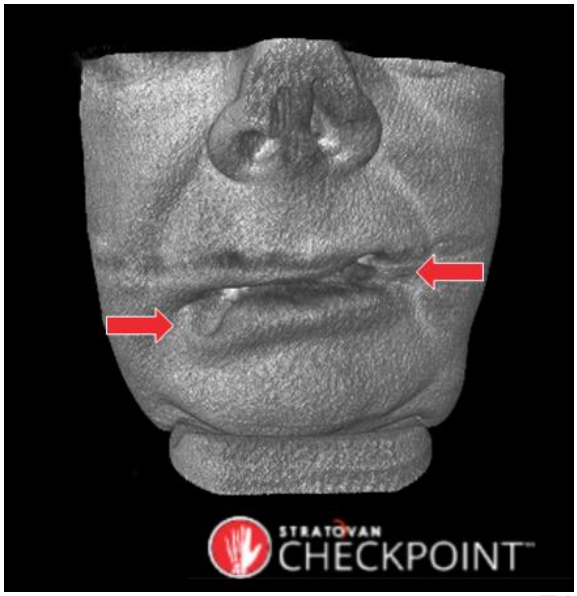

(Stratovan Checkpoint™)

Figure 39: The patient's mouth distorted (red arrows) by the placement of gauze or cotton to separate the patient's cheeks from the residual ridge or teeth to better view the patients mouth in the CBCT for diagnosis.

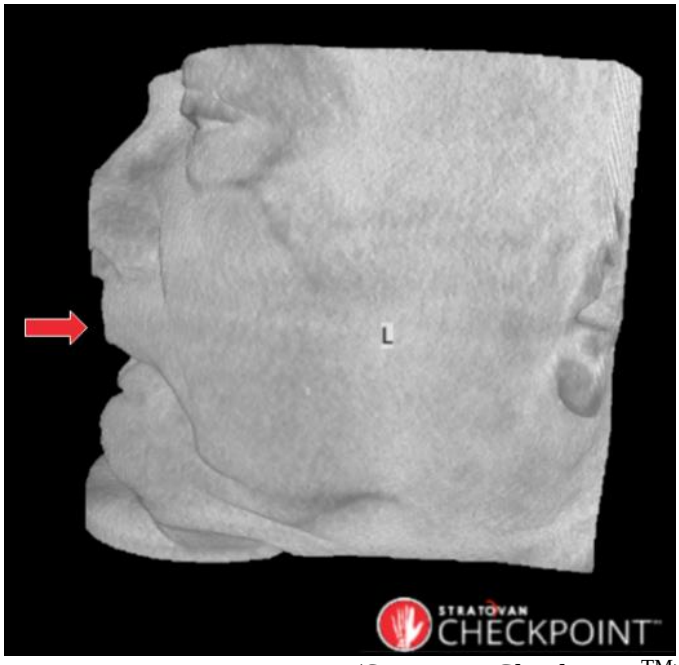

(Startovan Checkpoint™)

Figure 40: Example of an instance where the chin is distorted by chinrest but not the upper mouth (red arrow).

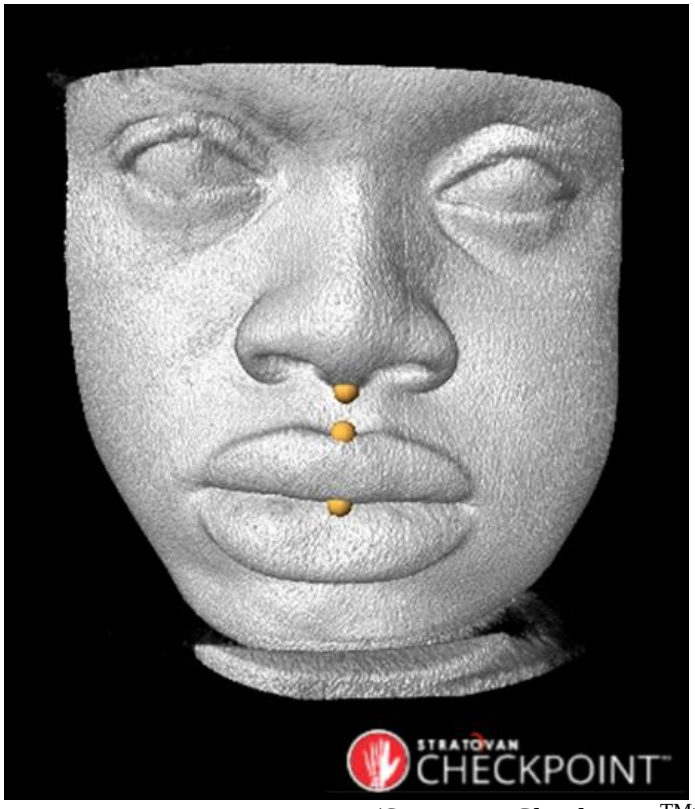

(Stratovan Checkpoint™)

Figure 41: Patient scanned without the bite plate. These were some of the scans included for this research. The orange landmarks seen in the CBCT scan are landmarks placed for geometrics morphometric.

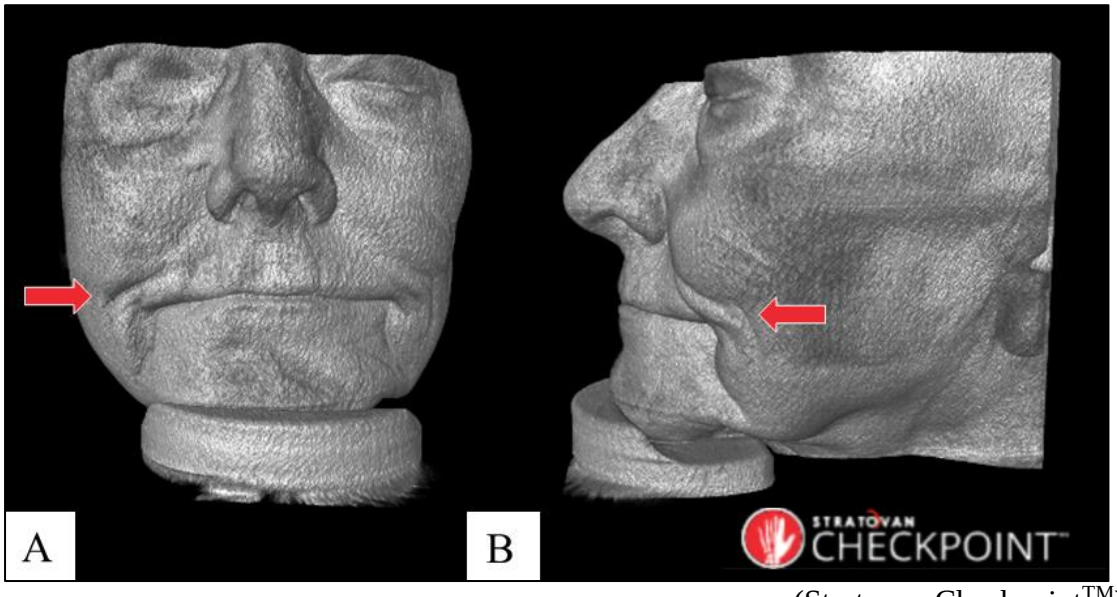

(Startovan Checkpoint™)

Figure 42: A patient that is not in a resting pose noted by the facial expression and pronounced smile lines (red arrow). Anterior view (A) and lateral view (B).

3.4.2 Indices

As mentioned, there were some instances where the entire individual's face and skull partially scanned due to the FOV for diagnostic purposes. For this research, it came as a limitation since certain osteometry could not be performed on various patients. In every patient, the maxilla-alveolar index (MAI) was measured. However, this was not possible for the upper facial index (UFI), gnathic index (GI) and subnasal gnathic index (SGI). If the nasion was not present in the scan as seen in Figure 43, the n-pr could not be measured, meaning the UFI could not be calculated. The same accounts for the SGI since the ba-n could not be measured. Therefore, the sample sizes for each index differ and none of the sample sizes met the powered sample size due to scan artefacts.

(Stratovan Checkpoint™)

Figure 43: Skull isosurface of CBCT scan with an absent frontal bone (red arrow) to demonstrate limited field of view.

3.4.2 Biological sex

Another limit placed on the sample size was the uneven number of males and females present in the PACS. In anthropometry, biological sex plays a significant role in tissue thicknesses where it is known that males present with thicker facial tissue than females, and that male skull dimensions are generally larger than females (Wilkinson *et al.* 2003; Briers *et al.* 2015). Therefore, it was made certain that males and females were analysed separately. However, some CBCT scans did not meet the selection criteria, resulting in an uneven number of males and females in the sample size. For the dentate patient scans, there were more males than females. For edentulous patients, the PACS consisted mostly of females in the treatment phase for dental implants. Therefore, the edentulous patient group had more females than males.

3.4.3 Facial anatomy

The lateral parts of the face, such as with the cheeks, could not be considered for anthropometry in this study, since being overweight could affect the STTs in these areas due to the various facial fat compartments (Figure 44). In an overweight individual, these fat compartments would be more adipose as opposed to an individual with a low body mass (Alghoul & Codner 2013). In this study, the patient's body mass was not made known, and therefore it was not controlled for in this study, and therefore, anthropometry of the lateral parts of face was not performed.

In the field of FA and FFD, a forensic anthropologist cannot always predict from human remains if the individual was overweight or not, where obesity would significantly influence the FFD. Therefore, body mass or the body mass index must be controlled in FFD studies (Wilkinson 2004). Since the bones of the skull cannot establish obesity or cheeks with high adiposity, the forensic anthropologist looks at the bones in the leg as they bear the majority of the bodyweight. It is theorised that in overweight individuals the femurs are more robust and sometimes osteophytes develop on the knee joints and ankle joints (Agostini & Ross 2011). This could give additional information to the FFD practitioner on how to depict the face.

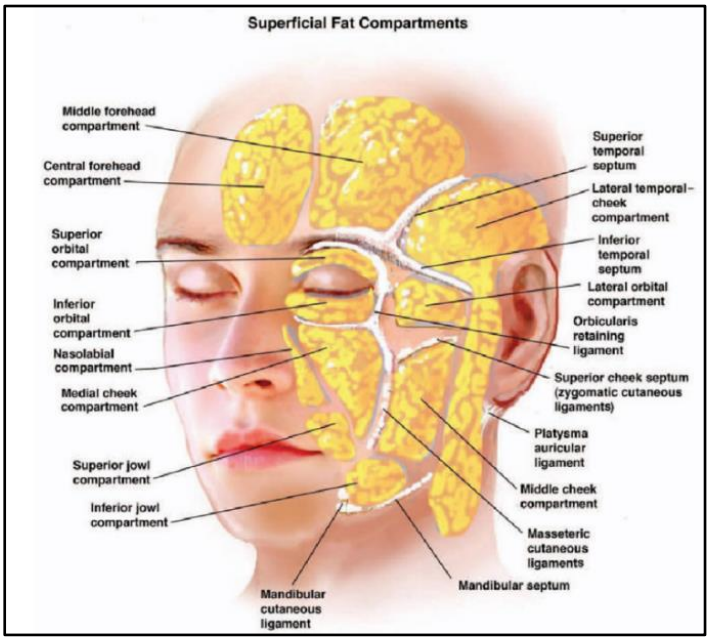

(Alghoul & Codner 2013)

Figure 44: Superficial fat compartments.

3.4.4 Isosurface values

The isosurface is a surface that represents points of a constant value. In this case, it will be bone or soft tissue density, within a volume of space (Botha, Preim, Kaufman, Takahashi, & Ynnerman 2014). To further simplify: to view the skull alone on a CBCT scan, it has its own isosurface threshold value, and the soft tissue has its own isosurface threshold value. Therefore, since bone density varies across the skull and between individuals, different isosurface values had to be used to view the bone in this research. Thus, the patient's bone mineral density (BMD) hindered data collection. It made setting an isosurface value for the skull intricate since the BMD varied between individuals, especially in older patients. Therefore, the isosurface value in Checkpoint™ had to be changed across individuals to expose majority of the skull. It was noted that the default isosurface value of 1000 was not suitable for older patients. This is observed in Figure 45 where both isosurfaces of the patients' skulls are set at an isosurface value of 1000. The patient in Figure 45A was aged 65 years at the time the scan was taken, while the patient in Figure 45B was 23 years of age at the time of the CBCT scan. The difference seen in the skulls is due to the patients' BMDs, since BMD decreases with age (Colón, Molina-Vicenty, Frontera-Rodríguez, García-Ferré, Rivera, Cintrón-Vélez & Frontera-Rodríguez 2018). Therefore, an isosurface value of 1000 cannot expose additional bone if the patient's BMD is relatively low. For older patients, the isosurface value had to be lowered to accommodate anthropometry. However, it proved difficult to do since the isosurface value also caused the tissue to be present around the maxilla. This is due to soft tissue having low isosurface values in Checkpoint™.

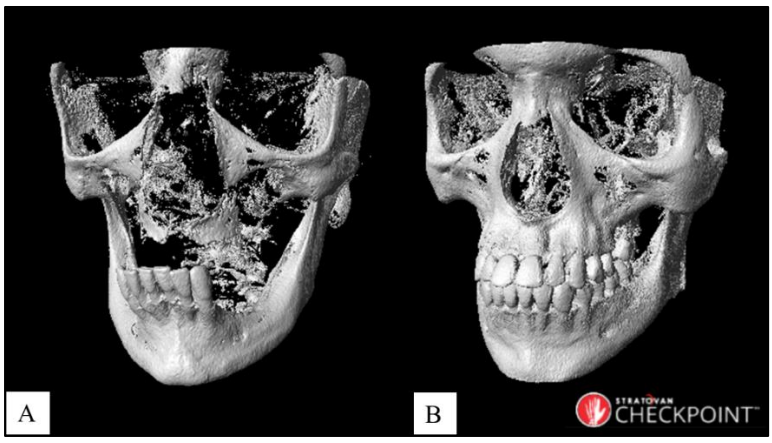

(Stratovan Checkpoint™)

Figure 45: Skull isosurfaces to show how isosurface values are dependent on an individual's age. The isosurface value set for the above scans was 1000. The patient in A was aged 65 at the time of the scan and B was aged 23.

3.5 METHODOLOGY

After the scans were accessed from PACS, the scans were uploaded to the software, Stratovan Checkpoint™. Checkpoint™ was used to perform geometric morphometrics on CBCT scan specimens by placing landmarks on the skull to measure the distance between these landmarks.

3.5.1 Isosurfacing

After opening the scan data with Checkpoint™, the CBCT scans were further assessed in its volumetric view. The volumetric view of the scan provided a 3D perspective of the specimen. Further assessing the scans in Checkpoint™ determined whether the scans met the scan selection criteria set out for this study, since IQ-WEB only allowed to view the specimen in a scout view, panorex, or in a volume slice.

Firstly, the scans were isosurfaced to expose the bone and soft tissue of the patient. This was done by rendering an isosurface using the data histogram to adjust the isosurface value as seen in Figure 46. Checkpoint™ automatically renders an isosurface using the threshold value of 1000 (Figure 46). For older individuals, this was not the appropriate value since older individuals present with a lower bone mineral density (Colón *et al.* 2018). This meant that the appropriate threshold value had to be lowered in order to increase the amount of hard tissue seen on the scan. As an example, in Figure 47, the isosurface value for the hard tissue was 800, and for the soft tissue, it was 250.

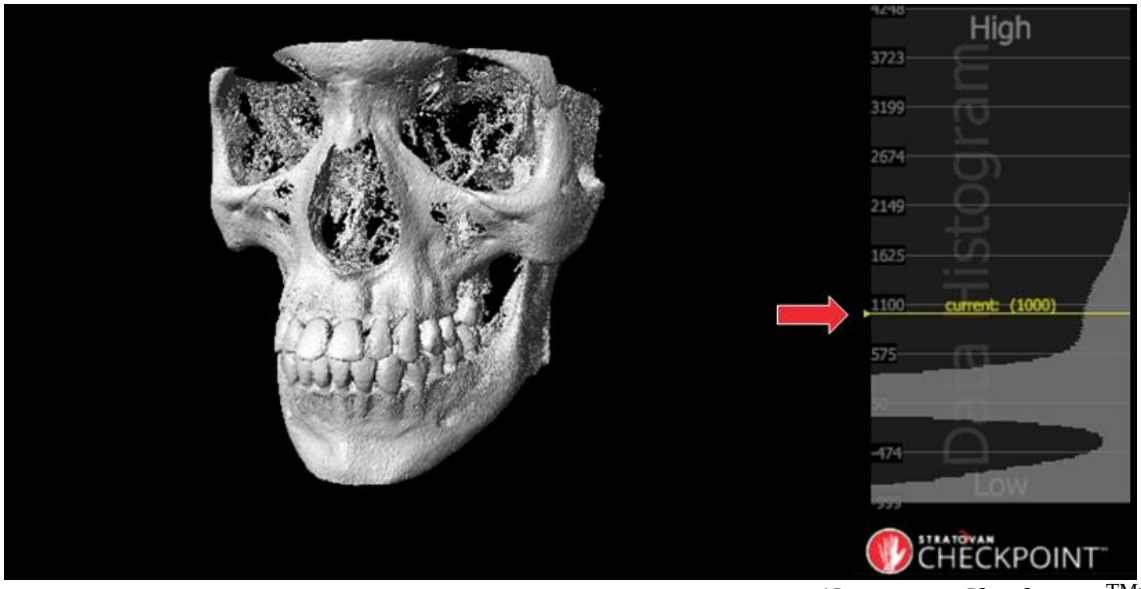

(Stratovan Checkpoint™)

Figure 46: A volumetric view of a CBCT scan to show the data histogram (red arrow) to adjust the isosurface value.

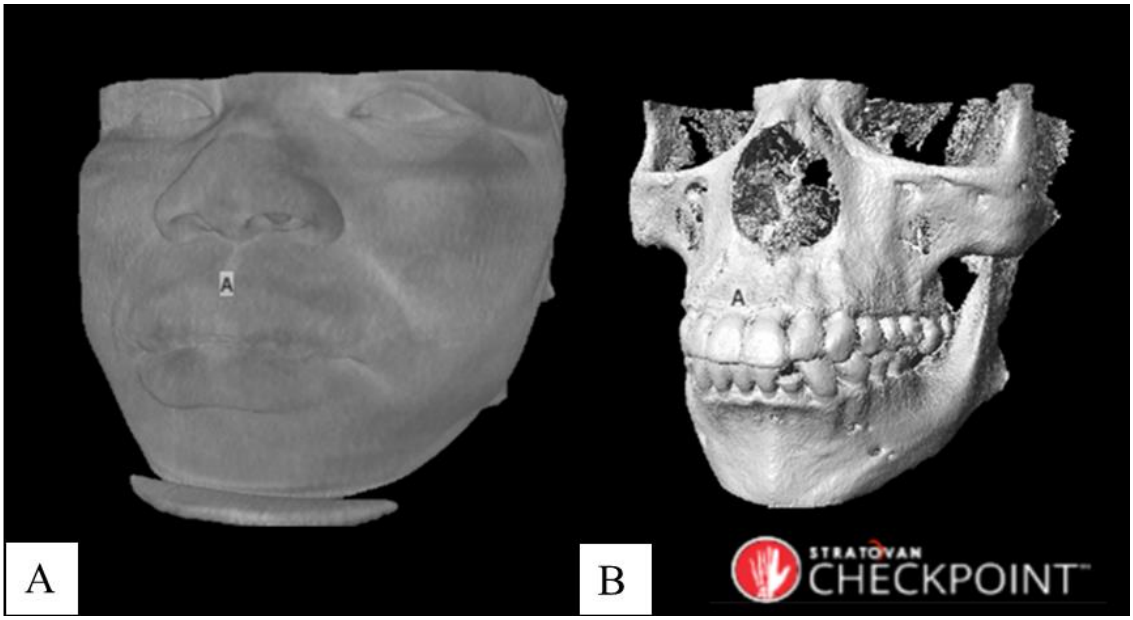

(Stratovan Checkpoint™)

Figure 47: Volumetric CBCT scan of the same patient with their isosurfaced soft tissue (A) and isosurfaced hard tissue (B).

3.5.2 Placing skull landmarks

To place the skull landmarks for osteometry, the isosurface of the skull was produced. These skull landmarks (Table 9) were used to measure the cranial lengths, which were used to calculate the skull indices related to the proportions of the mouth and face. This is further discussed in 3.5.3. Figure 48 to Figure 51 shows how these landmarks were placed on the skull's isosurface.

Table 9: Selected skull landmarks for this research.

Skull landmark	**Definition**
Alveolon (aIv)	The point where the mid-sagittal plane of the palate is intersected by a line connecting the posterior borders of the alveolar crests.
Basion (ba)	The point at which the anterior border of the foramen magnum is intersected by the mid-sagittal plane opposite the nasion.
Ectomolare (ecm)	The most lateral point on the buccal surface of the alveolar margin. This point is generally positioned on the alveolar margin of the second maxillary molar.
Nasion (n)	The point of intersection of the naso-frontal suture and the mid-sagittal plane
Prosthion (pr)	The most anterior point on the alveolar border of the maxilla between the central incisors in the mid-sagittal plane
Zygion (zy)	The most laterally positioned point on the zygomatic arches. The position of zygion is defined from the measurement of bizygomatic breadth

(Langley *et al.* 2016)

3.5.2.1 Nasion, prosthion, and zygion digital skull landmark placement

In Figure 48A the landmarks selected for the upper facial index (UFI) are seen in red. The UFI is used to describe the proportion of the upper face of the skull (Bass 2005). In Figure 48B, the landmarks are seen placed on the isosurfaced skull in Checkpoint™. In Figure 49, the same landmarks are placed on an edentulous skull, demonstrating how the prosthion is placed on the most anterior part of the residual ridge (Langley *et al.* 2016).

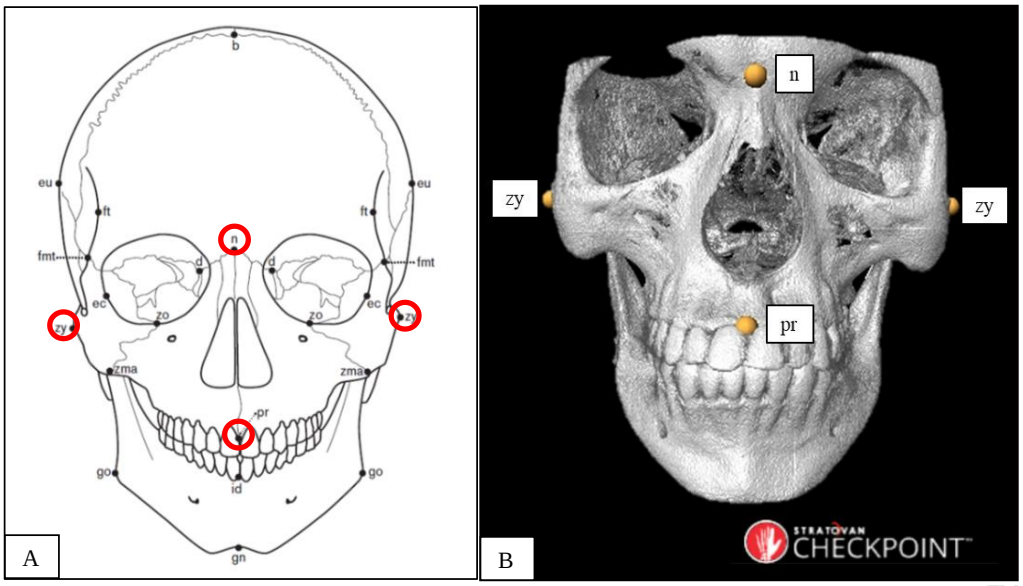

(Langley *et al.* 2016; Stratovan Checkpoint™)

Figure 48: The nasion (n), zygions (zy), and prosthion (pr) landmarks used for the calculation of the UFI shown in A. The placement of these landmarks on the skull isosurface shown in B.

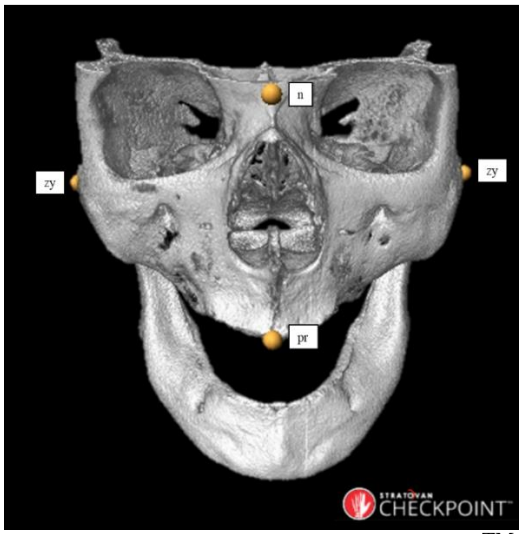

(Stratovan Checkpoint™)

Figure 49: Example of how the nasion (n), zygions (zy), and prosthion (pr) landmarks are placed on an edentulous individual for the UFI measurements.

3.5.2.2 Ectomolare and alveolon digital skull landmark placement

In Figure 50A the skull landmarks for ectomolare (ecm), alveolon (alv) and prosthion (pr) are seen indicated in red. In Figure 50B, the placement of the landmarks is seen on the axial volume slice. The axial slice of the CBCT scan was more convenient to use than the isosurface, since the ecm and alv landmarks could be placed by viewing the entire maxillary alveolar ridge.

Langely *et al.* (2016) mentions placing the alv on the point where the mid-sagittal plane of the palate is intersected by a line connecting the posterior borders of the alveolar crests. This was achieved on the axial scan where the landmark's quadrant lines were used to imitate Langley's method (Figure 50A). The alv landmark was first placed by estimating its position. Using the yellow quadrant line as seen in Figure 50B, the alv landmark was moved until its vertical quadrant line was in the mid sagittal plane. The horizontal quadrant line was then moved until it touched the posterior part of the alveolar crests. When the landmark was in this position, it was accepted as the alv. The ecm was placed on the axial scan as well, ensuring that they were at the most lateral parts of the alveolar bone.

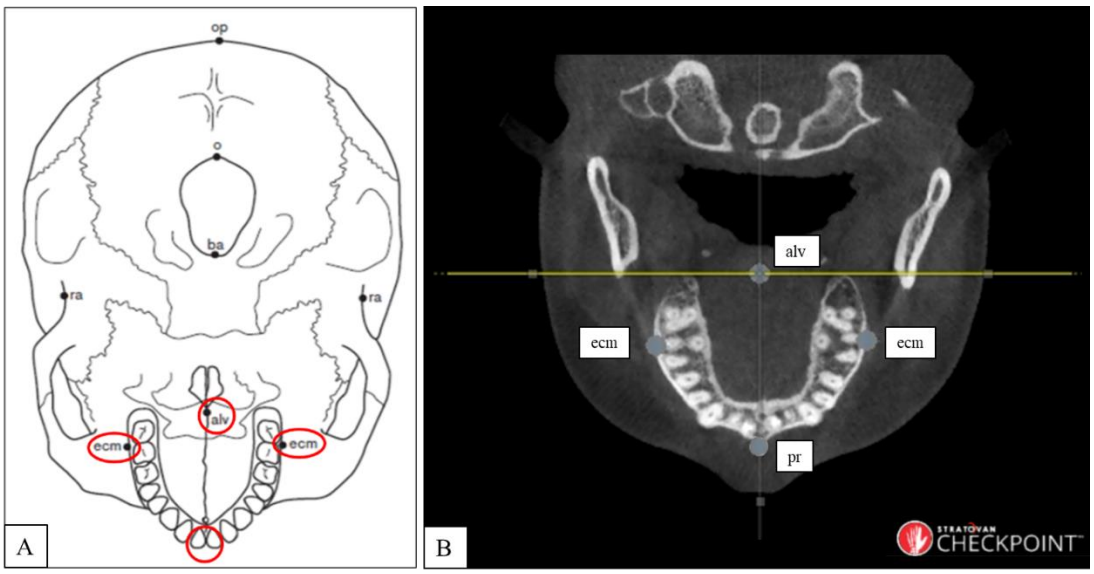

(Langley *et al.* 2016; Stratovan Checkpoint™)

Figure 50: Landmark placement for the ectomolare (ecm), alveolon (alv), and prosthion (pr) using an illustrated example (A) and using the axial volume slice of a CBCT scan at the level of the maxillary alveolar ridge (B).

3.5.2.3 Basion digital skull landmark placement

For the placement of the basion, the isosurface was used as well. In Figure 51A, the illustrated example is shown. In Figure 51B, the isosurface is seen, cropped, indicated in red to view the foramen magnum as it is in Figure 45A.

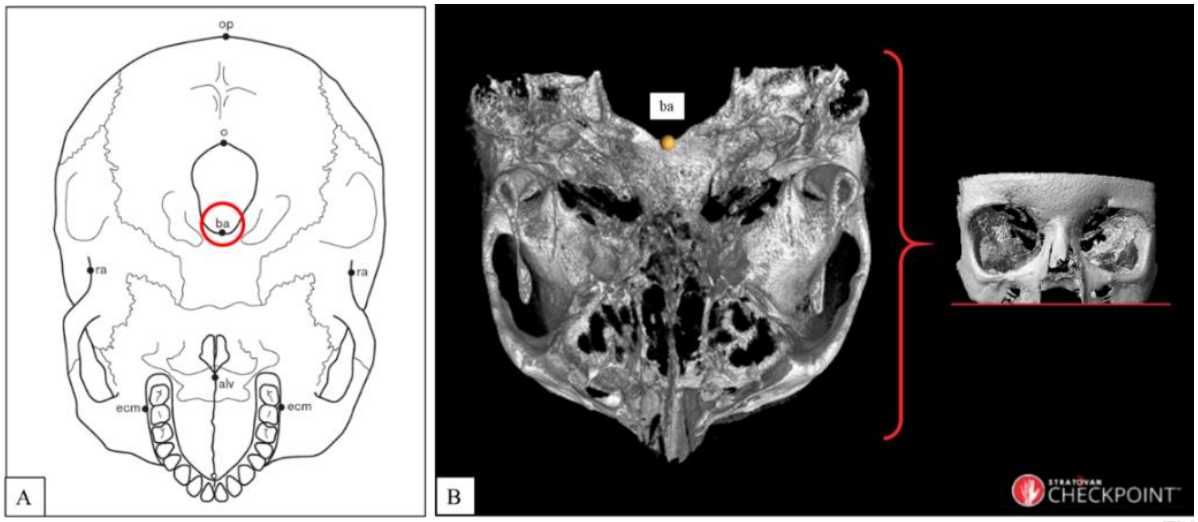

(Langley *et al.* 2016; Stratovan Checkpoint™)

Figure 51: Placement of the basion on the illustrated example (A) and the basion (ba) placed on the base of a cropped skull isosurface (B). In B, the volumetric CBCT scan has been cropped using the cropping tool in Checkpoint™ to view the placement of the ba.

3.5.3 Calculating indices from cranial landmarks

For this study, the proportion of the maxillary alveolar bone, the upper face, the level of prognacy, and subnasal prognacy was calculated. Respectively, these indices are known as the maxillo-alveolar, upper-facial, gnathic, and subnasal gnathic index.

The MAI represents the proportion of the maxillary-alveolar ridge, the UFI represents the proportion of the upper face, and the GI represents how far the maxillary alveolar ridge protrudes past the chin or mentum, and the SGI is a representation of how much the maxillary alveolar ridge protrudes passed the nasion (Liebenberg *et al.* 2015; Lesciotto *et al.* 2016).

After the landmarks were placed on the skull's isosurface, the distance was measured between the landmarks. The distances for the MAI include the maxillo-alveolar breadth (ecm-ecm, MAB) and length (pr-alv, MAL); for the UFI it was the bizygomatic breadth (zy-zy, ZYB) and the nasion-prosthion height (n-pr, NPH); the SGI consisted of the basion-prosthion length (ba-pr, BPL) and the cranial-base length (ba-n, BNL); and the GI consisted of the basion-prosthion (ba-pr) and basion-gnathion length (ba-gn). These cranial lengths are further defined in Table 10.

Table 10: Selected cranial lengths for this research.

Cranial length	**Definition**
Bizygomatic Breadth (zy-zy, ZYB)	The maximum breadth across the zygomatic arches, wherever found, perpendicular to the mid-sagittal plane
Basion-Prosthion Length (ba-pr, BPL)	The distance from basion (ba) to prosthion (pr)
Basion-Gnathion length (ba-gn)	The distance from basion (ba) to gnathion (gn)
Maxillo-Alveolar Breadth (ecm-ecm, MAB)	The maximum breadth across the alveolar borders of the maxilla measured on the lateral surfaces at the location of the second maxillary molars
Maxillo-Alveolar Length (pr-alv, MAL)	The distance from prosthion (pr) to alveolon (alv)
Nasion-Prosthion Height (n-pr, NPH)	The distance from nasion (n) to prosthion (pr)
Cranial Base Length (ba-n, BNL)	The distance from nasion (n) to basion (ba)

(Langley *et al.* 2016)

3.5.3.1 Calculating the maxillo-alveolar index using the maxilla-alveolar breadth and length

To calculate the MAI, the ecm-ecm and pr-alv was measured. The pr was determined using the method discussed in 3.5.2.2. Both the pr-alv and ecm-ecm was measured using the axial scan as well.

After selecting the respective landmarks, Checkpoint™ produces the length between landmarks. These measurements are seen in Figure 52. In Figure 52A the scan is volume rendered to give a transparent view of the hard tissue. Volume rendering allows the visualisation of specific tissue in a scan and does not use isosurface values. In Figure 52B, the lengths have been measured by Checkpoint™ in micrometres. These lengths were placed in Equation 2 to calculate the MAI.

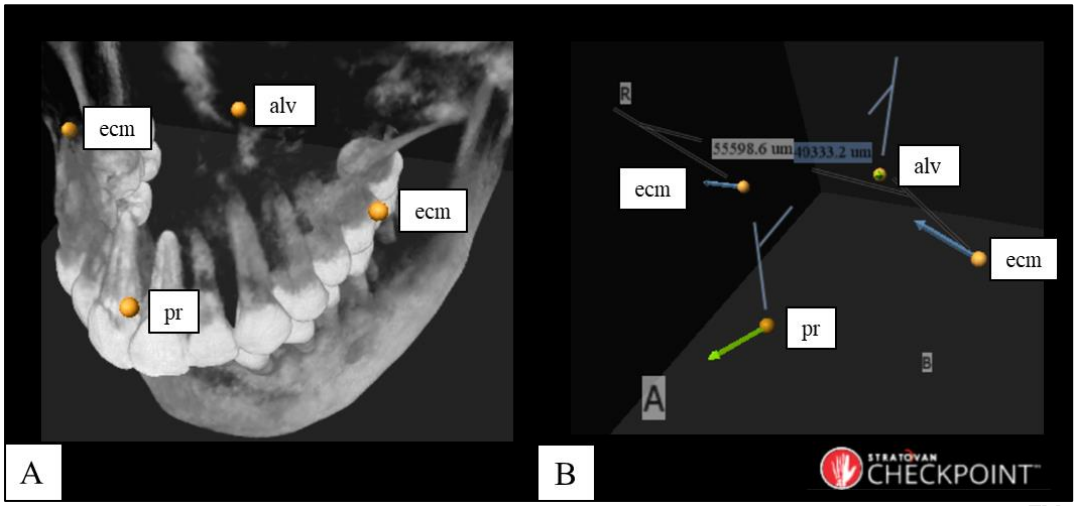

(Stratovan Checkpoint™)

Figure 52: Using the landmarks ectomolare (ecm), prosthion (pr), and alveolon (alv) to measure the maxillo-alveolar breadth (ecm-ecm) and maxilla-alveolar length (pr-alv) to calculate the MAI. Both A and B are of the same patient. In A, the landmarks are seen in a volume rendered scan to view how the landmarks were placed on the maxillary alveolar ridge; and after the landmarks were selected, using GM, the lengths were measured and isolated as seen in B.

$$MAI = \frac{\text{ecm} - \text{ecm}}{\text{pr} - \text{alv}} \times 100$$

(de Villiers 1979; Bass 2005; Liebenberg *et al.* 2015)

Equation 2: Calculating the maxillo-alveolar index using the maxilla-alveolar breadth (ecm-ecm) and maxilla-alveolar length (pr-alv).

3.5.3.2 Calculating the upper facial index using the bizygomatic breadth and nasion-prosthion height

To calculate the UFI, the n-pr and zy-zy were required. For these lengths, the landmarks were placed on the skull's isosurface seen in Figure 53. The respective landmarks were selected to calculate the lengths in millimetres required for the UFI using Checkpoint™. In Figure 53B the lengths are seen with the isosurface and without it. The lengths are seen in red as zy-zy = 126,4 mm, and n-pr = 60,4 mm. These measurements were placed in Equation 3.

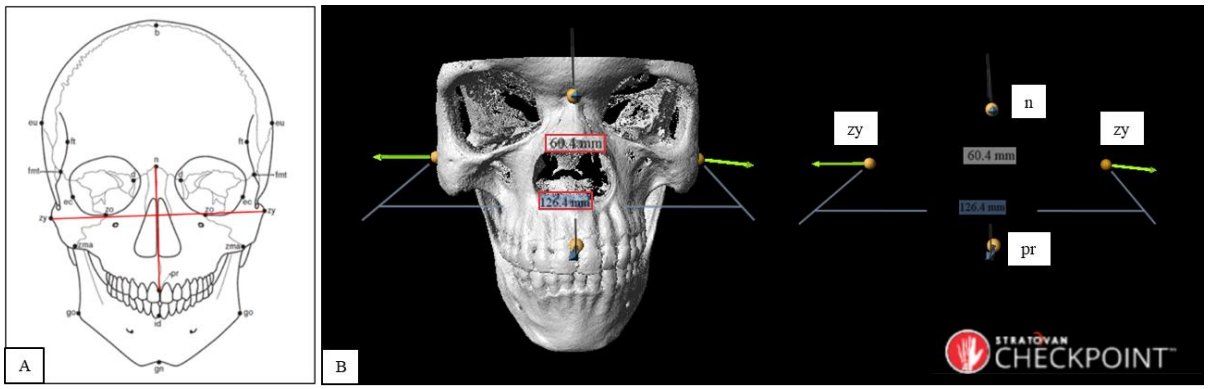

(Langley *et al.* 2016; Stratovan Checkpoint™)

Figure 53: Measuring the cranial lengths on an illustrated example (A) and on a CBCT scan (B) using the zygions (zy), nasion (n), and prosthion (pr). In B the isosurfaced skull and cranial lengths are isolated as the bizygomatic breadth (zy-zy) (126,4 mm) and the nasion-prosthion height (n-pr) (60,4 mm).

$$UFI = \frac{\mathrm{n} - \mathrm{pr}}{\mathrm{zy} - \mathrm{zy}} \times 100$$

(de Villiers 1979; Bass 2005; Liebenberg *et al.* 2015)

Equation 3: Calculating the upper-facial index using the nasion-prosthion height (n-pr) and bizygomatic length (zy-zy).

3.5.3.3 Calculating the subnasal Gnathic Index using the cranial base length and basion-prosthion length

To calculate the SGI, the ba-n and ba-pr were required. In Checkpoint™ the landmarks were selected (Figure 54A) using the example set out by Lesciotto *et al.* (2016), and measured as shown on the isosurface (Figure 54B). After the measurements were performed, the SGI was calculated using Equation 4. The corresponding SGI values are seen in Table 11. An SGI of more than 103 would indicate prognathism, an SGI between 98 and 102.9 indicates mesognathism, and an SGI less than 97.9 would show orthoganism (Lesciotto *et al.* 2016).

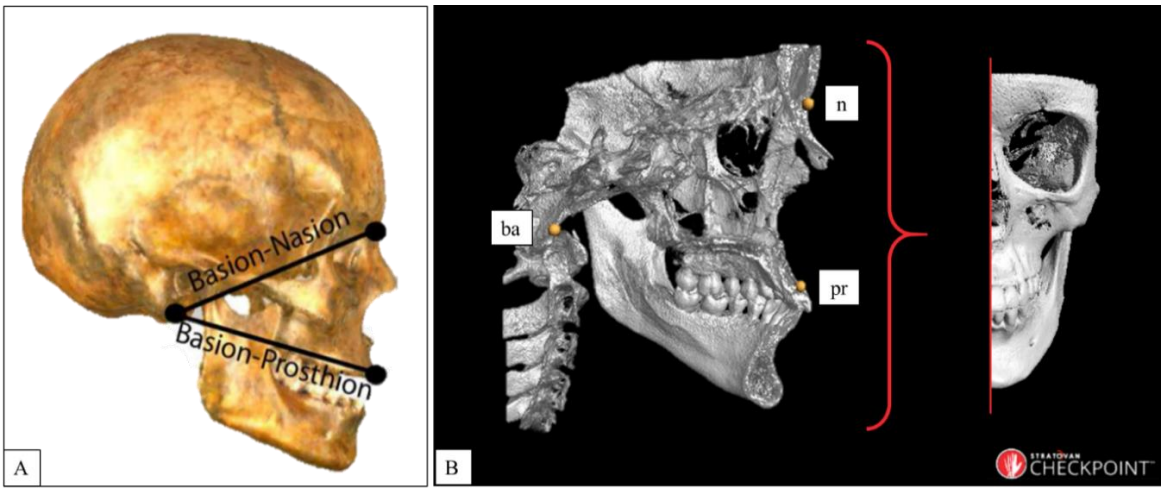

(Lesciotto *et al.* 2016; Stratovan Checkpoint™)

Figure 54: Selecting landmarks to measure the cranial base length (ba-n) and the basion-prosthion length (ba-pr) seen in example A and on CBCT scan (B). In B, the skull has been cropped, using the cropping tool in Checkpoint™ to better view the placement of the nasion (n), prosthion (pr), and basion (ba).

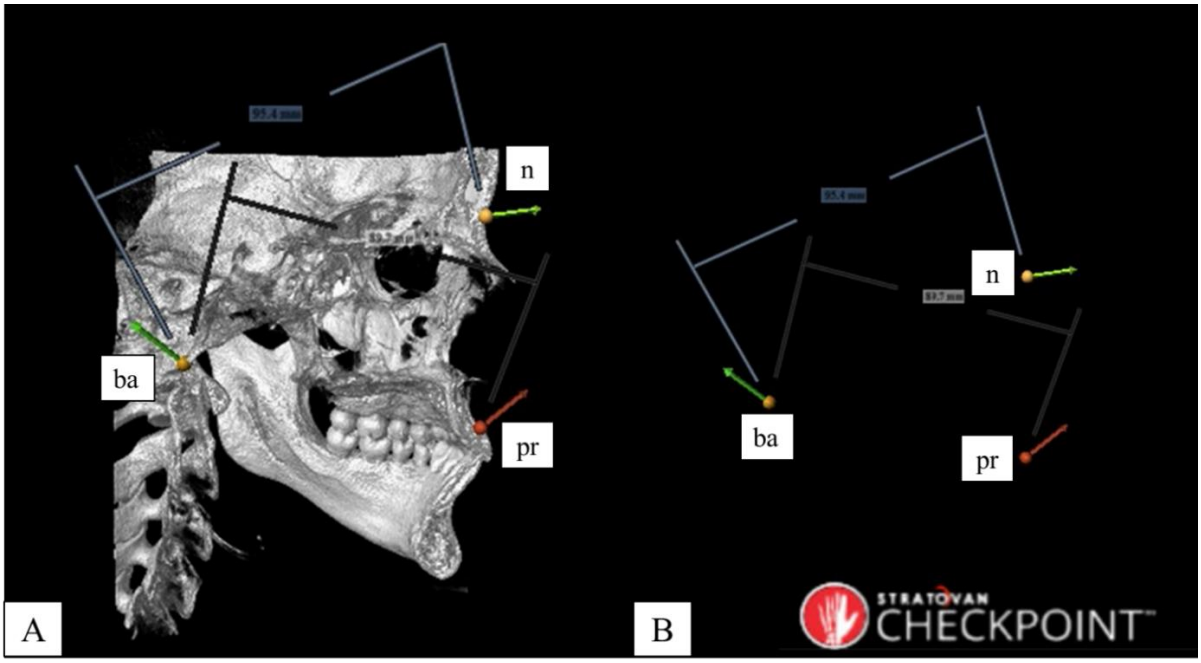

(Stratovan Checkpoint™)

Figure 55: Measuring the cranial base length (ba-n) and basion-prosthion length (ba-pr) on isosurface (A) and shown with the cranial lengths isolated with the landmarks nasion (n), basion (ba), and nasion (n).

$$SGI = \frac{\text{ba} - \text{pr}}{\text{ba} - \text{n}} \times 100$$

(de Villiers 1979; Bass 205; Lesciotto *et al.* 2016)

Equation 4: Calculating the SGI using the basion-prosthion length (ba-pr) and cranial base length (ba-n).

Table 11: Level of prognacy according to gnathic index.

Level of prognacy	**Subnasal gnathic index**
Prognathic (projecting)	>103.0
Mesognathic (medium)	98.0-102.9
Orthognathic (flat)	<97.9

(Liebenberg *et al.* 2015; Lesciotto *et al.* 2016)

3.5.3.4 Calculating the gnathic index

To calculate the GI, the ba-pr and ba-gn were measured. These landmarks and lengths are seen in Figure 56 and the calculation is shown in Equation 5.

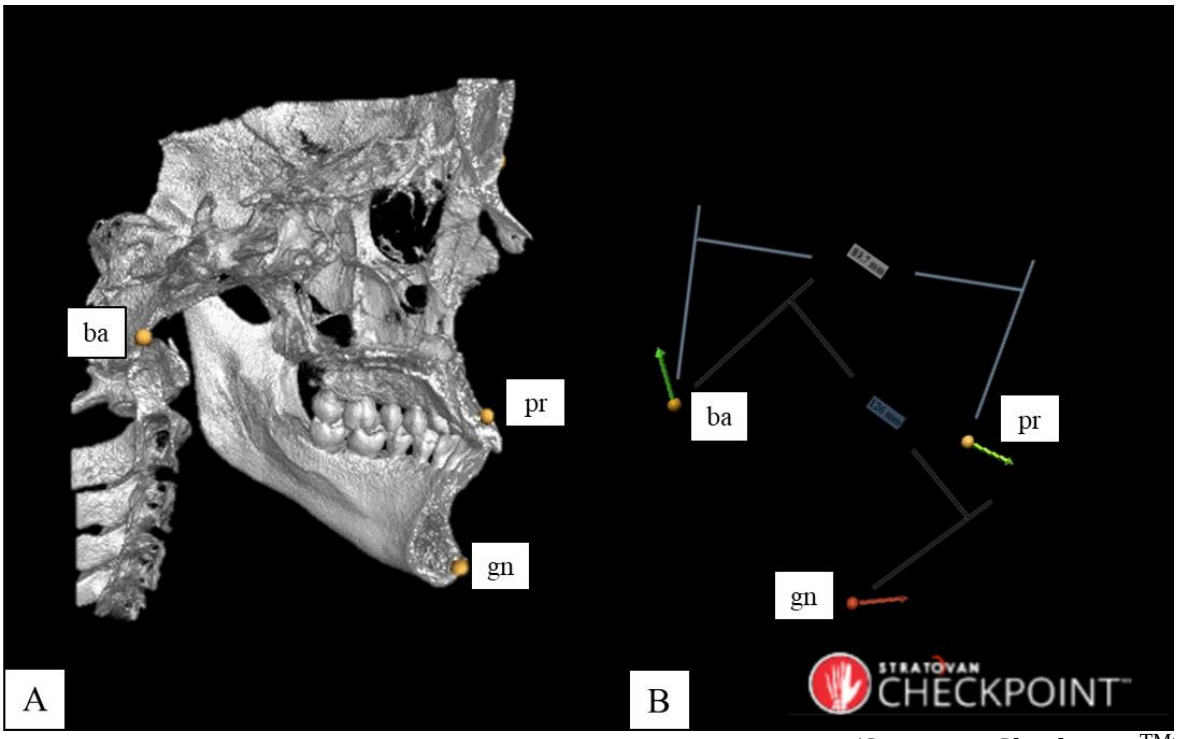

(Stratovan Checkpoint™)

Figure 56: Volumetric scan showing the placement of the basion (ba), prosthion (pr), and gnathion (gn) landmarks (A), and how the cranial base length (ba-n) and basion-gnathion (ba-gn) length was measured (B).

$$GI = \frac{\text{ba} - \text{pr}}{\text{ba} - \text{gn}} \times 100$$

(de Villiers 1979; Bass 2005; Liebenberg *et al.* 2015)

Equation 5: Calculating the GI using the basion-gnathion length (ba-gn) and basion-prosthion length (ba-pr).

3.5.4 Somatometry

An isosurface was not produced for the soft tissue since distances cannot be measured between isosurfaces using Checkpoint™. To measure the distances between skull and tissue, the volume slices (axial, cranial, and sagittal) (Figure 34) were used to place the landmarks.

3.5.4.1 Selected soft-tissue and tissue depth landmarks for this research

The soft tissue depths of the upper mouth were measured using the following tissue depths: Midphiltrum (H), mid-upper lip margin (I), upper-incisor (II), and supracanine (F) shown in, Figure 57, Figure 58, and Table 12. For II and F, both the right and left were analysed separately and denoted by the superscript “R” for right, and “L” for left. In Figure 58, only the H and I were selected on the edentulous skull since the other tissue depths require the teeth to be identified.

Furthermore, the philtrum length (PL) and lip height (LH) were measured in the midsagittal plane to gain further understanding of the mouth dimensions. The PL was measured between the columella and cupid’s bow, and the LH was measured between the cupid’s bow and oral fissure (Figure 59 & Figure 60). In some edentulous patients, the lips were not as visible, however, measurements were still performed as seen in Figure 61. It was ensured that the oral fissure landmark was not placed inside the mouth of edentulous patients, since most of the lip moves into the mouth, changing the original position of the oral fissure. The oral fissure remains outside the mouth as seen in Figure 61.

Due to the chinrest distorting the chin during a CBCT scan, all somatometry measured are of the upper mouth as the upper mouth showed a lower tendency to be influenced by the movement of the chin (Figure 40). However, if it was clearly seen that the upper lip was distorted, the scan was excluded from the study.

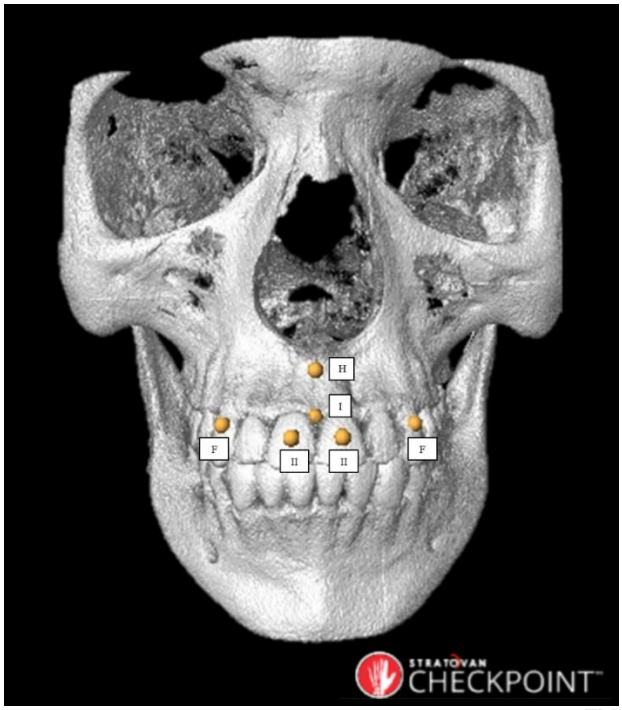

(Stratovan Checkpoint™)

Figure 57: Selected tissue depth landmarks of a dentate skull for this research as displayed on a CBCT scan. The landmarks include the midphiltrum (H), mid-upper lip margin (I), upper-incisor (II), and the supracanine (F).

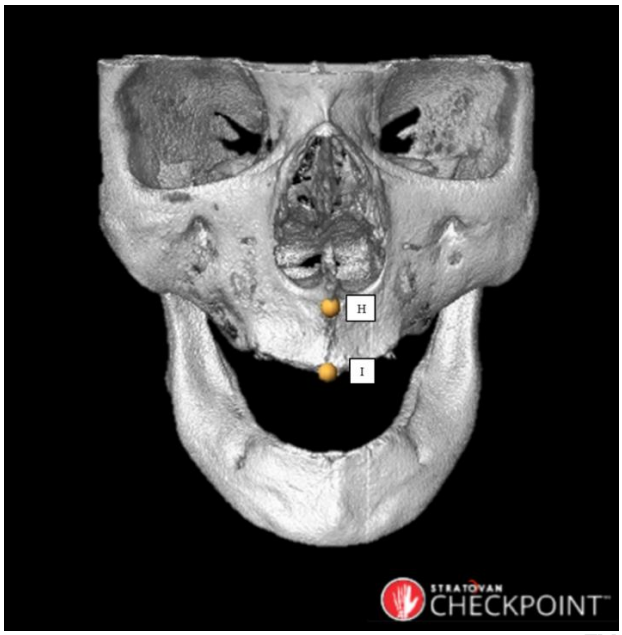

(Stratovan Checkpoint™)

Figure 58: Selected tissue depth landmarks of an edentulous skull for this research as displayed on a CBCT scan. The landmarks include the mid-philtrum (H) and mid-upper lip margin (I).

Table 12: Landmarks on the skull for tissue depth placement to be used in the proposed study further defined in Figure 20.

Landmark:		**Definition:**
F*	Lateral supra-labiale (supra canine)	A point on the maximum bulge of the maxillary/upper canine eminence
H	Mid-philtrum	Midline of the maxilla placed as high as possible before the curvature of the anterior nasal spine.
I	Mid upper lip margin	Centered between the maxillary (upper) central incisors at the level of the cementum–enamel junction
II*	Upper incisor	Halfway down the height of the enamel of the upper central incisors
PL	Philtrum length	Measured from the uppermost part of the philtrum to the cupids bow
LH	Lip height	Measured from cupids bow to oral fissure or the lowest margin of upper lip

(Wilkinson 2004; Iscan & Steyn 2013)

*Only to be measured on dentate patients.

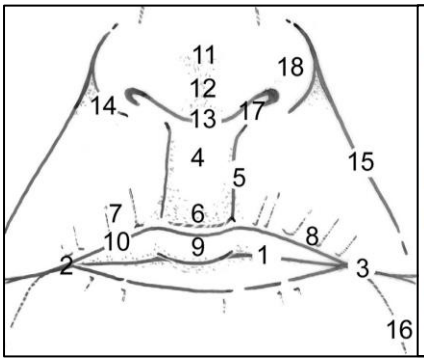

1	oral fissure	10	vermilion border
2	chelion point/corner of mouth	11	nasal tip
3	commissure crease	12	nose tip groove
4	philtrum	13	columella
5	philtral column	14	alar crease
6	cupid's bow	15	nasolabial crease
7	circumoral site/rhytides	16	marionette line
8	white roll	17	nostril
9	lip tubercle	18	ala/wing of nose

(Wilkinson 2004)

Figure 59: Soft-tissue landmarks in the area of the nose and mouth.

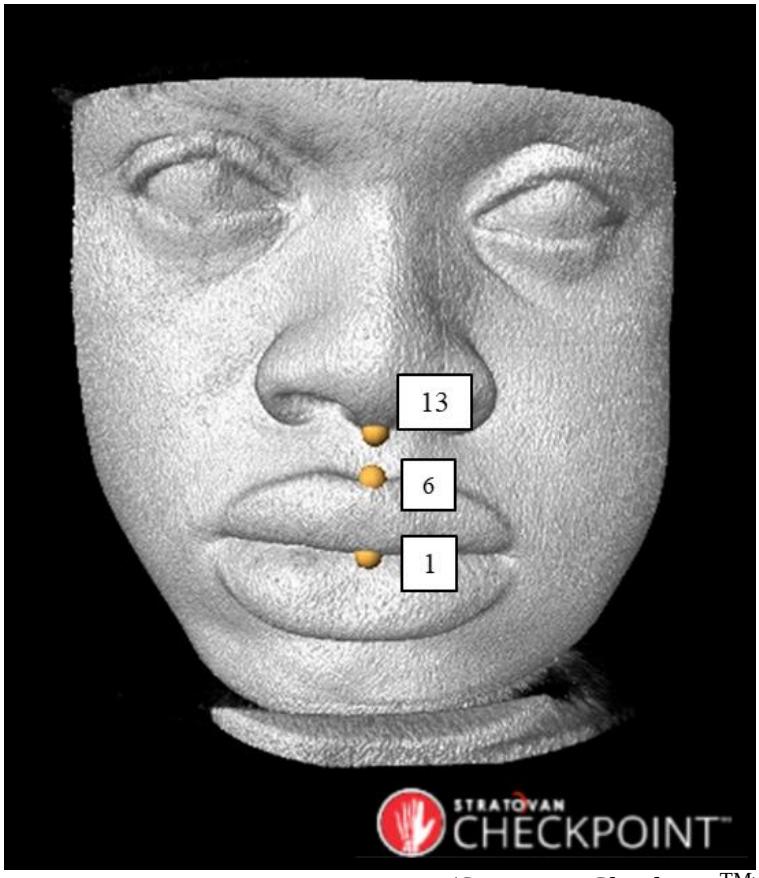

(Stratovan Checkoint™)

Figure 60: Soft-tissue landmarks selected for this research. With reference to Figure 59: 13-columella, 6 - cupid's bow, 1 - oral fissure.

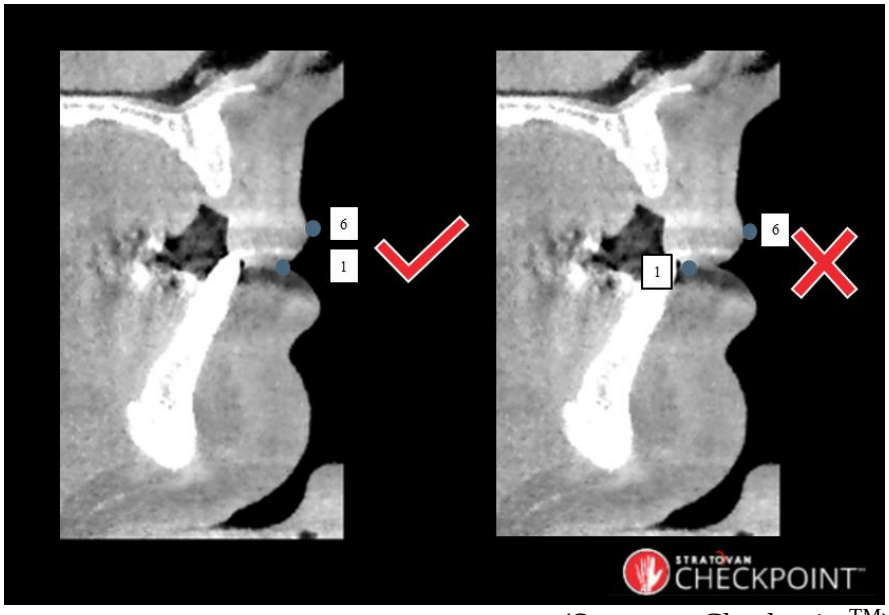

(Stratovan Checkpoint™)

Figure 61: Demonstrating the correct placement of: 1 - oral fissure and 6 - cupid's bow.

3.5.4.2 Perpendicular landmark placement for tissue depths.

It should be noted that each tissue depth was measured perpendicularly to the skull as suggested by Cavanagh & Steyn (2011) where Checkpoint's™ landmarks ensure this. In Figure 62, note the yellow landmark with its vector (blue arrow) pointing in a perpendicular direction of the surface it has been placed on, or as Checkpoint™ mentions, the arrow points in the "normal".

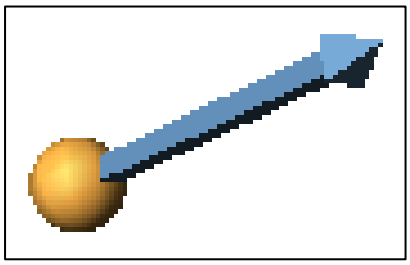

(Stratovan Checkpoint™)

Figure 62: Single point with normal vector in Checkpoint™.

When using Stratovan Checkpoint™, two landmarks were placed to measure the tissue depth. The first marker is placed on the skull at the respective tissue depth point (Figure 63A). This landmark's vector pointed in the direction that the second landmark will be placed (Figure 63B & Figure 64). The second landmark was then placed on the soft tissue in the direction of the first landmark's vector (Figure 64). To place the landmark on the soft tissue, the tissue was volume rendered in order to view it on the isosurfaced skull. Volume rendering allows the visualisation of certain tissue in a scan and Figure 65 shows how the skull has been isolated in volume rendering (Figure 65A), and how the tissue gets rendered until all the soft tissue is seen (Figure 65B to D). Since landmarks cannot be placed on a volume-rendered surface, the second landmark was placed on the tissue using the volume slices (Figure 34). If the soft tissue landmark was not in line with the skull landmark's normal, the soft tissue landmark was moved on the volume slices. To ensure that the soft tissue landmark was placed perpendicularly, a transparent version or volume slice of the volumetric scan was produced to superimpose the soft- and hard tissues (Figure 66).

The PL and LH uses the columella, cupid's bow, and oral fissure to measure these mouth dimensions. In this study, these landmarks were placed in the mid-sagittal plane. The PL and LH were measured to understand its relationship to the SGI, since prognathism influences the morphology of the mouth significantly. The landmarks were placed on the soft tissue alone and ,therefore, a soft tissue isosurface could be generated as seen in Figure 67A. Hereafter, the PL and LH were measured (Figure 67B).

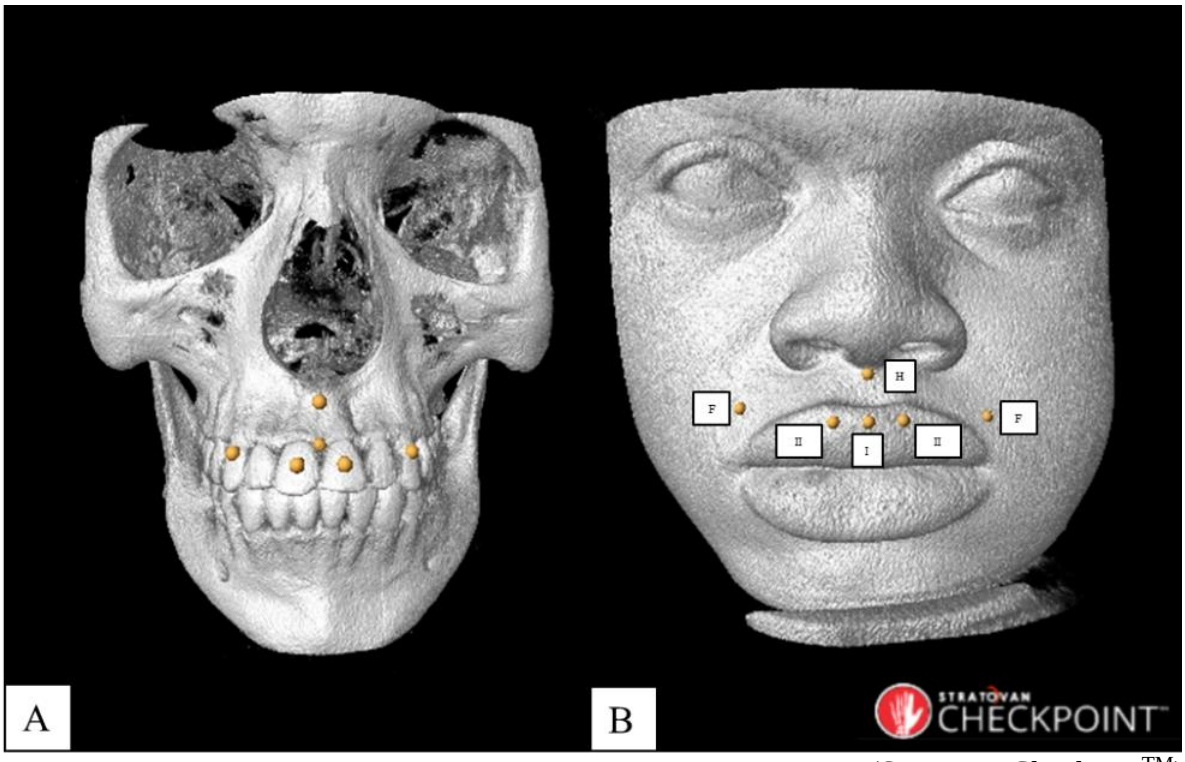

(Stratovan Checkoint^{TM})

Figure 63: Tissue depth landmarks placed on the skull and soft tissue of a CBCT scan to measure the soft tissue depths between the skull and soft tissue. The landmarks are shown as the midphiltrum (H), mid-upper lip margin (I), upper-incisor (II), and the supracanine (F).

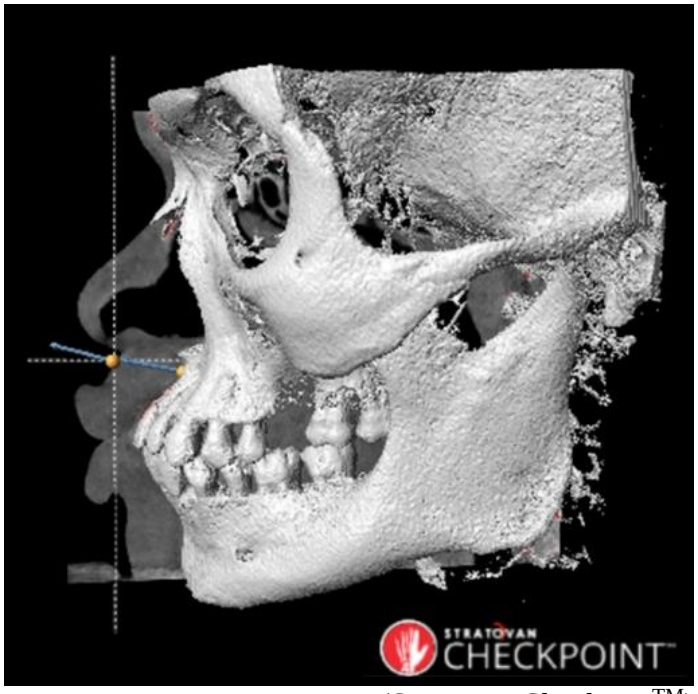

(Stratovan Checkoint™)

Figure 64: CBCT scan shown with its isosurface and superimposed sagittal slice to show the perpendicular placement of landmarks.It can be seen that the landmark's normal on the hard tissue points in the direction of the landmark of the soft tissue.

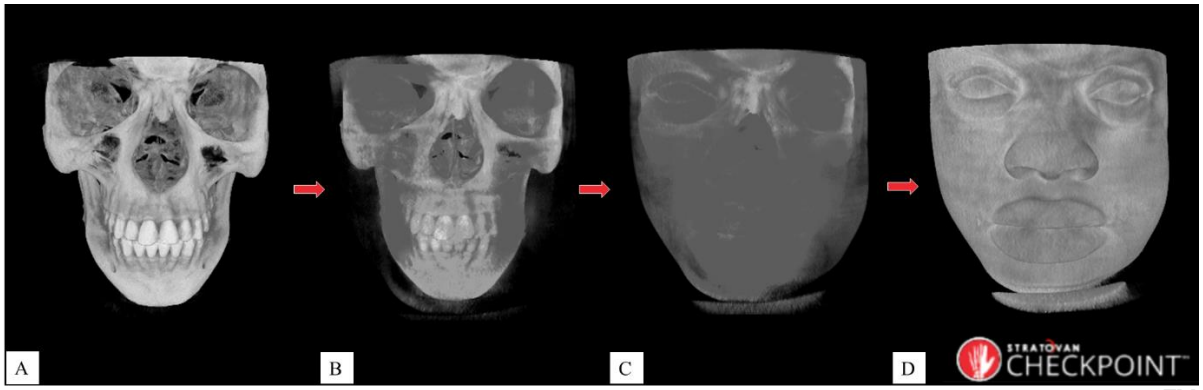

(Stratovan Checkoint™)

Figure 65: A volumetric CBCT scan demonstrating volume rendering of the skull by adding its soft tissue. In A, the patient's skull is volume rendered to its hard tissue only, in B to C, the soft tissue of the patient is volume rendered until all of the soft tissue is present as seen in D.

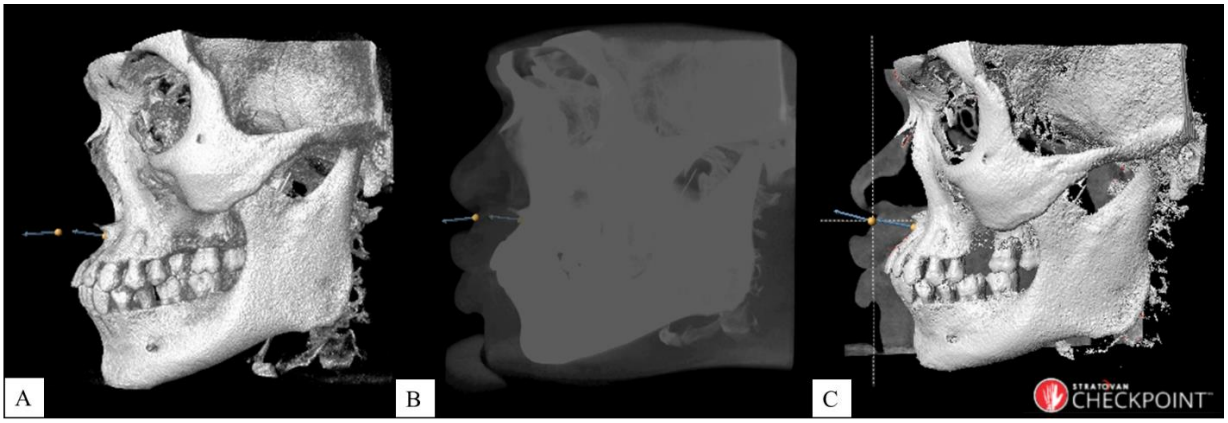

(Stratovan Checkoint™)

Figure 66: The various ways of identifying whether the tissue depth landmarks are placed perpendicularly using Checkpoint™; A – using the skull isosurface, B - transparent superimposition of soft tissue and hard tissue, and C - Superimposition of sagittal slice and skull isosurface.In all A, B, and C, note that the hard tissue landmark's normal points in the direction of the soft tissue landmark which ensures perpendicularity.

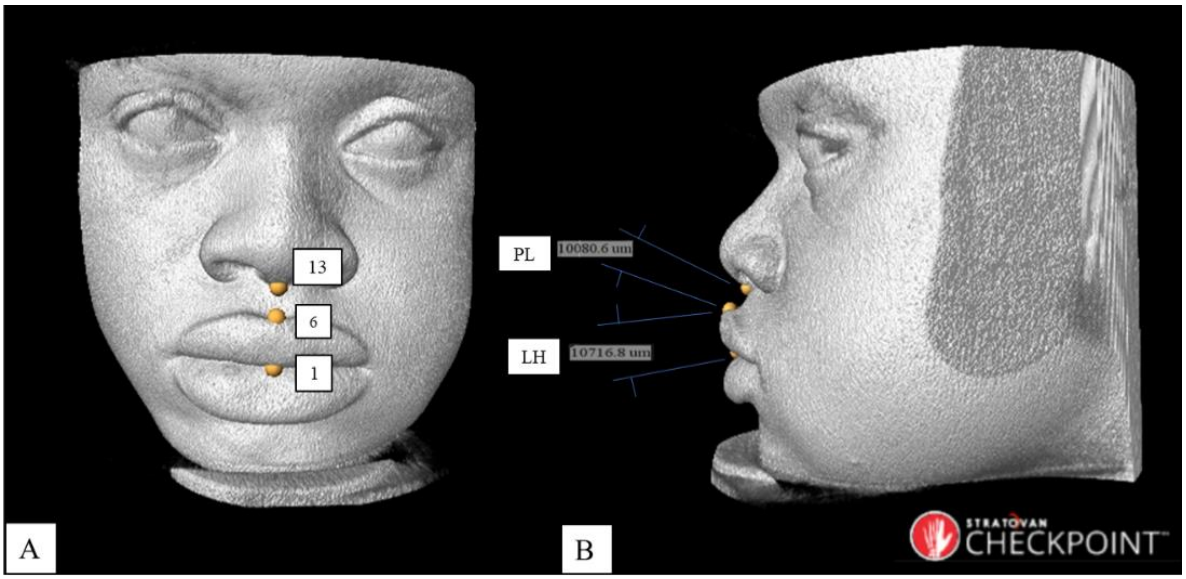

(Stratovan Checkoint™)

Figure 67: Measuring lip height (LH) and philtrum length (PL) on a isosurfaced CBCT scan using tissue landmarks seen in Figure 59. The oral fissue (1), cupids bow(6), and columella (13) were placed on the soft tissue isosurface (A) and the measurements were performed (B).

3.6 DATA RECORDING PROCEDURE

After all the measurements were performed, they were viewed on Checkpoint™ (Figure 68) and recorded on a table as displayed in addendum A. In Checkpoint™, the measurements are not labelled and therefore, the length had to be selected in the left column and it was highlighted on the specimen in orange as seen in Figure 68 indicated by the red arrow.

For the dentate sample, male and female anthropometry were recorded separately, and the indices and tissue lengths were grouped accordingly (Addendum A). For Pearson's correlation analysis in the edentulous group, only the females were analysed since the male group's sample size was below the required amount for correlation analysis ($n<10$). Furthermore, the patients of this study could not be grouped according to age since there was a limit placed on the sample size. If age were controlled in the current sample size, correlations could only be performed with groups consisting of less than 10 specimens, which was under the recommended sample size of this research.

In some instances, certain tissue lengths could not be measured due to scan artefacts. For example, the UFI and SGI could not be calculated if the nasion was absent in the scan. This limited the sample size when somatometry was correlated to these indices. Therefore, the sample size where the SGI was measured, was lower than the sample size where MAI was measured, the same applies to the other indices.

For further statistical analysis, an informal method was tested by summing the indices in various ways to identify whether the sum of indices could produce more statistically significant correlations when correlated to upper mouth somatometry. This was done by first calculating the indices and then adding the indices in various ways ensuring that each index was summed with one another, at least once. This method was tried since multiple linear regression (MLR) was not possible due to this research's low sample size (Knofczynski and Mundfrom 2008).

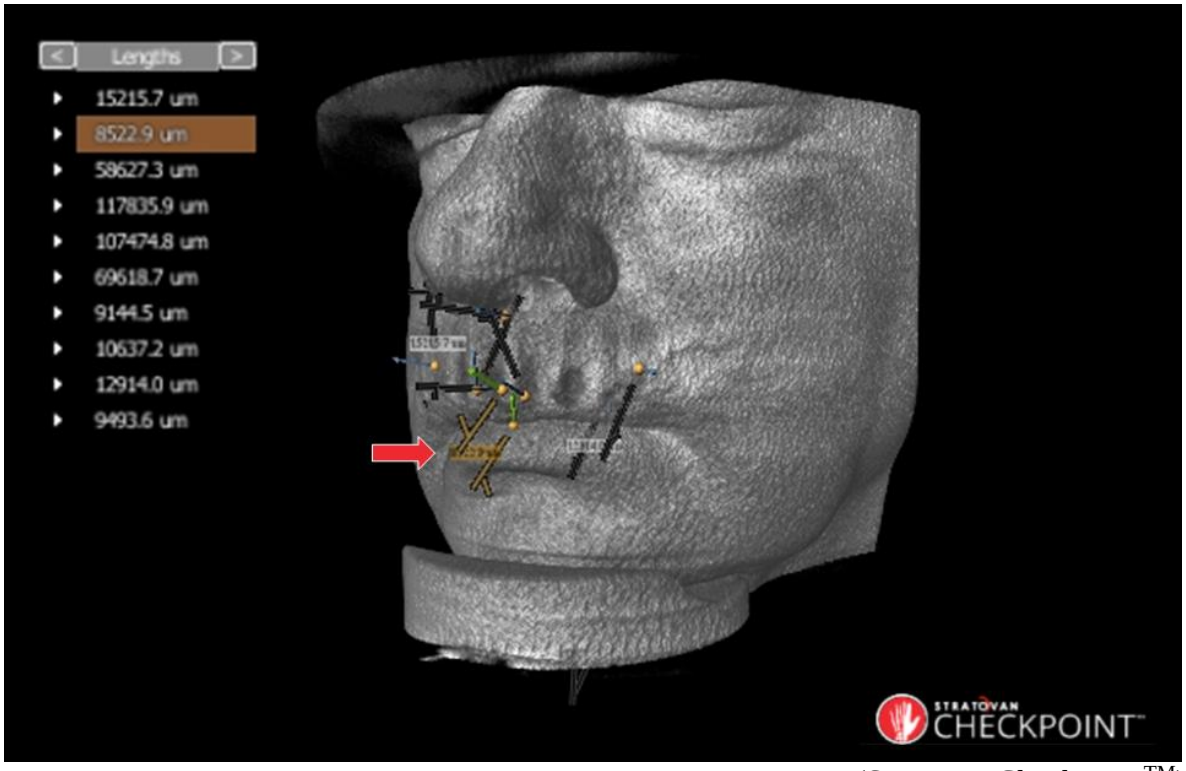

(Stratovan Checkpoint™)

Figure 68: Viewing the measurements performed on the CBCT scan. The red arrow indicates the selected length in the column.

3.7 STATISTICAL ANALYSES

A biostatistician was consulted and a sample size of n=25 per biological sex group was calculated. However, this sample size was not possible to achieve as many of the CBCT scans collected did not meet the selection criteria and many limitations were met. Therefore, a total of 63 scans were retrieved: for dentate patients, n=40 (24 males; 16 females); and for edentulous patients, n=23 (7 males; 16 females).

To assess the normality of the measurements, a Shapiro-Wilk test was performed before Pearson's correlation analysis could be applied. Pearson's correlation analysis was applied to assess the correlations between the skull indices and somatometry. The strength of these correlations was interpreted using Table 13.

For descriptive statistics, means and standard deviations of the measurements were calculated of each sex group and an independent t-test was used to test for anthropometric differences between the sexes.

To assess the degree of agreement between observers, Bland-Altman (BA) plots were used to visualise the inter- and intra-observer error. Only 10% of the sample was used to analyse the observer error. For this study, the observers were annotated as observer A for the PI, and observer B as the additional investigator. Observer B, for this research, was a postgraduate student in human anatomy with skills in osteometry and biological anthropometry.

Observer A2 was the PI as well, where "A2" defined the second set of measurements to establish the intra-observer error. The second set of measurements were performed four months after the first set measurements, by the PI. The BA plots were generated by plotting the difference between two measurements against their mean. The mean of the two measurements was plotted along the horizontal axis and the difference of the two measurements was plotted on the vertical axis. The bias between the two measurements was calculated by averaging the measurements' differences. The BA plots also required the upper and lower limits of agreement (LOA) (Giavarina 2015). When the degree of agreement was assessed between observers, it was taken into consideration that a measurement difference larger than 2 mm, was not considered acceptable (Verhoff *et al.*, 2008).

Significance was set at $p < 0.05$ for all statistical tests. All statistical analyses were carried out using IBM® SPSS® Statistics for Windows, version 27.

Table 13: Interpreting correlation coefficients.

Positive		**Negative**	
r =1	Perfect positive correlation	r = -1	Perfect negative correlation
0,95 ≤ r < 1	Very strong positive correlation	- 1 < r ≤ -0,95	Very strong negative correlation
0,87 ≤ r < 0,95	Strong positive correlation	- 0,95 < r ≤ -0,87	Strong negative correlation
0,7 ≤ r < 0,87	Moderate positive correlation	- 0,87 < r ≤ -0,7	Moderate negative correlation
0,5 ≤ r < 0,7	Weak positive correlation	- 0,7 < r ≤ -0,5	Weak negative correlation
0 < r < 0,5	Very weak positive correlation	- 0,5 < r < 0	Very weak negative correlation

(Adapted from Mukaka 2012)

3.7.1 Hypothesis

H_1: There is a weak correlation between skull indices and somatometry

H_0: There is a strong correlation between skull indices and somatometry

CHAPTER 4 RESULTS

A total of 63 CBCT scans were retrieved for this research and anthropometry was performed on the patients' skulls and soft tissue of the mouth. The measurements of the skull were used to calculate skull indices and the indices were correlated to the mouth's somatometry.

Of the 63 patients, 10% were selected for an inter- and intraobserver analysis. In Adendum B, the BA plots display the intra- and interobserver error of all the measurements performed in this research. In addendum B, Figure 1 to Figure 14 shows the intra- and interobserver errors found in osteometry, and Figure 15 to Figure 30 display the inter- and intraobserver errors of somatometry. It should be noted that for Figure 23 to Figure 30, in addendum B, that only three x-values are present, and this is due to these BA plots displaying the measurement error for the II and F tissue depth points which were not measured in the edentulous group.

Based on the BA plots, it can be confirmed that all measurements were reproducible. The BA plots show that almost all the measurements for the inter- and intra-observations were located within the 95% CI. This indicates a high degree of inter- and intra-observer agreement. Most of the measurements also lie within the accepted 2 mm error margin except in the instance of the interobserver error for n-pr (Figure 1) and zy-zy (Figure 3) (Addendum B) (Verhoff *et al.*, 2008). According to Giavarina (2015), all BA plots show a random variability trend, and the plots graphically display that there is no systematic difference between the observers' measurements.

The Shapiro-Wilk test determined that the continuous variables were all approximately normally distributed in the sample (Shapiro-Wilk test: p-value > 0.05). Due to normality of the measurements, Pearson's correlation analysis could be performed.

Table 14 presents the descriptive statistics and the significant differences between the anthropometry of dentate males and female patients of this research, and Table 15 shows the descriptive statistics and significant differences of somatometry between dentate males and female patients. According to Table 14, most dentate osteomtetry were significantly different between males and females ($p < 0,05$), however, the ecm-ecm, pr-alv, and n-pr were not. For dentate somatometry (Table 15) only the I was significantly different between the sexes ($p < 0,05$).

Table 16 shows the descriptive statistics and the significant differences between the anthropometry of edentulous males and female patients, and Table 17 shows the descriptive statistics and significant differences of somatometry between edentulous males and female patients. In Table 16 the edentulous ba-pr, ba-gn, ba-n, and ecm-ecm were significantly different ($p < 0,05$) between the sexes. In Table 17, only the edentulous H and I were significantly different ($p < 0,05$) between the sexes.

Table 18 shows the frequency of prognathism, mesognathism, and orthoganism in the entire study sample (dentate and edentulous), using the SGI as the determinant. According to the patients' SGI values, five patients were prognathic, six were mesognathic, and 14 were orthognathic.

Table 14: Mean and standard deviations of osteometry of the dentate patients to display significant osteometric sex differences.

Measurements (mm)	**Male**			**Female**			**Sex difference**
	Mean	**n**	**std dev.**	**Mean**	**n**	**Std dev.**	**p-value**
n-pr	66,88	14	4,73	64,51	11	3,71	0,19
zy-zy	130,79	14	4,99	121,94	11	5,56	p < 0,01
ba-pr	101,12	24	5,62	95,73	15	5,02	p < 0,01
ba-gn	113,13	7	6,18	101,28	14	6,46	p < 0,01
ba-n	103,23	12	4,33	98,53	7	4,32	p < 0,05
ecm-ecm	65,74	24	5,36	62,93	16	4,42	0,09
pr-alv	56,26	24	3,54	54,09	16	3,41	0,06

p<0,01/p<0,05 = significant

Table 15: Mean and standard deviations of somatometry of the dentate patients to display significant somatometric sex differences.

Measurements (mm)	**Male**			**Female**			**Sex difference**
	Mean	**n**	**Std dev.**	**Mean**	**n**	**Std dev.**	**p-value**
H	13,36	24	2,18	12,16	16	1,41	0,06
I	14,79	24	3,05	12,04	16	2,34	p < 0,01
II^R	10,96	24	2,46	13,89	16	20,86	0,49
II^L	10,95	24	2,48	9,01	16	1,81	0,011
F^R	10,71	24	1,68	9,41	16	1,56	0,02
F^L	10,51	24	1,96	9,48	16	1,75	0,09
PL	14,41	24	3,69	14,51	16	2,87	0,92
LH	11,54	24	2,97	10,11	16	2,37	0,12

p<0,01 = significant

Table 16: Mean and standard deviations of osteometry of the edentulous patients to display significant osteometric sex differences.

Measurements (mm)	**Male**			**Female**			**Sex difference**
	Mean	**n**	**Std dev.**	**Mean**	**n**	**Std dev.**	**p-value**
n-pr	66,94	3	1,74	62,28	11	4,91	0,14
zy-zy	128,98	3	1,17	121,78	11	5,78	0,06
ba-pr	96,45	7	1,83	88,13	14	5,69	p < 0,01
ba-gn	114,86	22	7,86	106,65	14	4,74	p < 0,01
ba-n	104,91	3	5,46	96,81	11	4,36	p < 0,05
ecm-ecm	59,88	7	3,61	55,68	16	3,66	p < 0,05
pr-alv	51,49	7	2,08	48,71	16	4,02	0,11

p<0,01/p<0.05 = significant

Table 17: Means and standard deviations of somatometry of edentulous patients to display significant somatometric sex differences.

Measurements (mm)	**Male**			**Female**			**Sex difference**
	Mean	**n**	**Std dev.**	**Mean**	**n**	**Std dev.**	**p-value**
H	13,14	7	2,58	10,61	16	2,19	p < 0,05
I	14,87	7	4,14	10,31	13	2,12	p < 0,05
PL	14,59	5	2,54	15,61	13	3,28	0,543
LH	6,84	5	3,47	6,17	13	2,58	0,661

p<0.05 = significant

Table 18: The frequency of prognathic, mesognathic, and orthognathic individuals in the sample of this research. The SGI could only be calculated of 25 individuals in the sample.

Dentate	**SGI n=25**
Prognathic (projecting) > SGI = 103.0	5
Mesognathic (medium) SGI = 98.0-102.9	6
Orthognathic (flat) < SGI = 97.9	14

4.1 CORRELATION ANALYSIS FOR EDENTULOUS PATIENTS

No significant correlations were found for the edentulous female group (Table 19 & Table 20). However, in Table 21, after summing the indices a significant correlation was found between GI+SGI and PL.

Table 19: Correlation coefficients between indices and the mid-philtrum in female edentulous patients.

Female	**n**	**H**
MAI	16	0,22
GI	14	-0,24
MAI+ GI	14	0,13
SGI	11	-0,19
MAI+SGI	11	0,06
UFI	11	-0,49
MAI+UFI	11	-0,14
GI+SGI	12	0,31
MAI+GI+SGI	12	-0,28

* Significant ($p < 0.05$)

Table 20: Correlation coefficients between the maxillary-alveolar and gnathic index, and somatometry in female edentulous patients.

Female	**n**	**I**	**PL**	**LH**
MAI	13	-0,03	0,04	-0,3
GI	12	-0,01	0,21	0,53

* Significant ($p < 0.05$)

Table 21: Correlation coefficients between the summed indices and somatometry in female edentulous patients.

Female	**I**	**PL**	**LH**
MAI+GI n=12	-0,05	0,21	0,09
GI+SGI	(n=10) 0,26	(n=9) 0.69*	(n=9) 0,21
MAI+GI+SGI	(n=10) -0,58	(n=9) 0,47	(n=9) 0,01

* Significant ($p < 0.05$)

4.2 CORRELATION ANALYSIS FOR DENTATE PATIENTS

For the dentate group, many significant correlations were found as opposed to the edentulous group. These results are displayed in Table 22 to Table 27

In Table 22, the MAI and II^R, MAI and II^L, and SGI and LH, showed significant correlations. In Table 23, the GI+SGI and F^R, GI+SGI and LH, and SGI+UFI and LH, had significant correlations. In Table 24, the MAI+GI+SGI and PL, and MAI+SGI+GI+UFI and PL, had significant correlations. In Table 25, the SGI and LH, SGI and II^L, and SGI and F^L, had significant correlations. In Table 26, the MAI+SGI and I, MAI+SGI and LH, GI+SGI and II^L, GI+SGI and F^L, GI+UFI and PL, SGI+UFI and II^L, and SGI+UFI and F^L, had significant correlations. In Table 27, the MAI+FI+SGI and I, MAI+SGI+UFI and LH, GI+SGI+UFI and II^L, GI+SGI+UFI and F^R, GI+SGI+UFI and F^L, and MAI+SGI+UFI and I, had significant correlations.

Table 22: Correlation coefficient between indices and somatometry in dentate male patients.

Dentate males	**n**	**H**	**I**	**II^R**	**II^L**	**F^R**	**F^L**	**PL**	**LH**
MAI	24	-0,01	0,22	0,469*	0,51*	0,26	0,11	0,16	0,11
GI	22	-0,51*	-0,01	-0,09	-0,11	-0,27	-0,25	0,16	0,36
SGI	14	-0,28	0,25	-0,33	-0,23	-0,48	-0,35	0,49	0,68**
UFI	14	-0,24	-0,16	-0,21	-0,31	-0,08	-0,31	0,04	0,06

* $p < 0.05$

**$p < 0.01$

Table 23: Correlation coefficient between summed indices and somatometry in dentate male patients.

Dentate males	**n**	**H**	**I**	**II^R**	**II^L**	**F^R**	**F^L**	**PL**	**LH**
MAI+GI	22	-0,22	0,17	0,37	0,39	0,09	-0,01	0,26	0,25
MAI+SGI	14	-0,09	0,51	0,21	0,31	-0,03	-0,09	0,49	0,47
MAI+ UFI	14	-0,03	0,35	0,37	0,38	0,26	-0,02	0,26	0,11
GI+SGI	12	-0,42	0	-0,53	-0,44	-0.67*	-0,54	0,55	0,66*
GI+UFI	12	-0,42	-0,31	-0,51	-0,53	-0,48	-0,56	0,30	0,24
SGI+UFI	14	-0,34	0,10	-0,36	-0,33	-0,41	-0,44	0,40	0,55*

* $p < 0.05$

Table 24: Correlation coefficient between summed indices and somatometry in dentate male patients.

Dentate males	n	H	I	II^R	II^L	F^R	F^L	PL	LH
MAI+GI+SGI	12	-0,16	0,36	-0,05	0,06	-0,28	-0,28	0,69*	0,56
MAI+GI+UFI	12	-0,11	0,18	0,07	0,08	-0,03	-0,25	0,54	0,19
MAI+SGI+UFI	14	-0,19	0,43	0,12	0,19	-0,06	-0,22	0,50	0,48
GI+SGI+UFI	12	-0,42	-0,07	-0,51	-0,47	-0,57	-0,55	0,46	0,54
MAI+SGI+GI+UFI	12	-0,23	0,27	-0,13	-0,07	-0,29	-0,37	0, 67*	0,53

* $p < 0.05$

Table 25: Correlation coefficient between indices and somatometry in female dentate patients.

Dentate females	n	H	I	II^R	II^L	F^R	F^L	PL	LH
MAI	16	-0,29	-0,05	0,05	-0,17	-0,23	-0,30	0,09	0,07
GI	14	-0,34	0,26	0,05	0,26	0,31	0,38	0,18	0,53
SGI	11	-0,06	0,50	0,55	0,71*	0,53	0,61*	-0,23	0,71*
UFI	11	-0,17	-0,15	-0,51	-0,50	-0,28	-0,30	0,48	-0,54

* $p < 0.05$

Table 26: Correlation coefficient between summed indices and somatometry in female dentate patients.

Dentate females	n	H	I	II^R	II^L	F^R	F^L	PL	LH
MAI+GI	14	-0,42	0,04	0,12	-0,13	-0,07	-0,13	0,21	0,11
MAI+SGI	11	-0,41	0.62*	0,39	0,42	0,36	0,38	-0,09	0,77**
MAI+ UFI	11	-0,46	0,22	-0,20	-0,28	-0,13	-0,19	0,26	0,07
GI+SGI	9	0,34	0,43	0,60	0.78*	0,64	0,72*	-0,19	0,52
GI+UFI	9	-0,31	0,22	-0,09	0,14	0,14	0,31	0,85**	-0,12
SGI+UFI	11	-0,18	0,55	0,41	0,61*	0,51	0,61*	-0,01	0,59

* $p < 0.05$
**$p < 0.01$

Table 27: Correlation coefficient between summed indices and somatometry in female dentate patients.

Dentate females	n	H	I	II^R	II^L	F^R	F^L	PL	LH
MAI+GI+SGI	9	0,04	0,71*	0,53	0,58	0,61	0,58	-0,13	0,66
MAI+GI+UFI	9	-0,36	0,28	-0,10	-0,17	-0,02	-0,07	0,27	0,08
MAI+SGI+UFI	11	-0,49	0,59	0,22	0,26	0,28	0,29	0,08	0,61*
GI+SGI+UFI	9	0,23	0,53	0,54	0,79*	0,67*	0,79*	-0,01	0,55
MAI+SGI+GI+UFI	9	-0,13	0,68*	0,35	0,41	0,49	0,48	0,06	0,56

* $p < 0.05$
**$p < 0.01$.

CHAPTER 5 DISCUSSION

This study aimed to determine whether there is a strong correlation between skull indices and somatometry of the mouth of edentulous patients. Since edentulous patients have no teeth, dentate patients were included in this research to understand the transition from dentate to edentulous morphology. Many of the correlations found in this study were negative, and weak or very weak (Table 13), which could indicate that the proportions of the skull are not good predictors of mouth somatometry or that additional factors were required to set additional controls for this study, such as with age, ancestry, hormonal factors, genetic make-up, epigenetic factors, skin ageing, and systemic factors (Ridel, *et al.* 2018) .The interdependence of these different factors could influence the morphology of the craniofacial skeleton and facial morphology (Wilkinson 2004; Briers *et al.* 2015).

5.1 DENTATE VS EDENTULOUS ANTHROPOMETRY

Many significant correlations were found in dentate patients as opposed to the edentulous patients. This indicated that the dimensions of the edentulous skulls of this research could not predict somatometry of the mouth as well as the dentate patients. This could be attributed due to edentulous patients undergoing RRR.

With RRR, an edentulous patient's pr changes from its original position, progressively, more severely than in dentate patients. This is due to the maxillary alveolar ridge resorbing over time. The reason RRR was not controlled for in this study was since it influences the ba-pr and n-pr which were used to calculate the UFI, GI and SGI. Therefore, it was assumed that the pr's position would have defined RRR severity, however, it did not seem effective based on the lack of significant correlations in the edentulous group.

In Figure 69, adapted from Reich *et al.* (2011), the pr of the maxilla shifts position as RRR progression takes place. Therefore, if the n-pr was measured of an individual before tooth extraction, the same individual's n-pr would be shorter if their RRR was as severe as in number 6 in Figure 69. However, this is not to say that n-pr can define RRR severity. The Cawood and Howell classing system (1988) (Figure 8 and Figure 9) should be employed in future research with a larger sample size to control RRR severity.

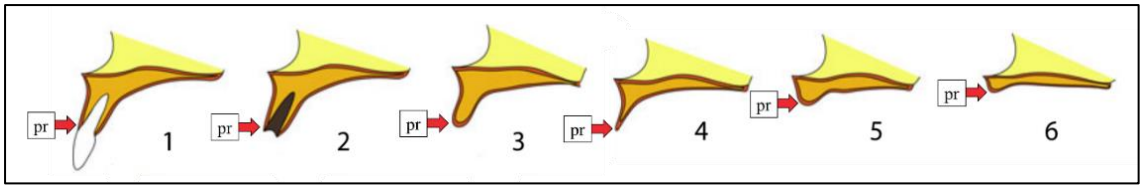

(Adapted from Reich *et al.* 2011)

Figure 69: The prosthion's position changes as residual ridge resorption progresses.

5.1.1 Edentulous anthropometry

In edentulous patients, the lips sink into the mouth over time. This is seen in Figure 70 which is a severe case of RRR. Relating to this research, the issue noted in edentulous morphology is that the morphology of the patient's lips and the length of the philtrum are influenced. This issue varied between all edentulous patients since many factors played a role in their morphology. Due to the inconsistency in the patients' rate of RRR and because of the lack of controls in the edentulous group, it led to inconclusive results. Therefore, none of the female edentulous correlations were significant as seen in Table 19 and Table 20. However, when the indices were summed for the edentulous females, the GI+SGI vs PL was significant (Table 21)

(Stratovan Checkpoint™)

Figure 70: Mouth morphology of patient with severe RRR.

By summing the edentulous GI and SGI, it yielded a weak-positive significant correlation for the PL (Table 21). The GI and SGI were summed as an attempt to represent the overall prognathism of the individual. Therefore, by summing GI and SGI, it could give a quantitative indication of prognathism. Due to the significant correlation, the SGI+GI shows that it may be linked with the PL, but this is not to say that this is statistically viable. The reason being is that the edentulous SGI and GI, separately, had no significant correlation with any somatometric length. Therefore, SGI and GI may influence the mouth differently in edentulous patients and to further assess this relationship, a larger sample is required that controls for age, biological sex, RRR severity. Perhaps ancestry will not have to be controlled since the SGI and GI rely on prognacy which is dependent on ancestry (Gerasimov 1971).

All other edentulous correlations were not significant since other factors are influencing the dimensions of somatometry other than the indices. With the edentulous MAI, no teeth were present, making the alveolar ridge's dimensions smaller than the dentate patient's alveolar ridge. The MAI is also influenced by RRR since no significant correlations were found as opposed to the dentate male group where significant weak-positive correlations were found with II^R and II^L (Table 22). Since significant correlations are found in the dentate MAIs, and not in edentulous MAIs, it can be concluded that RRR plays a role in determining somatometry as RRR distorts the mouth dimensions. However, age cannot be ignored as a cofactor to RRR.

5.1.2 Dentate anthropometry

It was noted that in some instances, the correlations increased and became significant when the dentate indices were summed (Table 22 to Table 27). This is more evident in Table 26 and Table 27. However, these significant correlations could not be statistically confirmed in this research since the sample size was too low for MLR.

Table 22 and Table 25 look at the indices on their own, correlated to the somatometry for males and females, respectively. For the MAI, GI and UFI, many of the correlations were either very weak or weak which shows that the MAI, GI, UFI could be predictors of upper mouth somatometry, however, the SGI yielded stronger and significant correlations. For the males, the SGI had a significant weak positive correlation to the LH; and for the females, the SGI had a significant moderate positive correlation to the II^{L}, a significant weak positive correlation to the F^{L}, and a significant moderate correlation with the LH. This indicates that prognacy of teeth may be good predictor of upper mouth somatometry in dentate patients. This could also emphasise the need to control for ancestry in future edentulous studies since prognacy and ancestry are dependent. Furthermore, because the dentate SGI is positively correlated to upper mouth somatometry, it further confirms Gerasimov's statement that prognathism indicates macrochelia, or fuller lips. Therefore, the more prognathic an individual is, the more likely for the individual is to present with macrochelia (Gerasimov 1971; Taylor 2000; Vermeulen 2012).

For the female dentate group where the indices were summed, correlations seemed to strengthen and ranged between weak and moderate. It could be assumed that the summing of indices could increase the amount of the skull morphology used to predict somatometry. It is known that many of the skull indices are specific for certain population groups (Bass 2005). By summing the indices, it further defined the skull's morphology and therefore, this may be the reason the correlations have strengthened and became significant.

5.2 AGE

With ageing comes the morphological and anatomical changes of the facial tissue and skeleton. The facial tissue changes in thickness and in its composition of subcutaneous tissue, the location of facial ligaments shift, and the contours of the skull change, giving the individual an overall superficial appearance of an aged face (Trojahn, Dobos, Lichterfeld, Blume-Peytavi & Kottner 2015).

The results of this research may have been influenced by age since the majority of the sample skews to middle-aged and more senior individuals. During data collection, the individuals that presented with edentulism were mostly older, which corresponds with the link between age and edentulism, which states that older individual will lose their teeth over time if not medically cared for and treated for by frequent visits to dental hospitals (Gupta *et al.* 2019).

The sample of this research's facial morphology was affected by the ageing process which contributed to the weak correlations. As the skin and facial tissue ages, collagen production is decreased, and the skin's firmness gradually declines; the production of elastin slows down, and the adiposity of the face diminishes (Coleman & Grover 2006). This leads to the overall sagging appearance of the skin and causes the height of the lips to decrease over time (Lévêquea & Goubanovab 2004). An example of these morphological age changes is seen in Figure 38 and Figure 70.

The change in the height of the lips is also attributed to the subcutaneous fat distribution. From the CBCTs, it was not possible to analyse fat distribution and therefore it was not assessed as a factor in this research. Even though this may have been the case, the thickness of the lips could still be measured. The thickness of the lip's changes in adiposity alongside adipose hypertrophy and hypotrophy of certain areas of the face (Coleman 2005). The areas of hypotrophy include the periorbital, forehead, malar, temporal, mandibular, mental, glabellar, and perioral sites; whereas hypertrophy and persistence of fat occur in the submental, lateral nasolabial fold, labiomental crease, jowl, infraorbital fat pouch, and malar fat pad sites (Gosain, Klein, Sudhakar, & Prost 2005) (Figure 42 & Figure 70). Therefore, the influence of age on fat distribution of the face could affect the somatometry of the mouth (Coleman & Grover 2006).

The weakening of ligaments in the face also contribute to the shifting of the positioning of certain parts of the face. The malar fat pad's ligaments weaken, causing it to shift, forming or intensifying the nasolabial fold. The muscles also begin to slacken, atrophy, and the skin loses tautness leading to facial sagging. Due to muscle weakness and fat atrophy, the lips move downward and elongate over time, where the philtrum thins in its depth as well (Coleman & Grover 2006). This gives enough evidence why age is an important factor when performing facial anthropometric research.

5.3 SYSTEMIC FACTORS

Many extrinsic and intrinsic factors that speed up the facial ageing process or alter facial tissue's morphology. Many intrinsic factors were not controlled in this study, such as genetics and various facial phenotypes or ancestry, nor were some extrinsic factors such as tobacco use and ultraviolet light exposure. Intrinsic and extrinsic factors should not be overlooked in future research; however, it can be said that ancestry, as an intrinsic factor, was controlled quantitatively in this research as the UFI, SGI, and GI. The UFI is used in biological anthropology to define skull facial shape, and the SGI and GI to define prognacy; these are some of the factors used to estimate ancestry in an individual (de Villiers 1979; Bass 2005; Liebenberg *et al.* 2015; Lesciotto *et al.* 2016)

Extrinsic factors are those which can be controlled to a certain degree. For example, an individual can quit using tobacco or spend less time in the sun. Therefore, the extrinsic factors that affect individuals vary significantly and cannot easily be identified from the skull. Tobacco use can be identified if the individual presents with brown-orange tobacco stains on their teeth (Figure 71). However, excessive coffee intake also stains teeth in similar ways. Unstained teeth may not rule out tobacco use either since the individual may have had their teeth cleaned (Prathap, Rajesh, Boloor & Rao 2013). This could give the FFD practitioner an indication of how to interpret the individual's age on the skin.

The use of tobacco increases the number of elastic fibres in the reticular dermis (Just, Ribera, Monsó, Lorenzo, Ferrándiz 2006; Kahky, Zuel-Fakkar, Ali, Mahdy, Farrag & Helmy 2007). This increase is attributed to fibre fragmentation and elastic tissue degradation rather than new synthesis. Tobacco use only affects the reticular dermis since tobacco constituents flow through its bloodstream, leading to the degradation of the elastic tissue. Therefore, the effects of tobacco are not noted in the macroscopic appearance of the skin, the exception being if the skin is frequently exposed to the sun. If the skin is not protected from the sun adequately by implementing photoprotective practices, this could induce photoaging or accelerated ageing of the skin due to excessive sun exposure (Han, Chien & Kang 2014).

Unlike with smoking, sun exposure triggers the epidermis and dermis of the skin. It can either cause atrophy in the spinous layer, or it could cause epidermal thickening (Kurban & Bhawan 1990). Additionally, ultraviolet exposure also causes a decrease in collagen production and if the skin is not photoprotected adequately, degraded collagen accumulates in the skin over time (Han *et al.* 2014). Therefore, UV exposure also contributes to the morphology of the facial tissue and may also be a factor that should be controlled for in facial anthropometric studies.

It could not be established whether the patients were tobacco users or presented with photo-ageing on the CBCT scans; these extrinsic factors may have altered the results of the study. This leads to the suggestion that if this study were more controlled, where the investigator would choose candidates, using a specific criterion, to be scanned by CBCT, perhaps the correlation coefficient may have increased statistical significance.

Therefore, it can not only be chronological age that affects skin morphology, but other systemic factors as well. This further proves that performing FFD on a skull where these extrinsic factors are not known, could result in an inaccurate representation of the individual's age (Just *et al.* 2007; Prathap *et al.* 2013).

(Illustration by L. Daniels)

Figure 71: Tobacco tooth stains on a skeletal specimen.

5.4 BIOLOGICAL SEX

Morphologically, the faces of males and females differ. The male skull is more robust and angular, leading to the facial tissue portraying these features. Morphologically, the female face is less angular and less robust, leaving the female with facial features that are more gracile. Furthermore, the STTs of male faces is much thicker than that of females as proven by countless research (Wilkinson 2004; Cavanagh & Steyn 2011; Briers *et al.* 2015).

According to Nascimento *et al.* (2012), the volume capacity of the male mouth is much larger than the female mouth. Nascimento *et al.* (2011) also found that the dimensions of the male lips are significantly larger than female lips in their research cohort. A similar trend is noted in this research's results in Table 14 and Table 15. Therefore, biological sex was regarded as a factor when pooling the sample for statistical analysis.

5.4.1 Dentate patients

The dentate patients showed significant differences between the sexes with the measurements of zy-zy, ba-pr, ba-gn, and ba-n. However, this was not so for n-pr, ecm-ecm, and pr-alv (Table 14). This could be due to the size of the samples or because the measurements that were significant were those taken from a greater part of the skull with a lesser margin for error, and they are also the parts of the skull that give the face its distinct features. The ecm-ecm, pr-alv, and n-pr may not have played a role in sex determination in this research; however, other research cannot be ignored as it states that mouth dimensions differ between sexes.

The height of the face (n-pr) may represent population affinity more than biological sex; therefore, significant differences did not arise in this measurement. These significant differences may also be inconclusive since age and ancestry were not controlled for as Ridel *et al.* (2018) and Lesciotto *et al.* (2016) did.

For the soft tissue measurements (Table 15), significant differences were seen between the sexes in I, II^{L}, and F^{R}, however, these results are not reliable since the dentate group was only controlled for sex, while Cavanagh & Steyn (2011), Briers *et al.* (2015), and Vermeulen (2012) proved that tissue depth differences exist between various population groups and not only between sexes. Age will also play a significant role as it was mentioned that soft tissue changes with age. The PL and LH were not significantly different either (Table 15) which is due to many of the patients presenting with similar SGIs (Table 18). Most of the individuals portrayed orthognathism and according to Gerasimov (1971), lip morphology is dependent on prognacy. Since most dentate individuals were orthognathic, many presented their population-specific mouth morphology (Table 18).

5.4.2 Edentulous patients

For edentulous patients ba-pr, ba-gn, ba-n, and ecm-ecm showed significant differences (Table 16). Once again, the results may be inconclusive since age and population group were not controlled. The reason the edentulous male and female ecm-ecm was significantly different and dentate ecm-ecm was not, is due to many of the edentulous patients that presented with a spectrum of RRR severities (Table 14 & Table 16). Therefore, it was certain that there would be significant differences in the edentulous ecm-ecm. Another reason some of the differences were not significant was due to the sample sizes of the sexes vastly differing.

Similarly, to the dentate group, H and I were significantly different between the sexes and the PL and LH were not. This cannot be attributed to prognacy since the patients had a resorbed alveolar ridge and no teeth, however, this could be due to edentulous mouth morphology and RRR.

In the dentate group, a similar amount of significant correlations were found in females (Table 22) when compared to the males (Table 25). The summed indices are not mentioned in this case since an informal and unvalidated method has been used to retrieve the summed indices. It is not known whether the same trend would be observed in edentulous patients, since the edentulous males were excluded from correlation analysis. If age and RRR severity are better controlled in future studies, this could be defined more clearly.

5.5 JAW MORPHOLOGY

Jaw and teeth morphology play a vital role in determining lip shape, understanding that male mouths are generally larger than females and that prognathism will determine the size and morphology of the lips (Gerasimov 1971; Nascimento *et al.* 2012). However, for edentulous patients, it may be difficult to predict the shape of the mouth. The research observed that due to the absence of teeth, the lips had limited structural support. Even measuring the SGI and GI in edentulous patients did not yield significant results since the teeth, alongside the alveolar ridge, are required to determine prognathism, therefore the edentulous SGI and GI could only quantitatively represent prognathism. The process of RRR also hinders measuring the SGI and GI, since the residual ridge is resorbed, and these indices require the pr, and in severe RRR cases the position of the pr shifts (Figure 69), therefore making GI and SGI unreliable to determine prognathism. This was proven since the GI and SGI yielded weak correlations when regressed with mouth somatometry.

During the initial stages of RRR, the sunken-in appearance is mild. However, as the individual ages and RRR progresses, there is a distinct morphological change in the mouth; to the point where the lips and majority of the philtrum is sunken into the mouth as well. This was noted in patients with severe RRR such as in Figure 70. In severe RRR patients such as in Class V or VI (Figure 8 & Figure 9; Table 1) the residual ridge has mostly been resorbed and prognathism cannot be determined, however, in patients with mild RRR (Class II to IV), prognathism could still be determined.

Furthermore, in the edentulous CBCT scans, it was noted that the edentulous patients' lips were thinner, this can be explained by the "sinking-in" phenomenon. Majority of the lip moves into the mouth since the teeth are no longer present to support them as in a dentate patient. Many patients presented with different degrees of protruding versus sunken in lips based on their RRR class.

5.6 THE MAIN LIMITATION OF THIS RESEARCH

The results of this study were mainly limited due to the sample size. Both male and female groups were analysed separately for the dentate patient sample. However, for the edentulous patients, females were analysed alone since the edentulous males were excluded from this study due to their low sample size. The small size of the study sample prevented linear regressions equations from being formulated or MLR analysis. If this were done and significant moderate to strong correlations were present, the equations from linear regression could have been used in forensic practice. Although significant correlations are present, these linear regression equations cannot be used in practice since the powered sample size was not reached. Therefore, the correlations yielded from this study are only to describe whether there may or may not be a relationship between skull indices and mouth somatometry.

5.7 FUTURE RESEARCH DEVELOPMENTS

Due to the digital era for FFD, future studies should consider CBCT scans and GM in its methodology and data collection. Not many studies in edentulism have been performed and not many use GM and CBCT scans, therefore, no edentulous morphological-anthropometric studies exist. Therefore, edentulous morphological research is needed in the field of FFD due to many SA individuals being edentulous. In this study, 261 patient CBCT scans out of 962 were found to be edentulous. Most of the 261 patients could not be selected for this research since these CBCT scans presented with many scan artefacts and did not meet the selection criteria.

Future studies should also consider using CBCT imaging archives from private sectors to increase the edentulous sample so that further research may be conducted. Private practices could own CBCT technology which scans patients with a mouth support that does not distort the chin. Access to such scans would allow the chin, bottom lip, and mandible to be further analysed. It could then be identified whether edentulism affects the upper mouth the same way it does the lower. The larger and more diverse edentulous sample will further be controlled for age and RRR severity to understand what effect RRR has on mouth morphology and to anthropometrically discuss the morphological implications RRR brings over time.

CONCLUSION

This research attempted to understand whether edentulous upper mouth morphology could be predicted from edentulous skull indices. From the results of this study, the residual ridge made data collection challenging since certain factors were not controlled for, specifically the severity of RRR, as RRR severity influences osteometry of the jaw and further influences the morphology of the mouth. The results of the study found that in the edentulous female group, no significant correlations were present between skull indices and somatometry of the upper mouth. Since no significant correlations were found, it can be concluded that the edentulous skull indices were not good predictors of edentulous upper mouth somatometry in this research sample. However, significant correlations were found in dentate individuals which may support that a dentate skull index could be good predictors of dentate upper mouth somatometry. Therefore, the interpretation that could be made is that in edentulous skulls, RRR and the morphology of the edentulous upper mouth is determined by an array of factors. In comparison with the dentate group, significant correlations were present, since RRR was not an anomaly seen in these patients. Furthermore, the mean age of the dentate group was younger than the edentulous group, taking into consideration that age also plays a pivotal role in determining facial morphology and anthropometry (Trojahn *et al.* 2015).

The method of anthropometry and GM in this study is novel as it has never been performed in this capacity before. Using GM for data collection on CBCT scans is recommended to achieve accuracy and precision for anthropometric research results (Ismail *et al.* 2018). Additionally, CBCT scans also ensure the presence of both hard and soft tissue, other than performing GM on the dry bone with no soft tissue present. Therefore, the scans of this research were able to identify the effect edentulism had on the soft tissue in real-time, therefore making it convenient to place the digital landmarks for anthropometry. It is suggested that further FFD research continue in a digital capacity since current methods of FFD are moving to a digital platform using various software (Bulut *et al.* 2017).

REFERENCES

Agostini, G.M. and Ross, A.H., 2011. The effect of weight on the femur: a cross-sectional analysis. *Journal of Forensic Sciences*, *56*(2), pp.339-343.

Alamri, H.M., Sadrameli, M., Alshalhoob, M.A. and Alshehri, M.A., 2012. Applications of CBCT in dental practice: a review of the literature. *General Dentistry*, *60*(5), pp.390-400.

Al-Bashaireh, A.M., Haddad, L.G., Weaver, M., Chengguo, X., Kelly, D.L. and Yoon, S., 2018. The effect of tobacco smoking on bone mass: an overview of pathophysiologic mechanisms. *Journal of Osteoporosis*, *2018*.

Alghoul, M. and Codner, M.A., 2013. Retaining Ligaments of the Face. Review of Anatomy and Clinical Applications. *Aesthetic Surgery Journal*, *33*(6), pp.769-782.

Amler, M.H., Johnson, P.L. and Salman, I., 1960. Histological and histochemical investigation of human alveolar socket healing in undisturbed extraction wounds. *The Journal of the American Dental Association*, *61*(1), pp.32-44.

Angel, J.L., 1978, February. Restoration of head and face for identification. In *Proceedings of Meetings of American Academy of Forensic Science* (pp. 125-142).

Atwood, D.A., 1958. Cephalometric Study of the Clinical Rest Position Following Removal of Occlusal Contacts, Part III. Clinical Factors Related to Variability of the Clinical Rest Position Following the Removal of Occlusal Contacts. *Journal of Prosthetic Dentistry*, *8*, pp.693-708.

Aulsebrook, W.A., İşcan, M.Y., Slabbert, J.H. and Becker, P., 1995. Superimposition and reconstruction in forensic facial identification: a survey. *Forensic Science International*, *75*(2-3), pp.101-120.

Baer, M. and Kachelrieß, M., 2012. Hybrid scatter correction for CT imaging. *Physics in Medicine & Biology*, 57(21), p.6849.

Bass, W. M., 2005. *Human Osteology: A Laboratory and Field Manual.* 5th edition. Springfield: Missouri Archaeological Society

Bergman, B.O. and Carlsson, G.E., 1985. Clinical long-term study of complete denture wearers. *Journal of Prosthetic Dentistry*, *53*(1), pp.56-61.

Bhayat, A. and Madiba, T.K., 2017. Is dental caries contagious?. *South African Dental Journal*, *72*(7), pp.302-304.

Bookstein, F.L., 1990. Introduction to methods for landmark data. In *Proceedings of the Michigan morphometrics workshop* (Vol. 2, pp. 215-226). Ann Arbor: The University of Michigan Museum of Zoology.

Bookstein, F.L., 1997. *Morphometric tools for landmark data.* Cambridge UK: Cambridge University Press

Botha, C.P., Preim, B., Kaufman, A.E., Takahashi, S. and Ynnerman, A., 2014. From individual to population: challenges in medical visualization. In *Scientific Visualization* (pp. 265-282). Springer, London.

Bradley, J.C., 1975. A radiological investigation into the age changes of the inferior dental artery. *British Journal of Oral Surgery*, 13(1), pp.82-90.

Bras, J., Van Ooij, C.P. and Van den Akker, H.P., 1985. Mandibular atrophy and metabolic bone loss: Mandibular ridge augmentation by combined sandwich-visor osteotomy and resorption related to metabolic bone state. *International Journal of Oral Surgery*, 14(1), pp.16-21.

Briers, N., Briers, T.M., Becker, P.J. and Steyn, M., 2015. Soft tissue thickness values for black and coloured South African children aged 6–13 years. *Forensic Science International*, 252, pp.188-e1.

Bulut, O., Liu, C.Y.J., Koca, F. and Wilkinson, C., 2017. Comparison of three-dimensional facial morphology between upright and supine positions employing three-dimensional scanner from live subjects. *Legal Medicine*, *27*, pp.32-37.

Campbell, R.L., 1960. A comparative study of the resorption of the alveolar ridges in denture-wearers and non-denture-wearers. *The Journal of the American Dental Association*, *60*(2), pp.143-153.

Carlsson, G.E. and Persson, G., 1967. Morphologic changes of the mandible after tooth extraction and denture treatment. *Odontologisk Revy*, *18*, pp.27-54.

Carlsson, G.E., 2004. Responses of jawbone to pressure. *Gerodontology*, *21*(2), pp.65-70.

Carlsson, G.E., 2006. Facts and fallacies: an evidence base for complete dentures. *Dental Update*, *33*(3), pp.134-142.

Cavanagh, D. and Steyn, M., 2011. Facial reconstruction: soft tissue thickness values for South African black females. *Forensic Science International*, 206(1-3), pp.215-e1.

Cawood, J.I. and Howell, R., 1988. A classification of the edentulous jaws. *International Journal of Oral and Maxillofacial Surgery*, *17*(4), pp.232-236.

Coleman, S.R. and Grover, R., 2006. The anatomy of the aging face: volume loss and changes in 3-dimensional topography. *Aesthetic Surgery Journal*, 26(1_Supplement), pp.S4-S9.

Coleman, S.R., 2005. Structural Fat Grafting. *Plastic and Reconstructive Surgery*, *115*(6), pp.1777-1778.

Colman, K.L., De Boer, H.H., Dobbe, J.G., Liberton, N.P., Stull, K.E., Van Eijnatten, M., Streekstra, G.J., Oostra, R.J., Van Rijn, R.R. and Van der Merwe, A.E., 2019. Virtual forensic anthropology: the accuracy of osteometric analysis of 3D bone models derived from clinical computed tomography (CT) scans. *Forensic Science International*, 304, p.109963.

Colón, C.J.P., Molina-Vicenty, I.L., Frontera-Rodríguez, M., García-Ferré, A., Rivera, B.P., Cintrón-Vélez, G. and Frontera-Rodríguez, S., 2018. Muscle and Bone Mass Loss in the Elderly Population: Advances in diagnosis and treatment. *Journal of Biomedicine* (Sydney, NSW), *3*, p.40.

Correa, L.R., Spin-Neto, R., Stavropoulos, A., Schropp, L., da Silveira, H.E.D. and Wenzel, A., 2014. Planning of dental implant size with digital panoramic radiographs, CBCT-generated panoramic images, and CBCT cross-sectional images. *Clinical Oral Implants Research*, *25*(6), pp.690-695.

de Villiers, H., 1979. Verslag oor menslike skeletmateriaal. *Die Kulture van Greefswald, Deel III*.

Devlin, H. and Sloan, P., 2002. Early bone healing events in the human extraction socket. *International Journal of Oral and Maxillofacial Surgery*, *31*(6), pp.641-645.

Dewake, N., Ishioka, Y., Uchida, K., Taguchi, A., Higashi, Y., Yoshida, A. and Yoshinari, N., 2020. Association between Carotid Artery Calcification and Periodontal Disease Progression in Japanese Men and Women: A Cross-Sectional Study. *Journal of Clinical Medicine*, *9*(10), p.3365.

El-Kahky, H.M., Zuel-Fakkar, N.M., Ali, D.G., Mahdy, A.S., Farrag, A.R.H. and Helmy, N.A., 2013. Effect of smoking on skin elastic fibers: a morphometric and immunohistochemical analysis. *Journal of The Arab Society for Medical Research*, *8*(2), p.74.

El Maroush, M.A., Benhamida, S.A., Elgendy, A.A. and Elsaltani, M.H., 2019. Residual ridge resorption, the effect on prosthodontics management of edentulous patient: an article review. *Int. J. Sci. Res. Manag.*, *7*, pp.260-7.

Fedosyutkin, B.A. and Nainys, J.V., 1993. *The relationship of skull morphology to facial features* (Vol. 199). Wiley-Liss, New York.

Ferro, K.J., Morgano, S.M., Driscoll, C.F., Freilich, M.A., Guckes, A.D., Knoernschild, K.L., McGarry, T.J. and Twain, M., 2017. The glossary of prosthodontic terms. *Journal of Prosthetic Dentistry*, *117*(5S).

Flygare, L. and Öhman, A., 2008. Preoperative imaging procedures for lower wisdom teeth removal. *Clinical Oral Investigations*, *12*(4), pp.291-302.

Ford, J.M. and Decker, S.J., 2016. Computed tomography slice thickness and its effects on three-dimensional reconstruction of anatomical structures. *Journal of Forensic Radiology and Imaging*, *4*, pp.43-46.

Franco, F.C.M., Araujo, T.M.D., Vogel, C.J. and Quintão, C.C.A., 2013. Brachycephalic, dolichocephalic and mesocephalic: Is it appropriate to describe the face using skull patterns?. *Dental Press Journal of Orthodontics*, *18*(3), pp.159-163.

Franklin, D., Swift, L. and Flavel, A., 2016. 'Virtual anthropology'and radiographic imaging in the Forensic Medical Sciences. *Egyptian Journal of Forensic Sciences*, *6*(2), pp.31-43.

Fujita, H., 2012. Periodontal diseases in anthropology. *Periodontal Diseases–A Clinician's Guide (Manaki, K ed)*, pp.279-294.

Gerasimov, M.M., 1975. The Reconstruction of the Face from the Basic Structure of the Skull, trans. *W. Tshernezky, Russia:* Publishers unknown.

Giavarina, D., 2015. Understanding bland altman analysis. *Biochemia Medica*, *25*(2), pp.141-151.

Gosain, A.K., Klein, M.H., Sudhakar, P.V. and Prost, R.W., 2005. A volumetric analysis of soft-tissue changes in the aging midface using high-resolution MRI: implications for facial rejuvenation. *Plastic and Reconstructive Surgery*, *115*(4), pp.1143-1152.

Guiglia, R., Di-Fede, O., Lo-Russo, L., Sprini, D., Rini, G.B. and Campisi, G., 2013. Osteoporosis, jawbones and periodontal disease. *Medicina Oral, Patología oral y Cirugía Bucal*, 18(1), p.e93.

Gupta, S., Singh, S.V. and Arya, D., 2019. Residual ridge resorption-a review of etiology. *Polymorphism*, 2, pp.107-113.

Guyomarc'h, P. and Bruzek, J., 2010. Cranial sexual dimorphism of identified subjects (collection Olivier, MNHN, Paris): An evaluation by geometric morphometrics. *Bulletins et mémoires de la Société d'anthropologie de Paris*, *22*, pp.216-229.

Heymsfield, S.B., Bourgeois, B., Ng, B.K., Sommer, M.J., Li, X. and Shepherd, J.A., 2018. Digital anthropometry: a critical review. *European Journal of Clinical Nutrition*, *72*(5), pp.680-687.

Hummel, S.K., Wilson, M.A., Marker, V.A. and Nunn, M.E., 2002. Quality of removable partial dentures worn by the adult US population. *The Journal of Prosthetic Dentistry*, *88*(1), pp.37-43.

Iscan, M.Y. and Steyn, M., 2013. *The human skeleton in forensic medicine*. Charles C Thomas Publisher.

Ismail, N.A., Abdullah, N., Noor, M.H.M., Lai, P.S., Shafie, M.S. and Nor, F.M., 2019. Accuracy and reliability of virtual femur measurement from CT scan. *Journal of forensic and legal medicine*, *63*, pp.11-17. Ismail NA, Abdullah N, Noor MH, Lai PS, Shafie MS, Nor FM. 2019. Accuracy and reliability of virtual femur measurement from CT scan. *Journal of Forensic and Legal Medicine*. Apr 1;63:11-7.

Józefowicz, W., 1970. Method of compensation for resiliency of soft tissues under the prosthesis by covering the plates of dentures with elastic material. *Protetyka Stomatologiczna*, *20*(2), pp.99-102.

Just, M., Ribera, M., Monso, E., Lorenzo, J.C. and Ferrandiz, C., 2007. Effect of smoking on skin elastic fibres: morphometric and immunohistochemical analysis. *British Journal of Dermatology*, *156*(1), pp.85-91.

Jyoti, N., Shah, N. and Karthik, M.M., 2010. Prosthodontic Rehabilitation of patients with Combination syndrome. *International Journal of Dental Clinics*, *2*(3).

Kalk, W. and de Baat, C., 1989. Some factors connected with alveolar bone resorption. *Journal of Dentistry*, *17*(4), pp.162-165.

Kau, C.H., Souccar, N.M., English, J.D., Kamel, S.G. and Wong, M.E., 2012. The surgical and orthodontic management of cherubism in a growing child. *Journal of Cranio-Maxillofacial Surgery*, *40*(3), pp.229-233.

Kaur, R., Kumar, M., Jindal, N. and Badalia, I., 2017. Residual Ridge Resorption–Revisited. *Dental Journal of Advance Studies*, *5*(02), pp.076-080.

Klemetti, E. and Vainio, P., 1993. Effect of bone mineral density in skeleton and mandible on extraction of teeth and clinical alveolar height. *The Journal of Prosthetic Dentistry*, *70*(1), pp.21-25.

Knofczynski, G.T. and Mundfrom, D., 2008. Sample sizes when using multiple linear regression for prediction. *Educational and Psychological Measurement*, *68*(3), pp.431-442.

Krastl, G., Filippi, A., Zitzmann, N.U., Walter, C. and Weiger, R., 2011. Current aspects of restoring traumatically fractured teeth. *The European Journal of Esthetic Dentistry*, *6*.

Kurban, R.S. and Bhawan, J., 1990. Histologic changes in skin associated with aging. *The Journal of Dermatologic Surgery and Oncology*, *16*(10), pp.908-914.

Kuzminsky, S.C. and Gardiner, M.S., 2012. Three-dimensional laser scanning: potential uses for museum conservation and scientific research. *Journal of Archaeological Science*, *39*(8), pp.2744-2751.

Langley, N.R., Jantz, L.M., Ousley, S.D., Jantz, R.L. and Milner, G., 2016. Data collection procedures for forensic skeletal material 2.0. *University of Tennessee and Lincoln Memorial University*.

Lesciotto, K.M., Cabo, L.L. and Garvin, H.M., 2016. A morphometric analysis of prognathism and evaluation of the gnathic index in modern humans. *Homo*, *67*(4), pp.294-312.

Lévêque, J.L. and Goubanova, E., 2004. Influence of age on the lips and perioral skin. *Dermatology*, *208*(4), pp.307-313.

Liebenberg, L. and Krüger, G.C., 2020. Standardization and quality assurance in skeletal landmark placement and osteometry. *Forensic Science International*, *308*, p.110168.

Liebenberg, L., Stull, K.E., L'Abbé, E.N. and Botha, D., 2015. Evaluating the accuracy of cranial indices in ancestry estimation among South African groups. *Journal of Forensic Sciences*, *60*(5), pp.1277-1282.

Lindholm, J., Steiniche, T., Rasmussen, E., Thamsborg, G., Nielsen, I.O., Brockstedt-rasmussen, H.E.L.L.E., Storm, T., Hyldstrup, L. and Schou, C., 1991. Bone disorder in men with chronic alcoholism: a reversible disease?. *The Journal of Clinical Endocrinology & Metabolism*, *73*(1), pp.118-124.

Mark, A.M., 2019. Dealing with tooth pain. *The Journal of the American Dental Association*, *150*(9), p.812.

Mezzomo, L.A., Shinkai, R.S., Mardas, N. and Donos, N., 2011. Alveolar ridge preservation after dental extraction and before implant placement: a literature review. *Revista Odonto Ciência*, *26*(1), pp.77-83.

Mukaka, M.J.M.M.J., 2012. Statistics corner: a guide to appropriate use of correlation in medical research. *Malawi Medical Journal*, *24*(3), pp.69-71.

Nascimento, W.V., Cassiani, R.A. and Dantas, R.O., 2012. Gender effect on oral volume capacity. *Dysphagia*, *27*(3), pp.384-389.

Nazir, S.A., Benamore, R. and Gleeson, F., 2013. Missed lung cancers on the scout view: do we look every time?. *Case Reports in Medicine*, *2013*.

New Tom VGi evo EXPANDED.VISION. 2021. Italy.

Oka, K., Murase, T., Moritomo, H., Goto, A., Sugamoto, K. and Yoshikawa, H., 2009. Accuracy analysis of three-dimensional bone surface models of the forearm constructed from multidetector computed tomography data. *The International Journal of Medical Robotics and Computer Assisted Surgery*, *5*(4), pp.452-457.

Ortega, A., Pedrosa, J., Heyde, B., Tong, L. and D'hooge, J., 2017. Automatic definition of an anatomic field of view for volumetric cardiac motion estimation at high temporal resolution. *Applied Sciences*, *7*(7), p.752.

Pagni, G., Pellegrini, G., Giannobile, W.V. and Rasperini, G., 2012. Postextraction alveolar ridge preservation: biological basis and treatments. *International Journal of Dentistry*, *2012*.

Pauwels, R., Jacobs, R., Bosmans, H. and Schulze, R., 2012. Future prospects for dental cone beam CT imaging. *Imaging in Medicine*, *4*(5), p.551.

Pietrokovski, J., Azuelos, J., Tau, S. and Mostavoy, R., 1995. Oral findings in elderly nursing home residents in selected countries: oral hygiene conditions and plaque accumulation on denture surfaces. *The Journal of Prosthetic Dentistry*, *73*(2), pp.136-141.

Pietrokovski, J., Starinsky, R., Arensburg, B. and Kaffe, I., 2007. Morphologic characteristics of bony edentulous jaws. *Journal of Prosthodontics*, *16*(2), pp.141-147.

Pinto, J.R., Bosco, Á.F., Okamoto, T., Guerra, J.B. and Piza, I.G., 2002. Effects of nicotine on the healing of extraction sockets in rats. A histological study. *Brazilian Dental Journal*, *13*(1), pp.3-10.

Pisulkar, S.K., Agrawal, R., Belkhode, V., Nimonkar, S., Borle, A. and Godbole, S.R., 2019. Perception of buccal corridor space on smile aesthetics among specialty dentist and layperson. *Journal of International Society of Preventive & Community Dentistry*, *9*(5), p.499.

Poštić S. Osteopenic and osteoporotic changes insegments of mandibles. 1st ed. Belgrade: *Zadužbina Andrejević*; 2000. pp. 14-83.

Prathap, S., Rajesh, H., Boloor, V.A. and Rao, A.S., 2013. Extrinsic stains and management: A new insight. *Journal of Academia and Industrial Research*, *1*(8), pp.435-442.

Priyadharshini, K.I., Idiculla, J.J., Sivapathasundaram, B., Mohanbabu, V., Augustine, D. and Patil, S., 2015. Age estimation using development of third molars in South Indian population: A radiological study. *Journal of International Society of Preventive & Community Dentistry*, *5*(Suppl 1), p.S32.

Ray, B.T. and Mathews, V.L., 1957. Artistic relationships in surface anatomy op the face: Application to reconstructive surgery. *Plastic and reconstructive surgery*, *20*(1), pp.1-17.

Reich, K.M., Huber, C.D., Lippnig, W.R., Ulm, C., Watzek, G. and Tangl, S., 2011. Atrophy of the residual alveolar ridge following tooth loss in an historical population. *Oral Diseases*, *17*(1), pp.33-44.

Rhine, J.S. and Campbell, H.R., 1980. Thickness of facial tissues in American blacks. *Journal of Forensic Science*, *25*(4), pp.847-858.

Richtsmeier, J.T., Paik, C.H., Elfert, P.C., Cole, T.M. and Dahlman, H.R., 1995. Precision, repeatability, and validation of the localization of cranial landmarks using computed tomography scans. *The Cleft palate-craniofacial Journal*, *32*(3), pp.217-227.

Ridel, A.F., Demeter, F., Liebenberg, J., L'Abbé, E.N., Vandermeulen, D. and Oettlé, A.C., 2018. Skeletal dimensions as predictors for the shape of the nose in a South African sample: A cone-beam computed tomography (CBCT) study. *Forensic Science International*, *289*, pp.18-26.

Rosenquist, J.B., Baylink, D.J. and Berger, J.S., 1978. Alveolar atrophy and decreased skeletal mass of the radius. *International Journal of Oral Surgery*, *7*(5), pp.479-481.

Ross, A.H. and Williams, S., 2008. Testing repeatability and error of coordinate landmark data acquired from crania. *Journal of Forensic Sciences*, *53*(4), pp.782-785.

Rynn, C., Balueva, T. and Veselovskaya, E., 2012. Relationships between the skull and face. *Craniofacial Identification*, p.193.

Sampson, H.W., Perks, N., Champney, T.H. and DeFee, B., 1996. Alcohol consumption inhibits bone growth and development in young actively growing rats. *Alcoholism: Clinical and Experimental Research*, *20*(8), pp.1375-1384.

Scarfe, W.C. and Farman, A.G., 2008. What is cone-beam CT and how does it work?. *Dental Clinics of North America*, *52*(4), pp.707-730.

Shiroma, C.Y., Terrado-Naguinlin, P.M. and Zuerlein, C.L., 2019. Healing alveolar sockets in skeletonized remains: A report on cases from one month to twelve months post-extraction. *Forensic Science International*, *301*, pp.e38-e43.

Slice, D.E., 2007. Geometric morphometrics. *Annual Review of Anthropology*, *36*, pp.261-281.

Smith, K., 2020. *Laws of the Face: Re-Staging Forensic Art as a counter-forensic device* (Doctoral dissertation, Liverpool John Moores University).

Stull, K.E., Tise, M.L., Ali, Z. and Fowler, D.R., 2014. Accuracy and reliability of measurements obtained from computed tomography 3D volume rendered images. *Forensic Science International*, *238*, pp.133-140.

Taylor, K.T., 2000. *Forensic art and illustration*. CRC press. Taylor KT. 2000 *Forensic Art and Illustration*. CRC press; Sep 15.

Trojahn, C., Dobos, G., Lichterfeld, A., Blume-Peytavi, U. and Kottner, J., 2015. Characterizing facial skin ageing in humans: disentangling extrinsic from intrinsic biological phenomena. *BioMedical Research International*, *2015*.

Trombelli, L., Farina, R., Marzola, A., Bozzi, L., Liljenberg, B. and Lindhe, J., 2008. Modeling and remodeling of human extraction sockets. *Journal of Clinical Periodontology*, *35*(7), pp.630-639.

Tuteja, M., Bahirwani, S. and Balaji, P., 2012. An evaluation of third molar eruption for assessment of chronologic age: A panoramic study. *Journal of Forensic Dental Sciences*, *4*(1), p.13.

Verhoff, M.A., Ramsthaler, F., Krähahn, J., Deml, U., Gille, R.J., Grabherr, S., Thali, M.J. and Kreutz, K., 2008. Digital forensic osteology—possibilities in cooperation with the Virtopsy® project. *Forensic science international*, *174*(2-3), pp.152-156. Vermeulen L. Manual forensic facial reconstruction. *Craniofacial Identification*. 2012 May 3;184.

Vermeulen, L., 2012. Manual forensic facial reconstruction. *Craniofacial Identification*, *184*.

von Cramon-Taubadel, N., Frazier, B.C. and Lahr, M.M., 2007. The problem of assessing landmark error in geometric morphometrics: theory, methods, and modifications. *American Journal of Physical Anthropology: The Official Publication of the American Association of Physical Anthropologists*, *134*(1), pp.24-35.

von Wowern, N. and Kollerup, G., 1992. Symptomatic osteoporosis: a risk factor for residual ridge reduction of the jaws. *The Journal of Prosthetic Dentistry*, *67*(5), pp.656-660.

Wärmländer, S.K., Garvin, H., Guyomarc'h, P., Petaros, A. and Sholts, S.B., 2019. Landmark typology in applied morphometrics studies: What's the point?. *The Anatomical Record*, *302*(7), pp.1144-1153.

White, S.C. and Rudolph, D.J., 1999. Alterations of the trabecular pattern of the jaws in patients with osteoporosis. *Oral Surgery, Oral Medicine, Oral Pathology, Oral Radiology, and Endodontology*, *88*(5), pp.628-635.

Wilkinson, C. and Neave, R., 2003. The reconstruction of a face showing a healed wound. *Journal of Archaeological Science*, 30(10), pp.1343-1348.

Wilkinson, C., 2004. *Forensic Facial Reconstruction*. Cambridge University Press.

Wilkinson, C., 2010. Facial reconstruction–anatomical art or artistic anatomy?. *Journal of anatomy*, *216*(2), pp.235-250.

Wilkinson, C., Rynn, C., Peters, H., Taister, M., Kau, C.H. and Richmond, S., 2006. A blind accuracy assessment of computer-modeled forensic facial reconstruction using computed tomography data from live subjects. *Forensic Science, Medicine, and Pathology*, *2*(3), pp.179-187.

Wilkinson, C.M., Motwani, M. and Chiang, E., 2003. The relationship between the soft tissues and the skeletal detail of the mouth. *Journal of Forensic Sciences*, *48*(4), pp.728-732.

Zelditch, M.L., Lundrigan, B.L. and Garland Jr, T., 2004. Developmental regulation of skull morphology. I. Ontogenetic dynamics of variance. *Evolution & Development*, *6*(3), pp.194-206.

Zmysłowska, E., Ledzion, S. and Jędrzejewski, K., 2007. Factors affecting mandibular residual ridge resorption in edentulous patients: a preliminary report. *Folia Morphologica*, *66*(4), pp.346-352.

ADDENDA

ADDENDUM A: TABLE FOR DATA COLLECTION

Table 1: Table used to record patient information, osteometry, somatometry for this research.

Patient information			Osteometry						Skull Indices					Somatometry							
Patient number	Age (years)	Sex (M/F)	ecm-ecm	pr-alv	zy-zy	n-pr	ba-pr	ba-gn	ba-n	MAI	UFI	SGI	H	I	II^R	II^L	F^R	F^L	PL	LH

ADDENDUM B: BLAND-ALTMAN PLOTS TO SHOW THE INTRA- AND INTEROBSERVER ANALYSIS

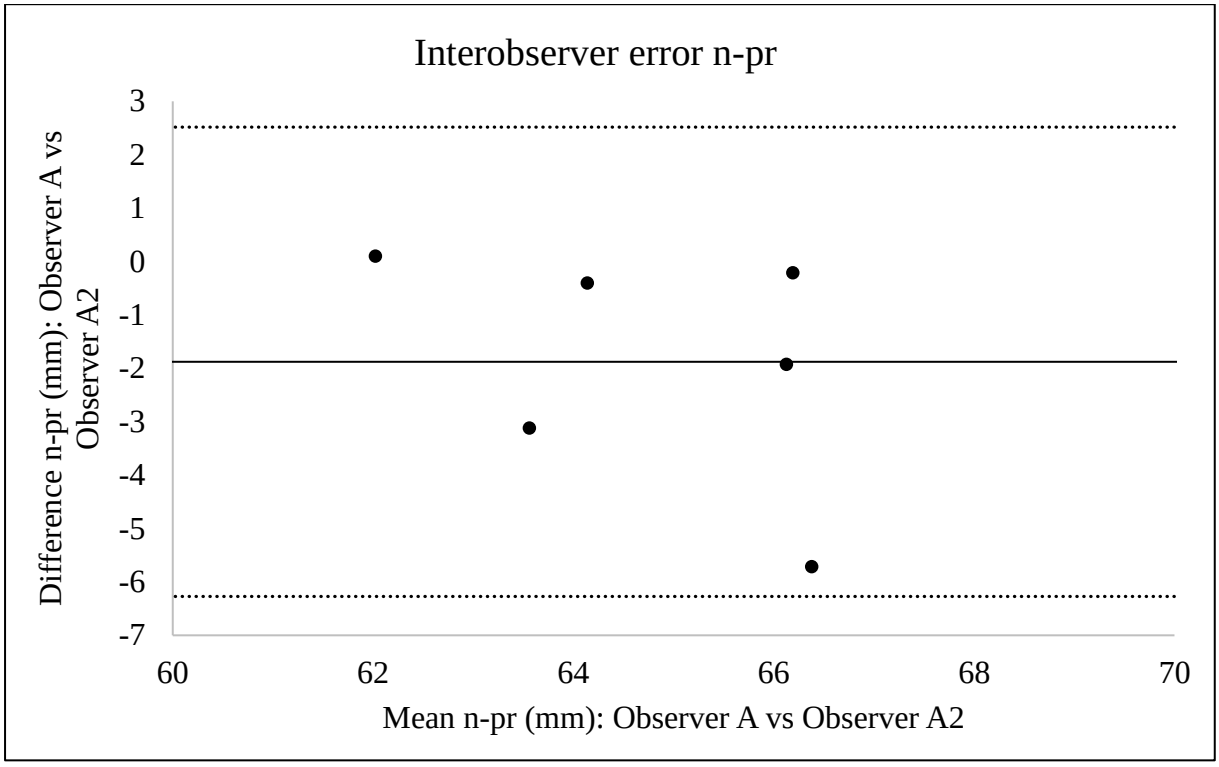

Figure 1: Interobserver error n-pr.

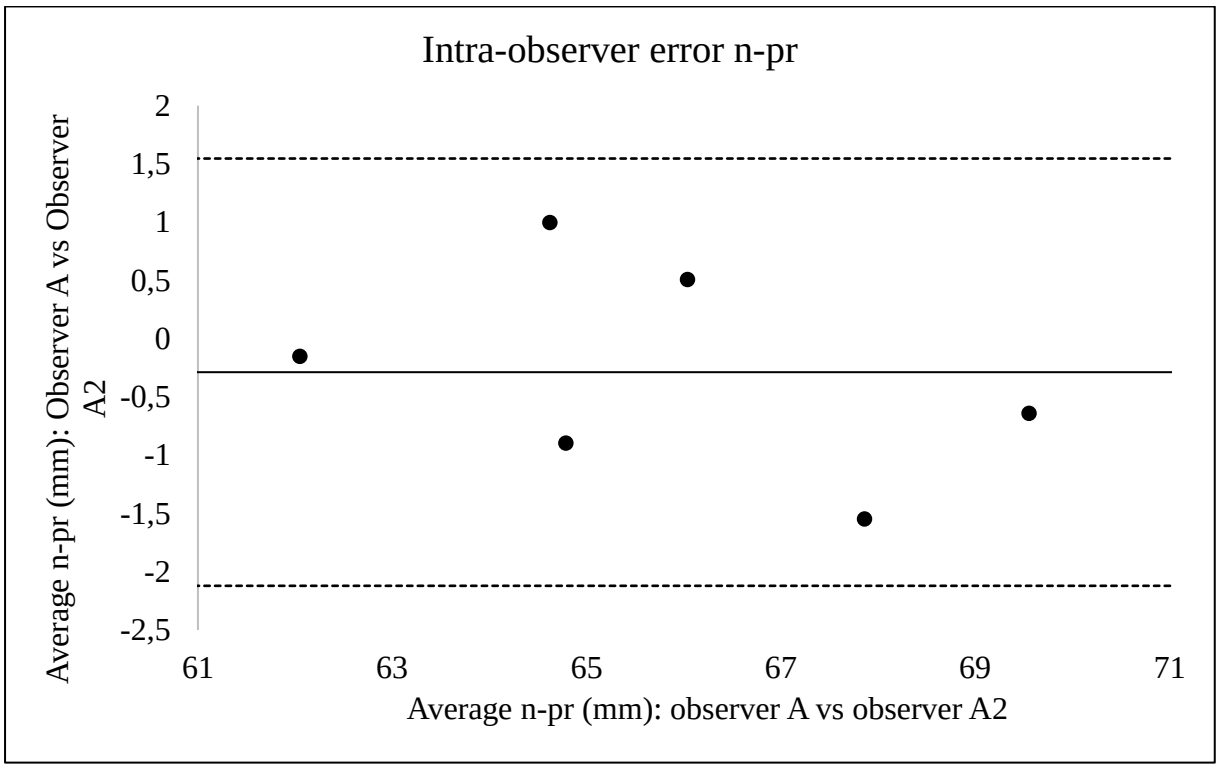

Figure 2: Intra-observer error n-pr.

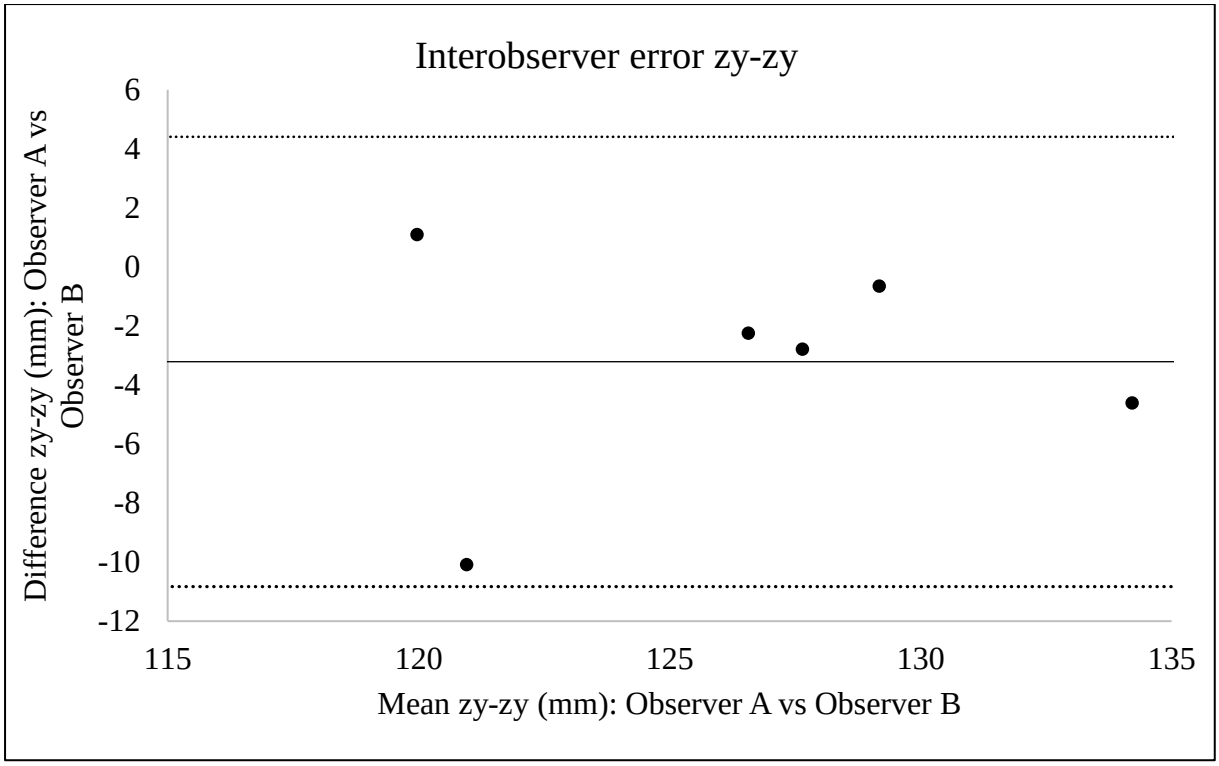

Figure 3: Interobserver error zy-zy.

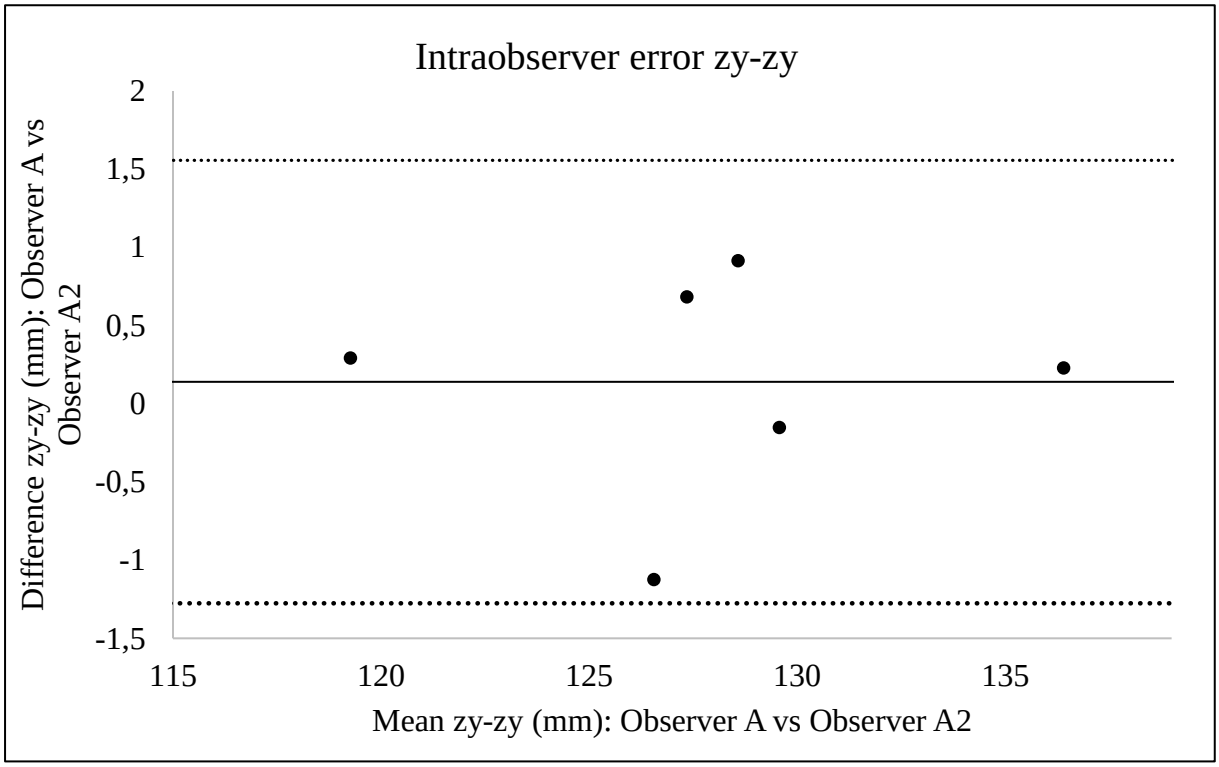

Figure 4: Intra-observer error zy-zy.

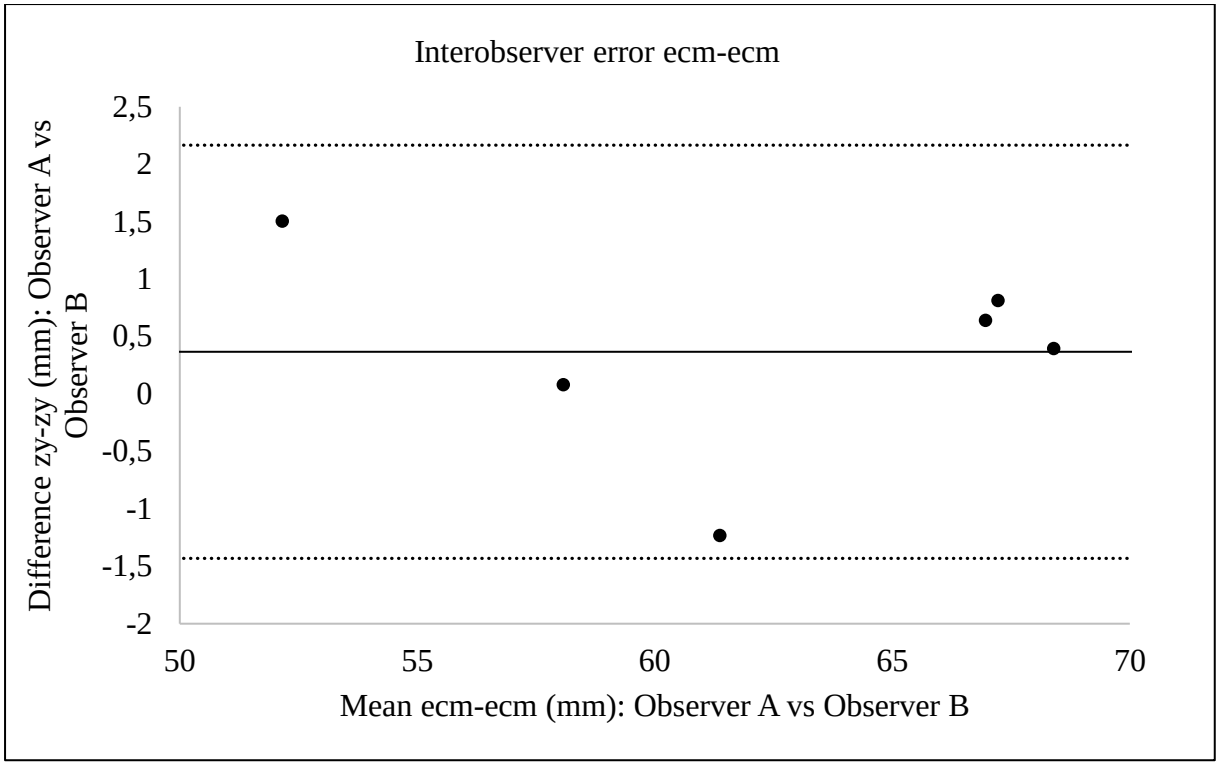

Figure 5: Interobserver error ecm-ecm.

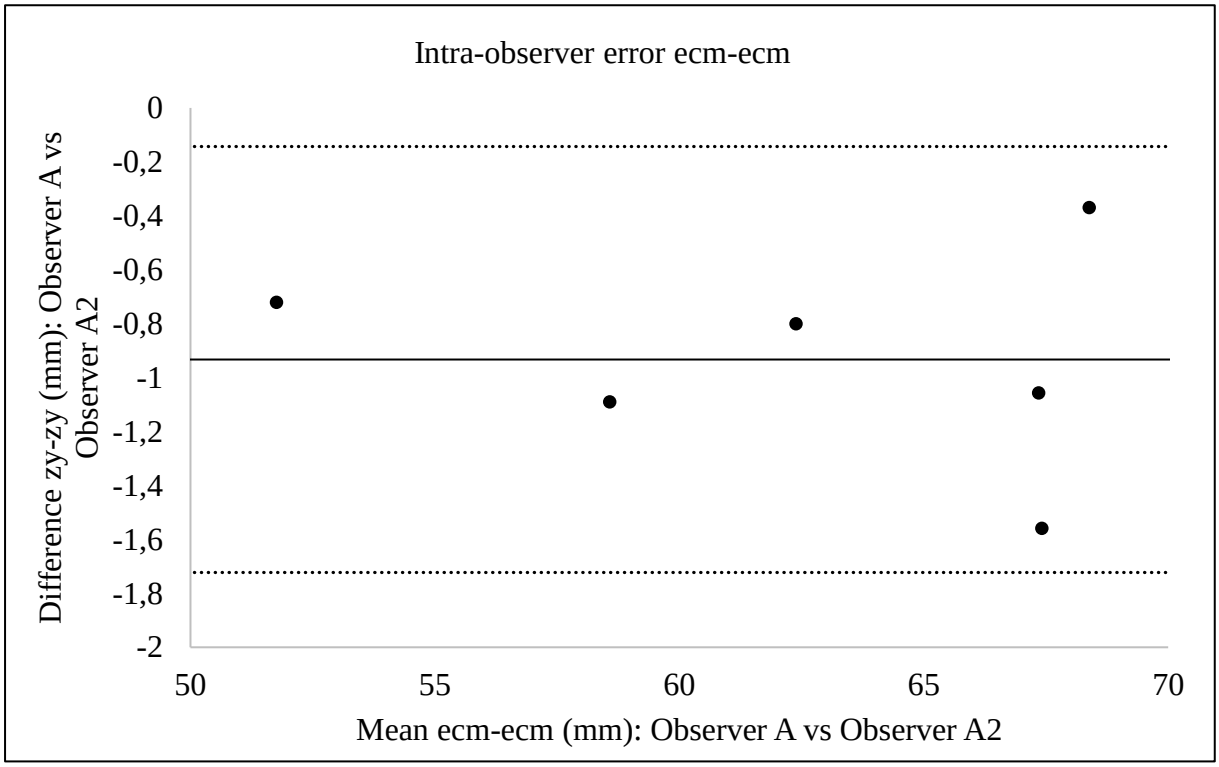

Figure 6: Intra-observer error ecm-ecm.

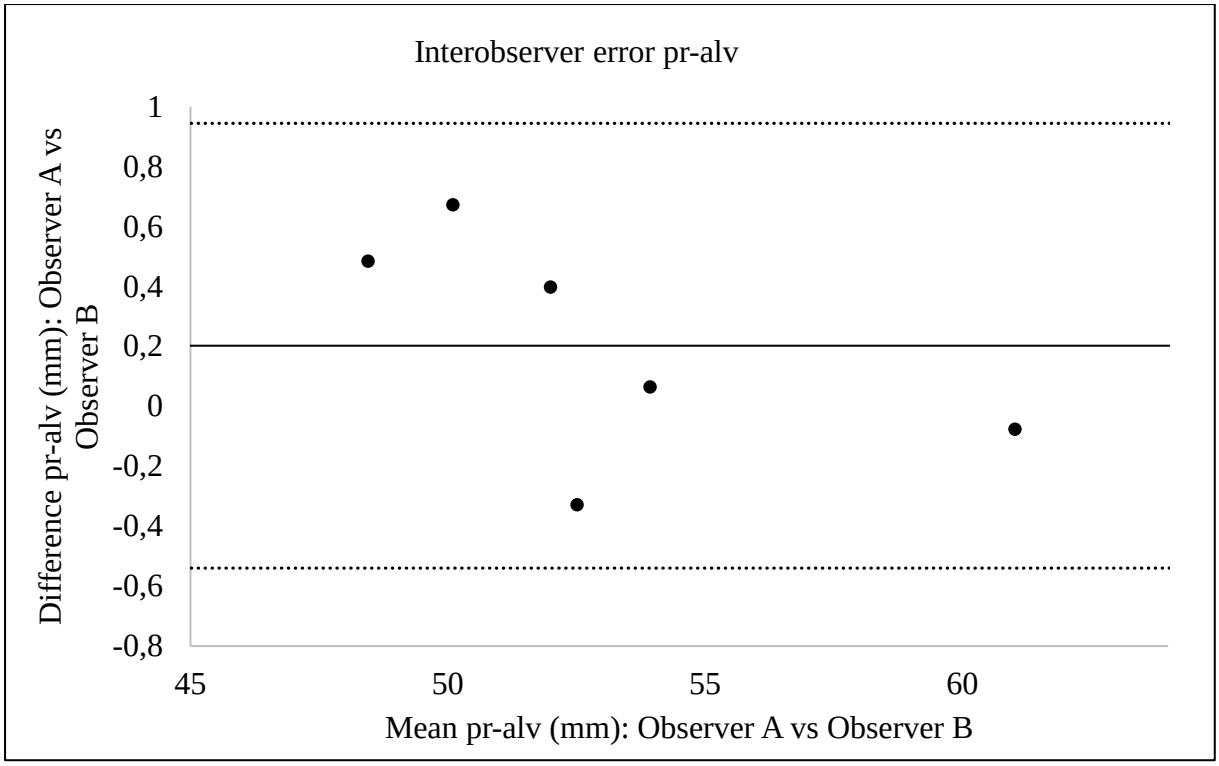

Figure 7: Interobserver error pr-alv.

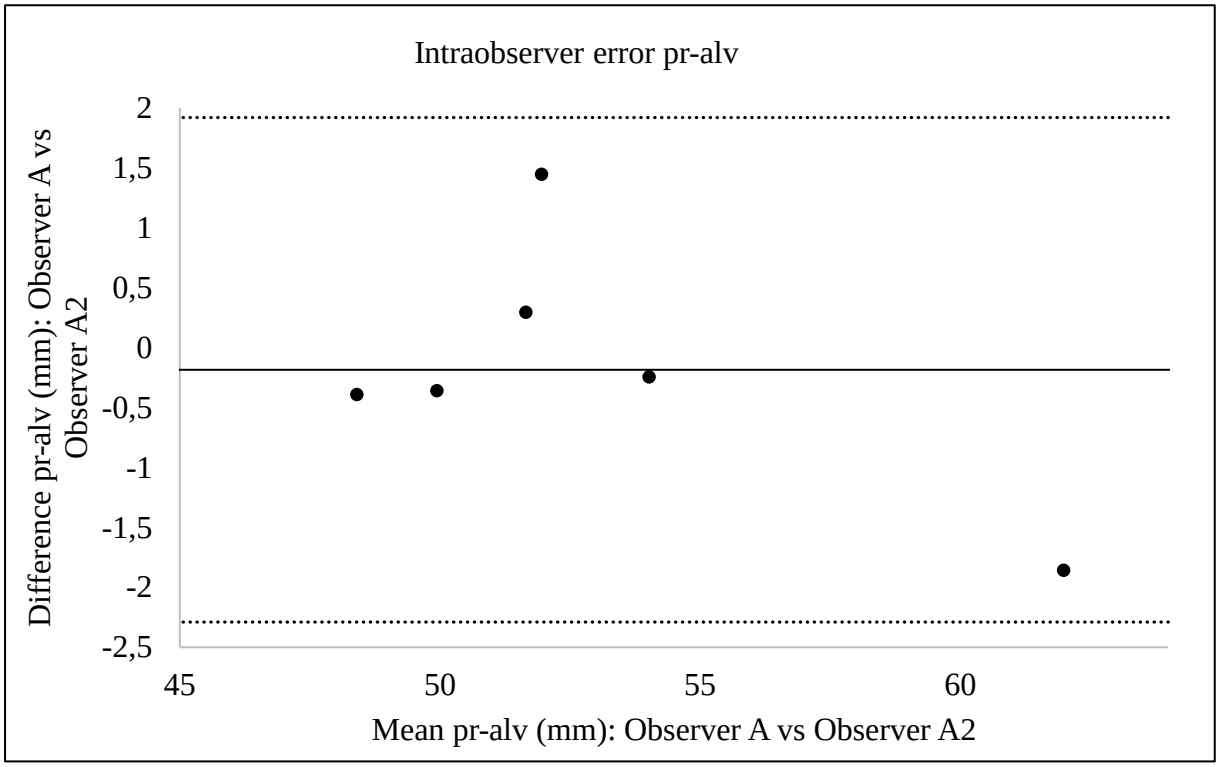

Figure 8: Intra-observer error pr-alv.

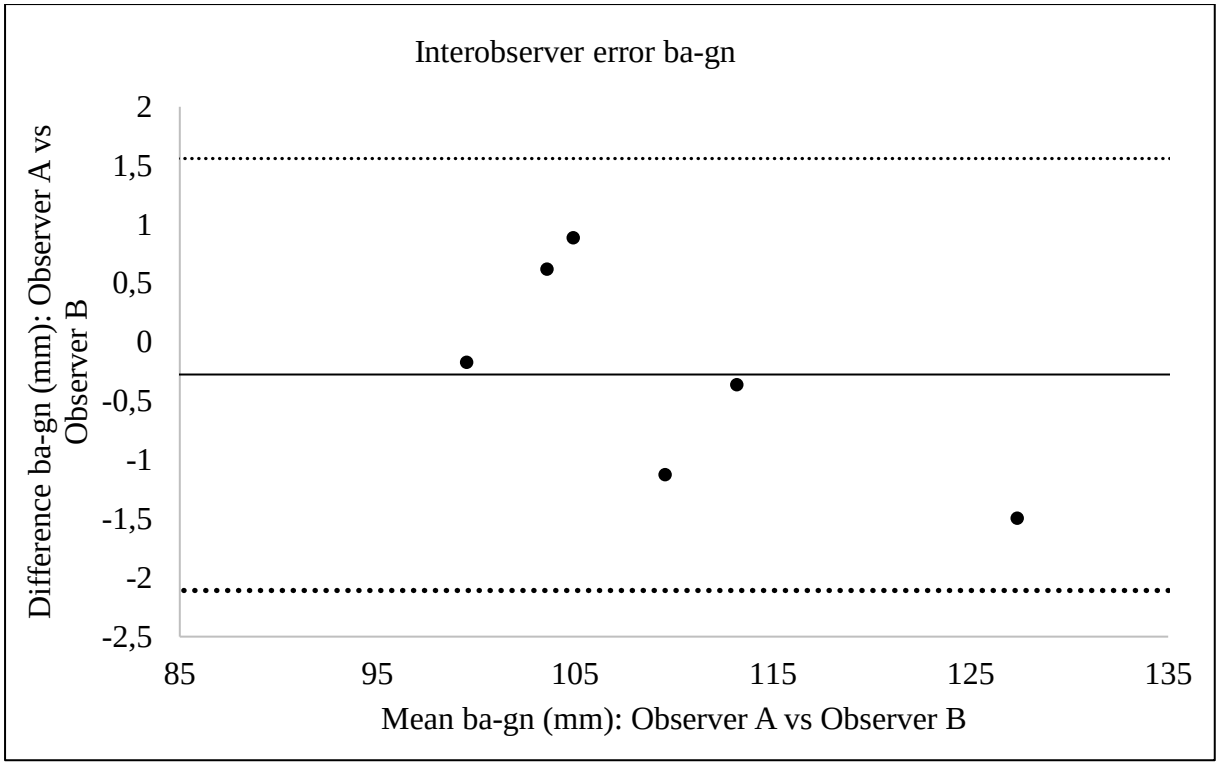

Figure 9: Interobserver error ba-gn.

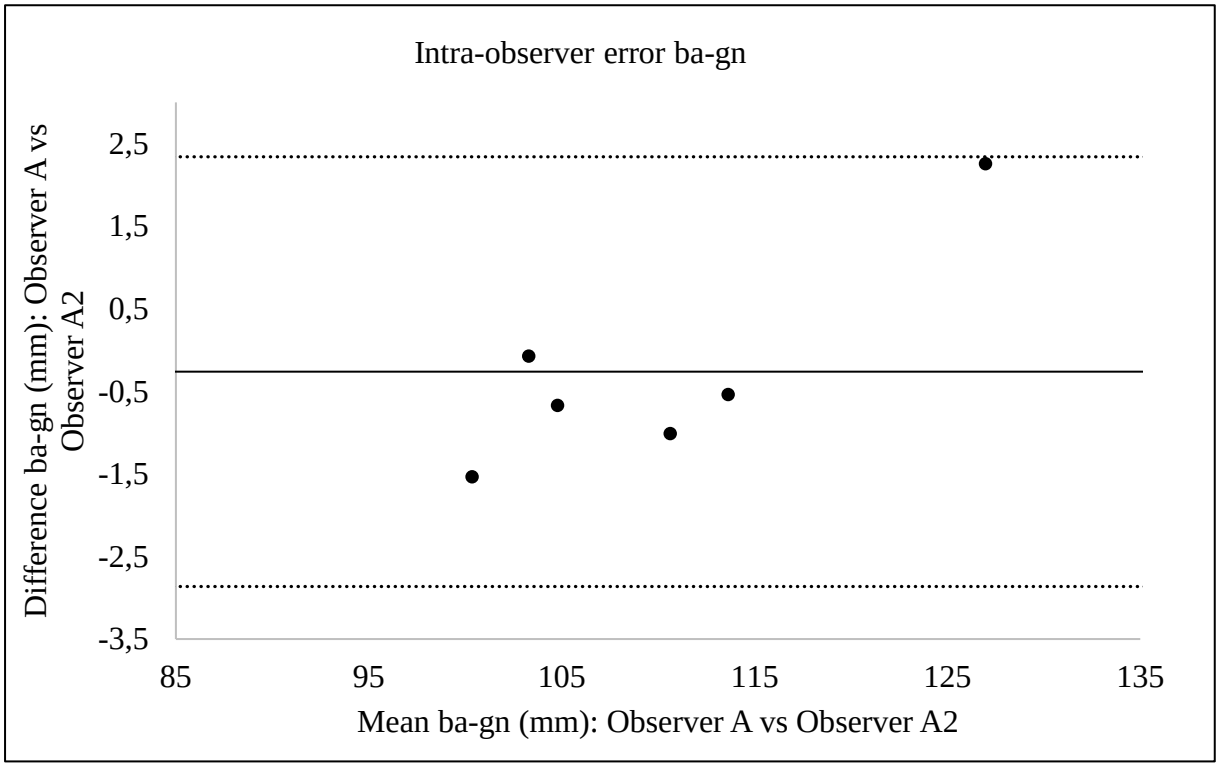

Figure 10: Intra-observer error ba-gn.

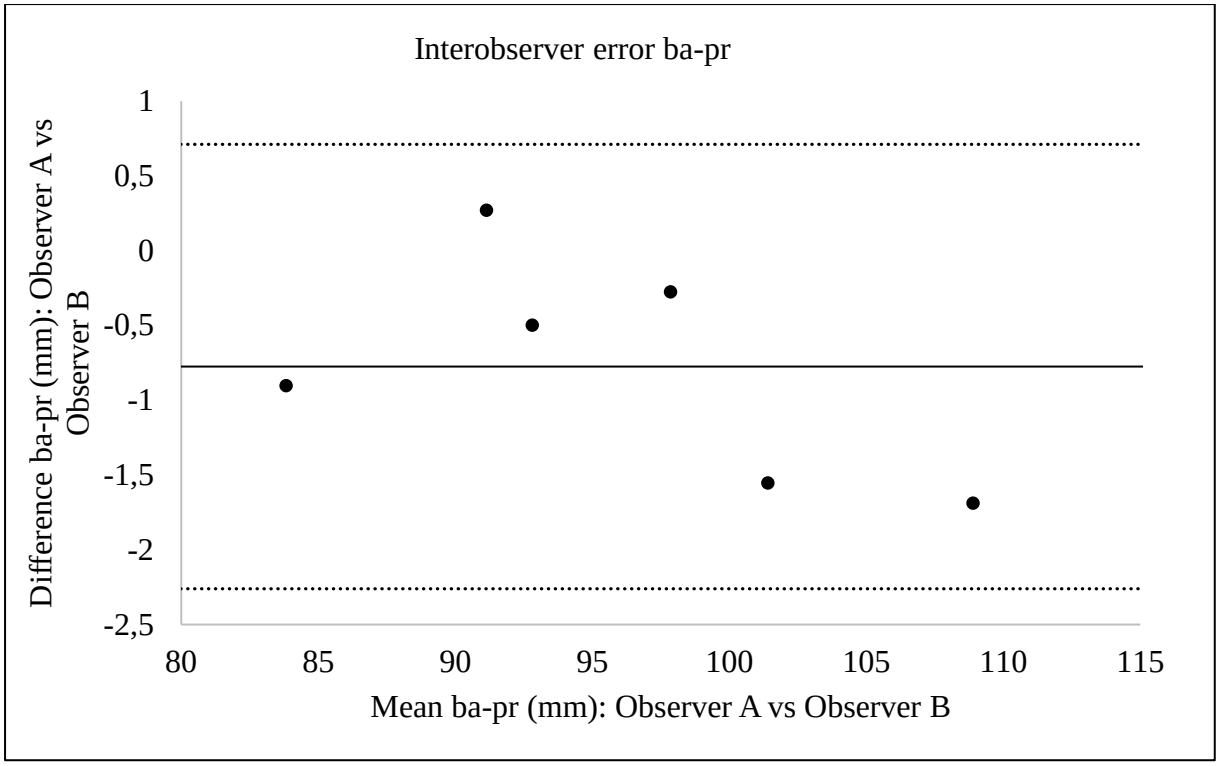

Figure 11: Interobserver error ba-pr.

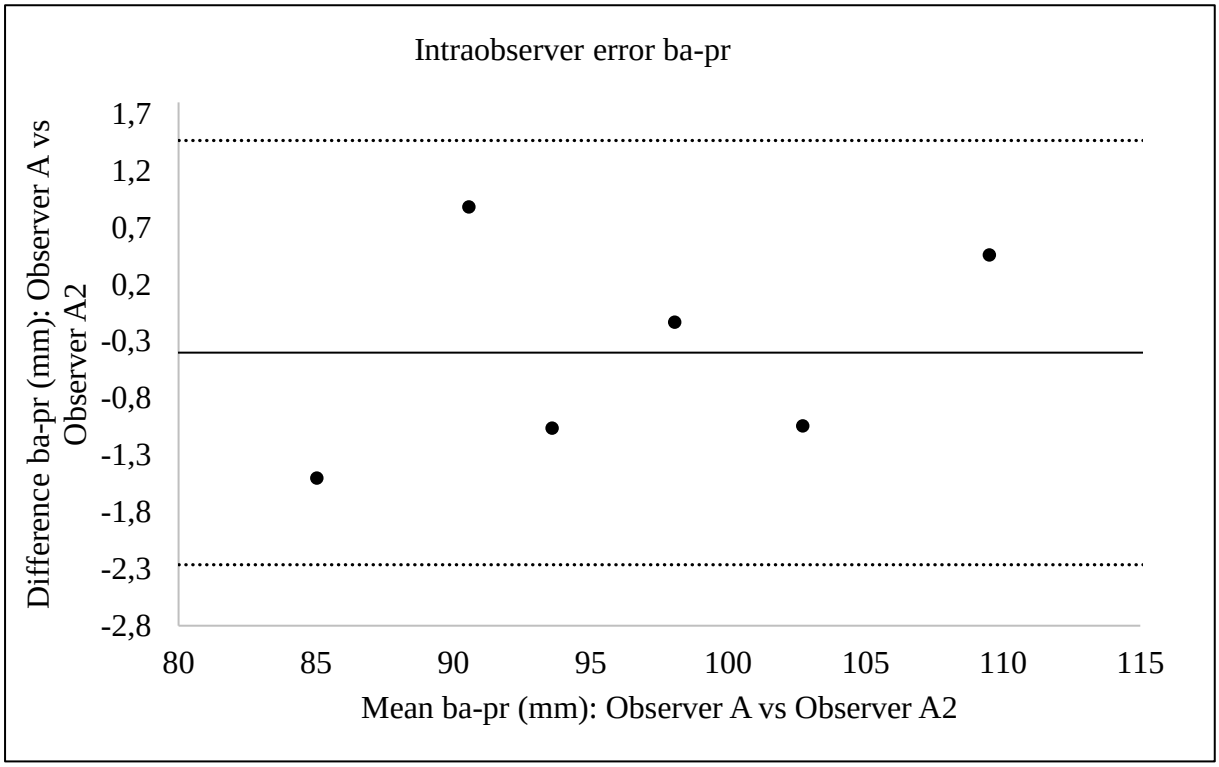

Figure 12: Intra-observer error ba-pr.

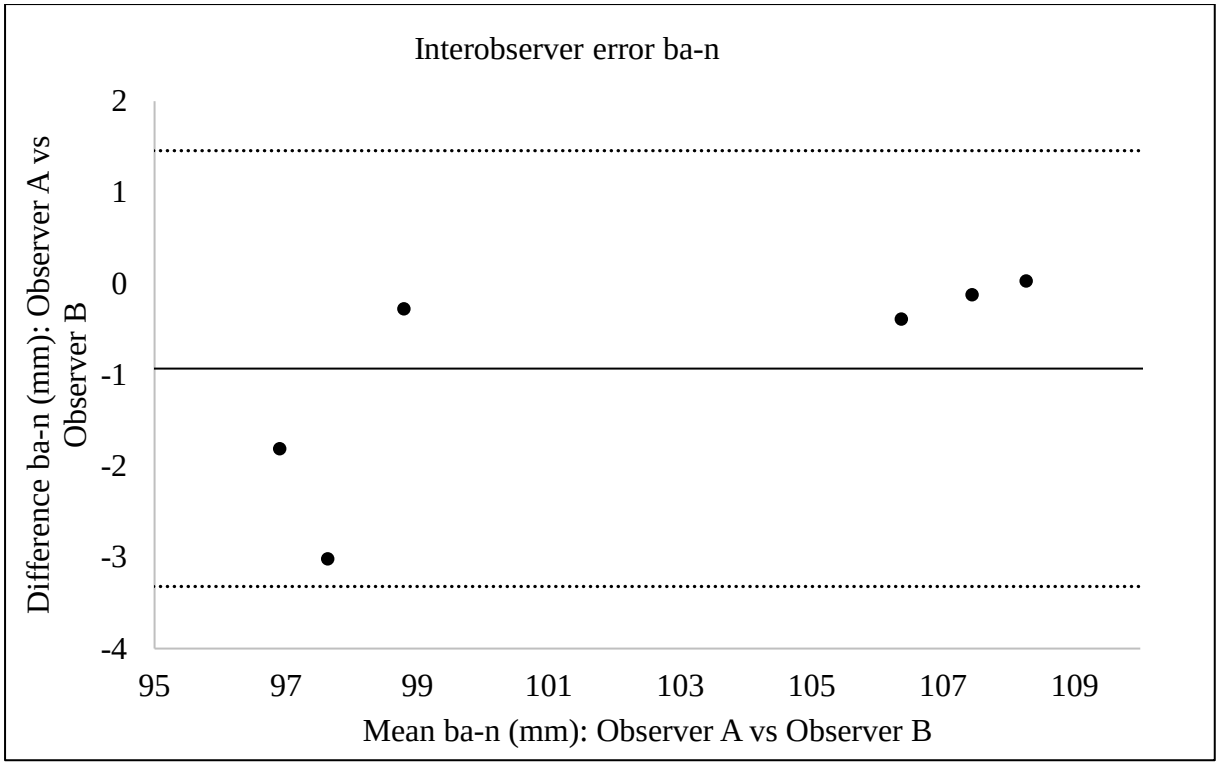

Figure 13: Interobserver error ba-n.

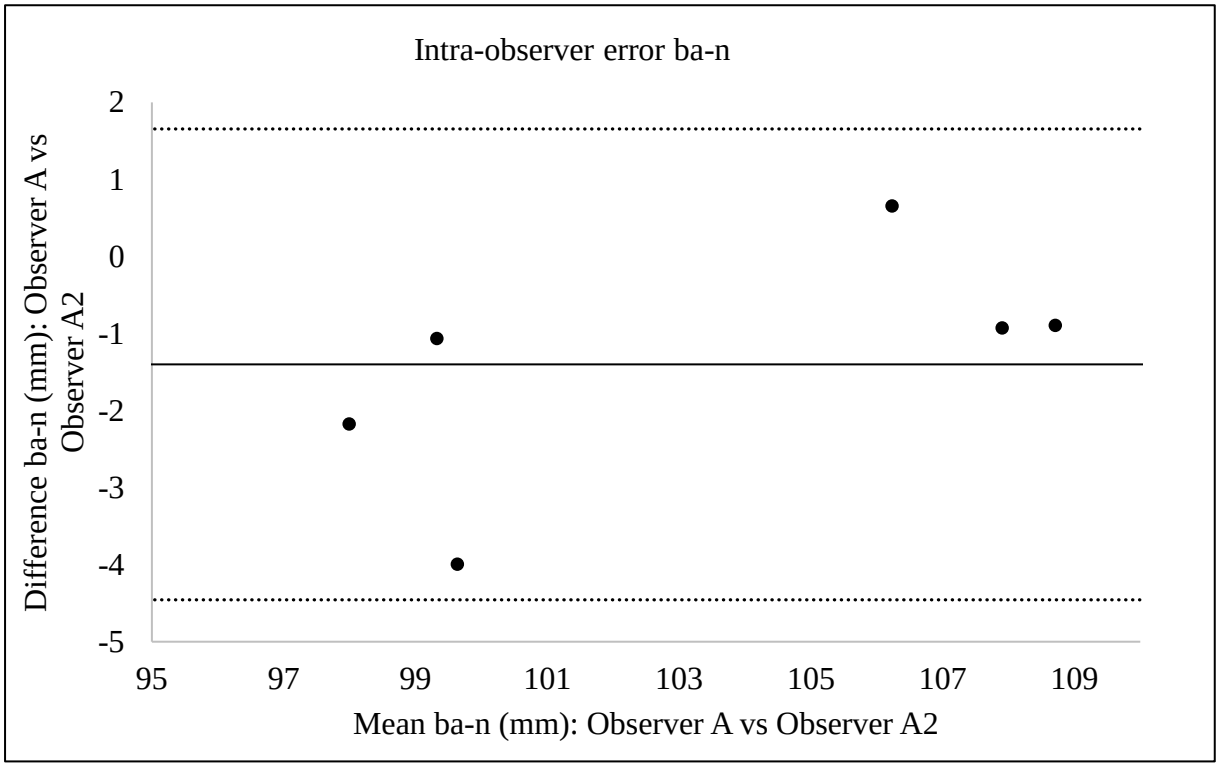

Figure 14: Intra-observer error ba-n.

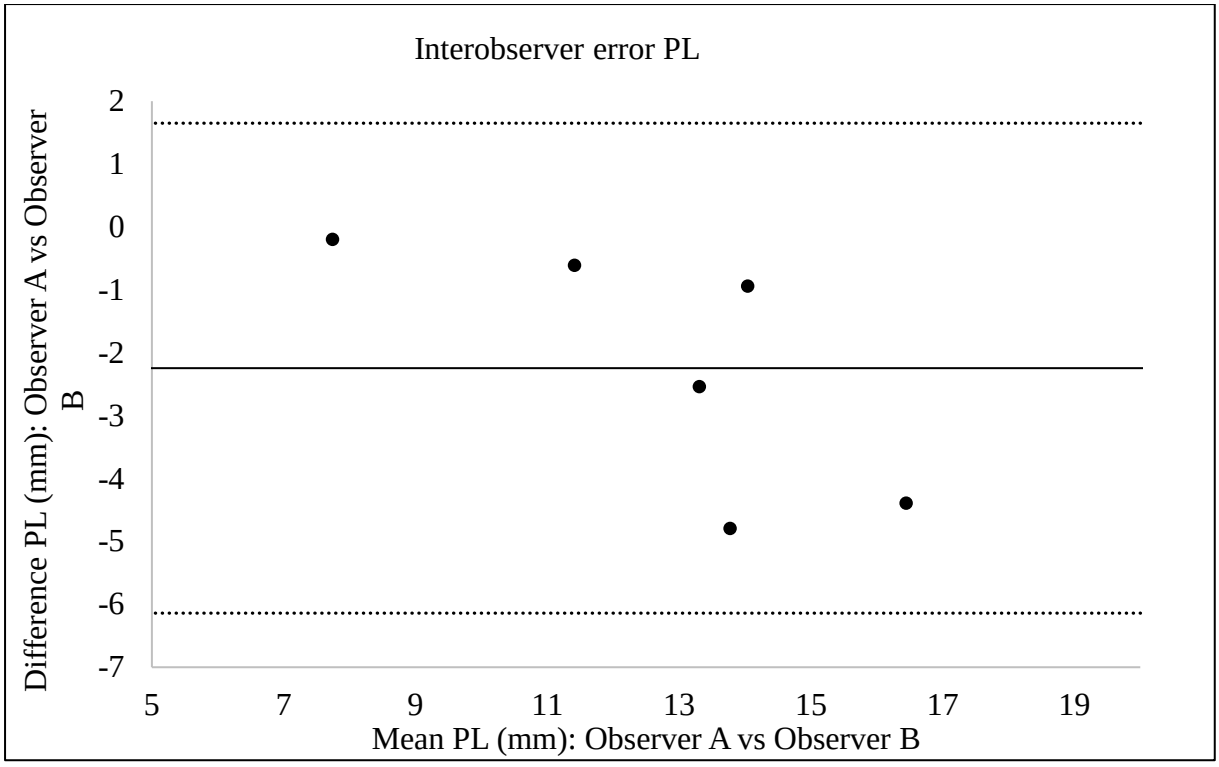

Figure 15: Interobserver error PL.

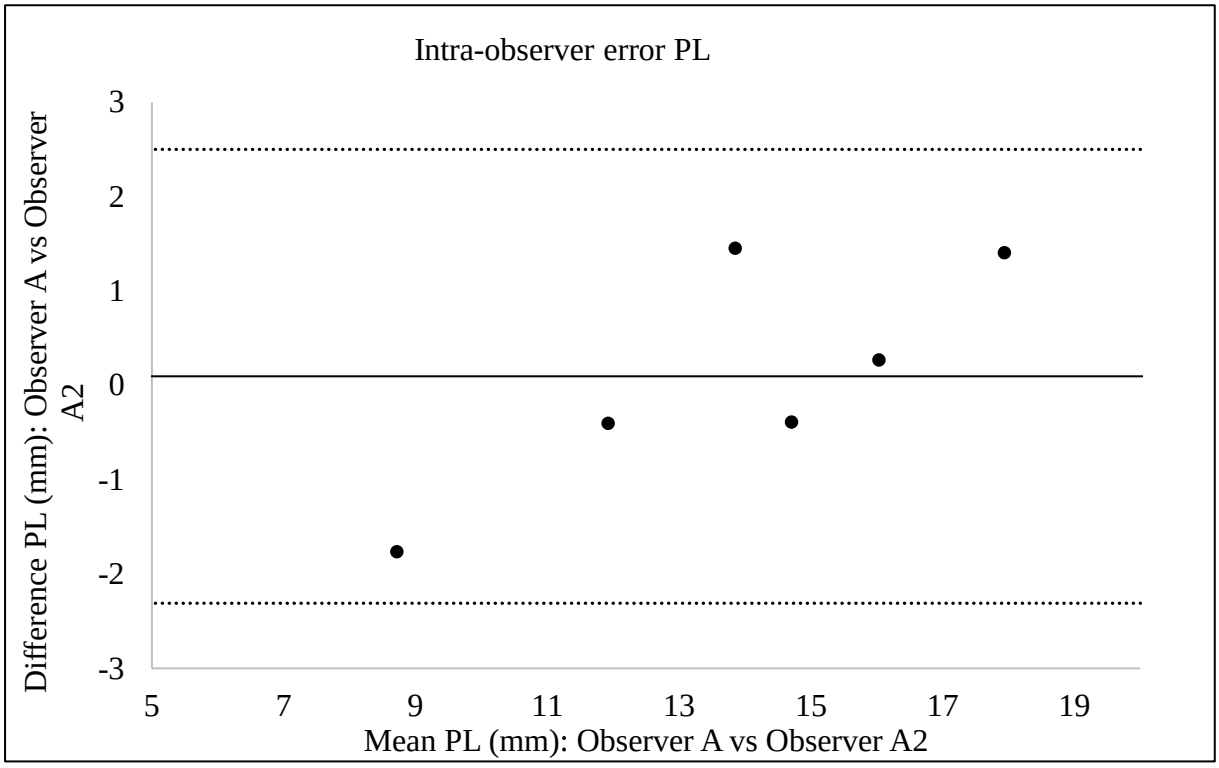

Figure 16: Intra-observer error PL.

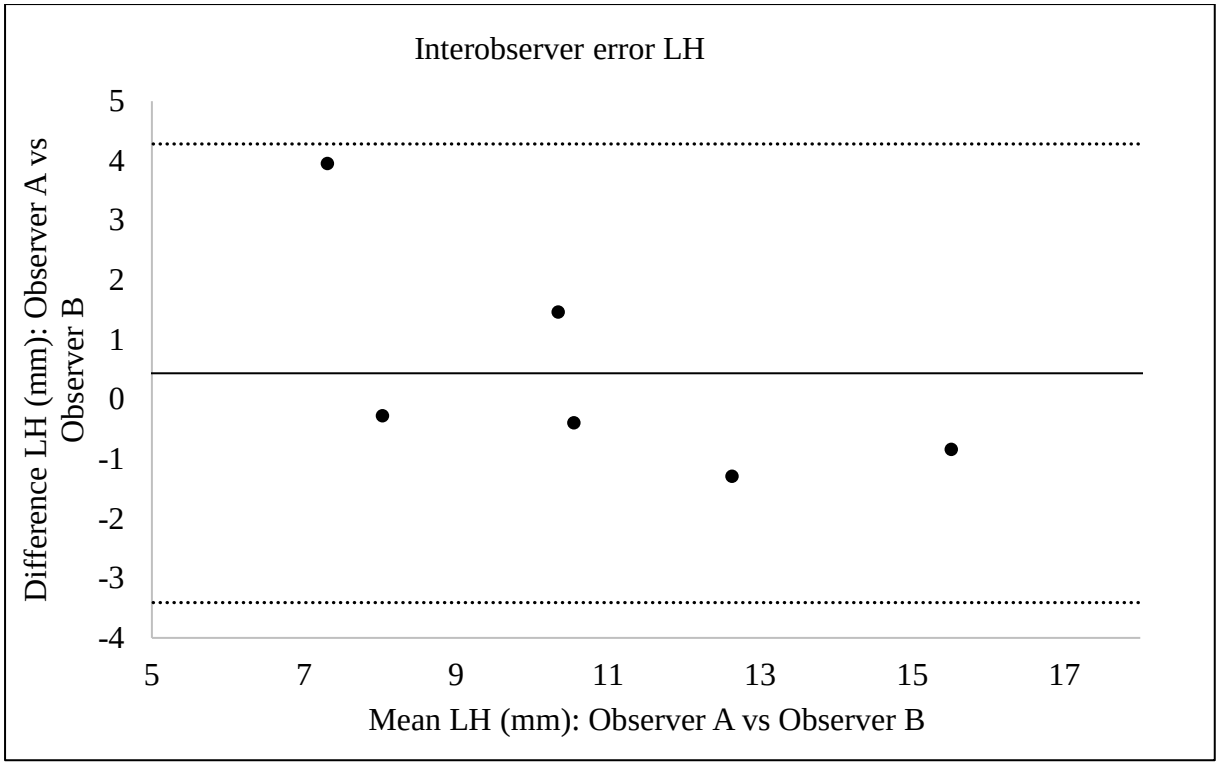

Figure 17: Interobserver error LH.

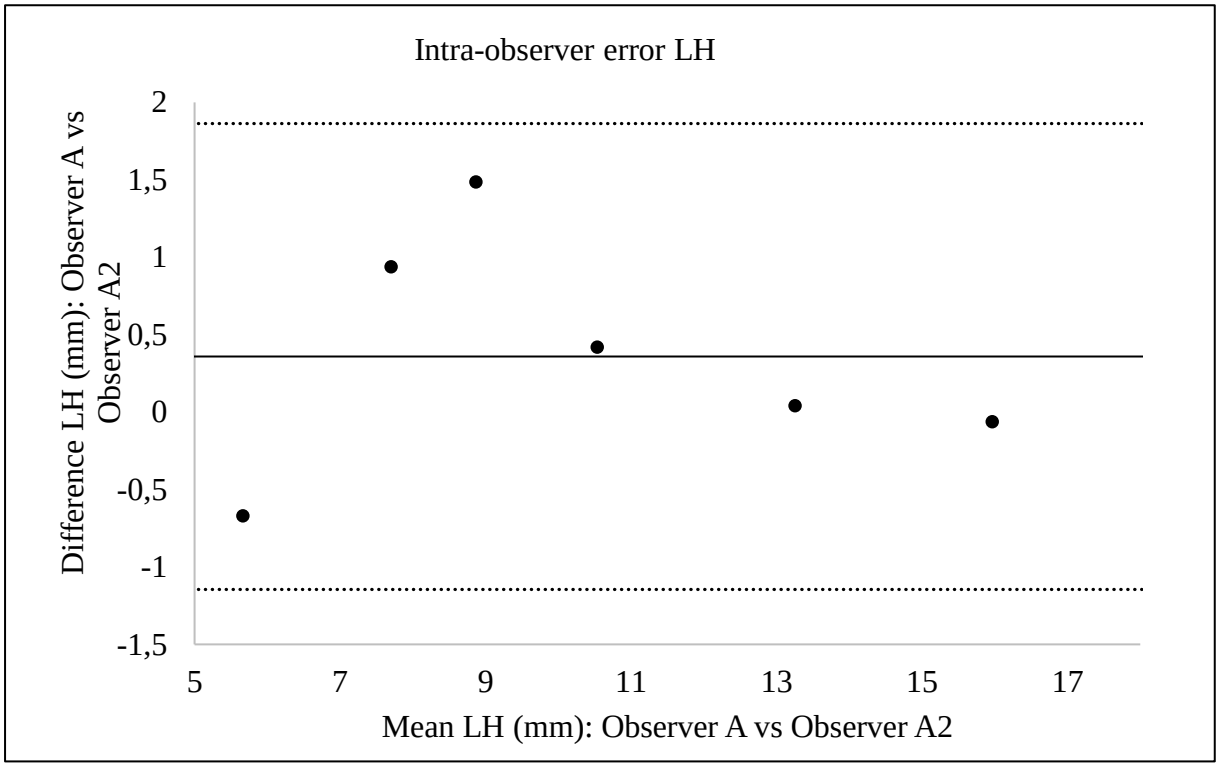

Figure 18: Intra-observer error LH.

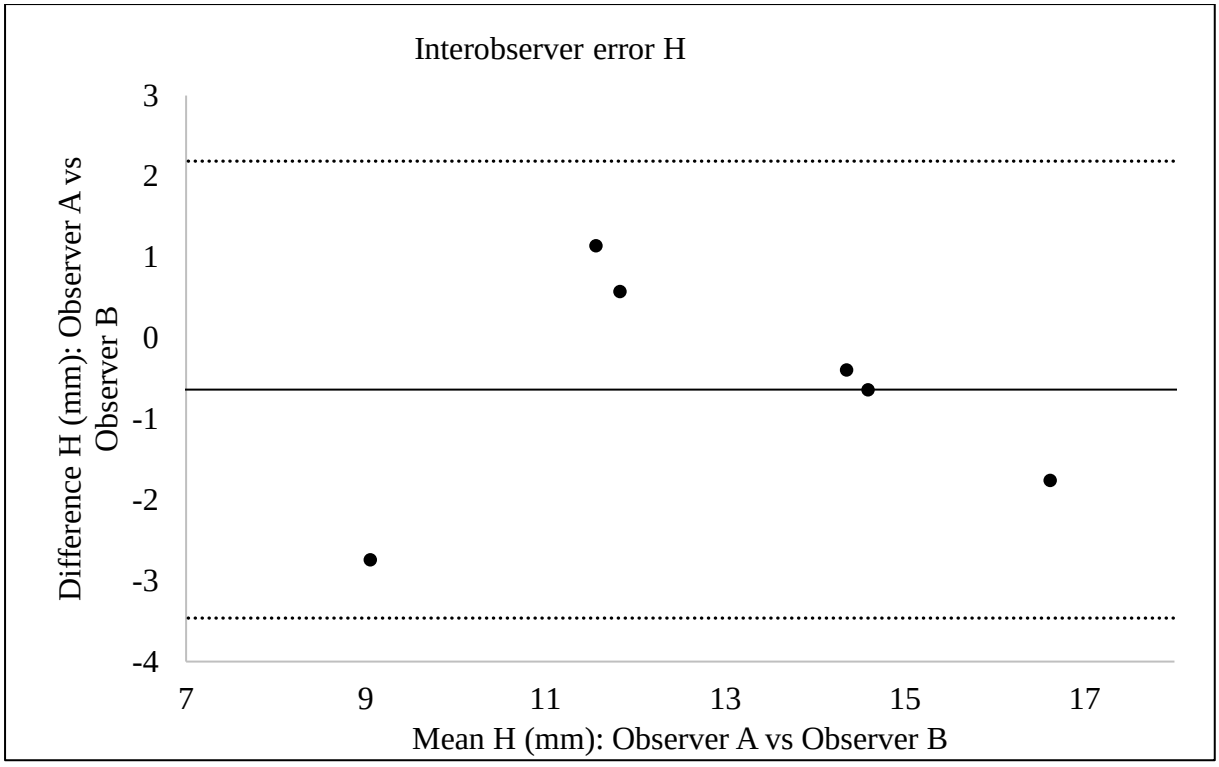

Figure 19: Interobserver error H.

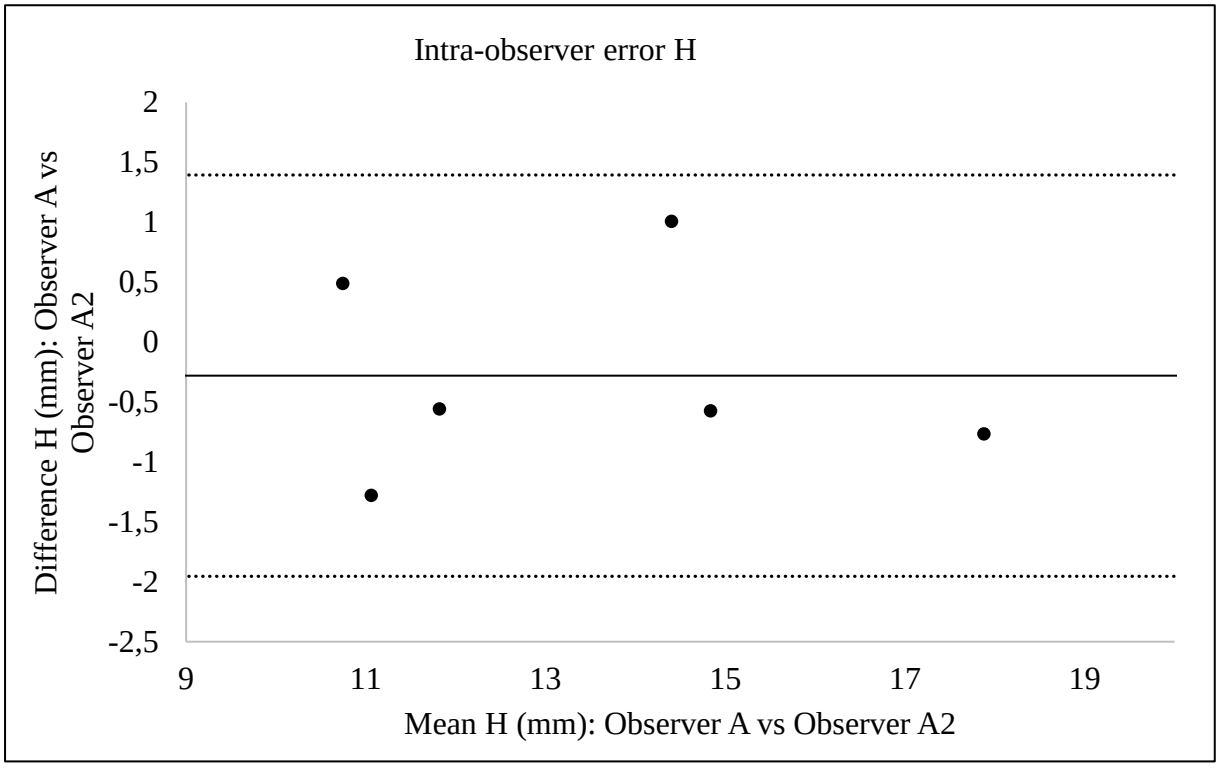

Figure 20: Intra-observer error H.

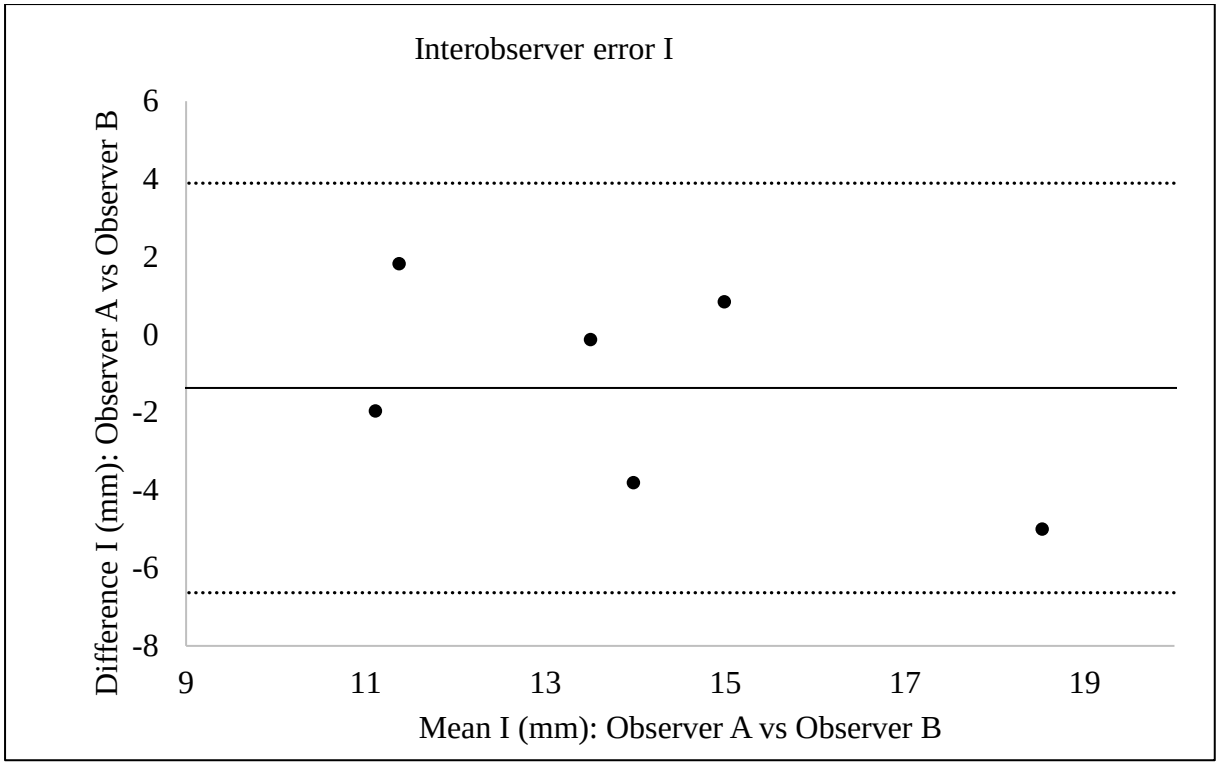

Figure 21: Interobserver error I.

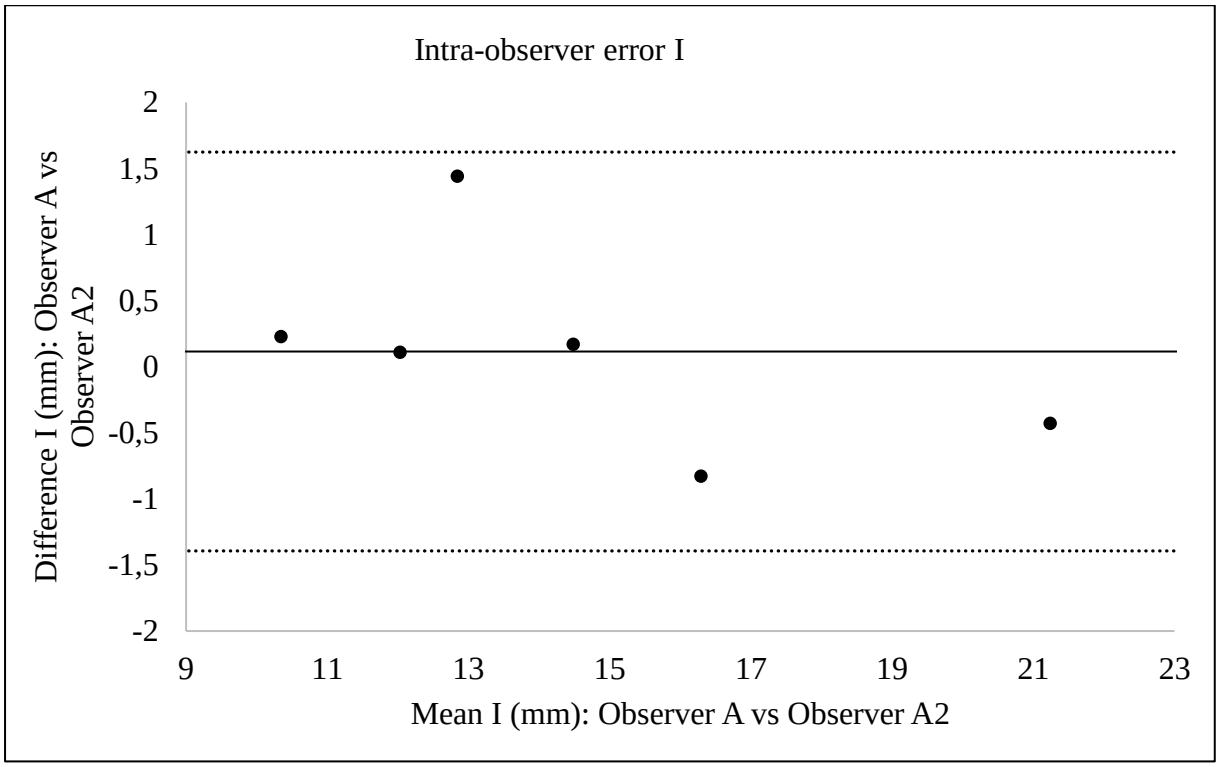

Figure 22: Intra-observer error I.

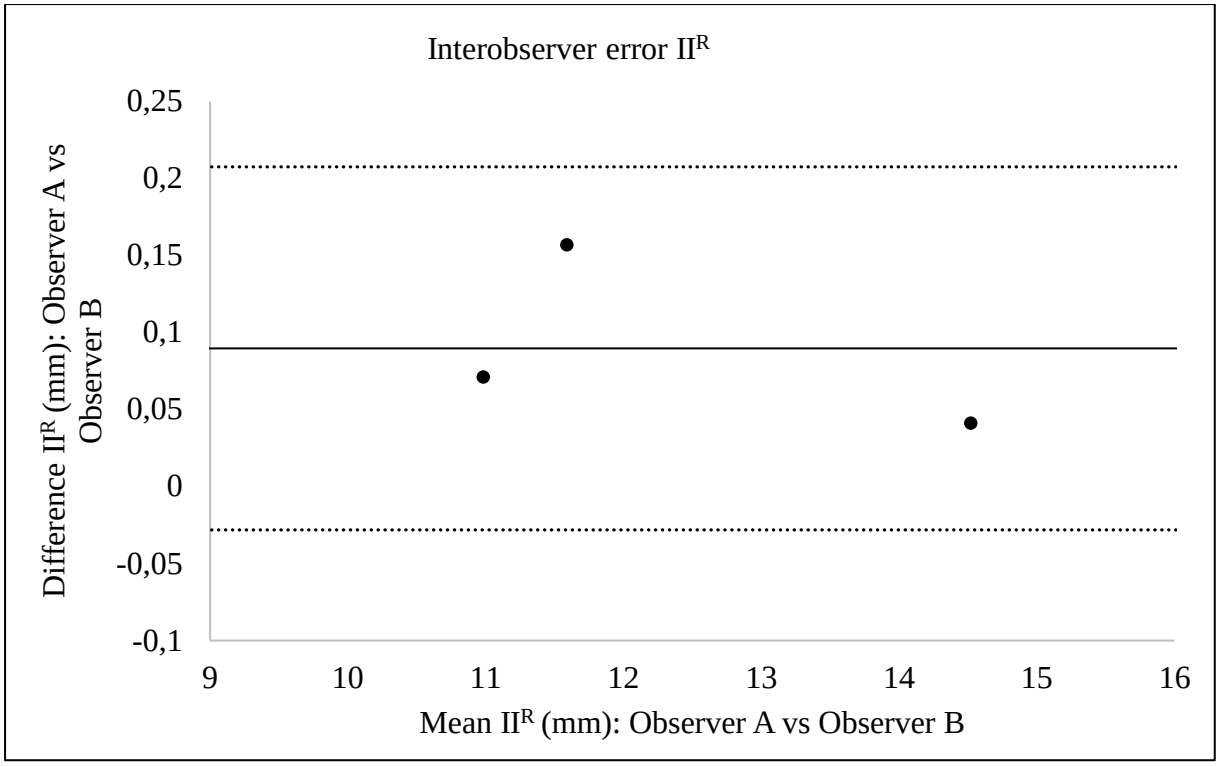

Figure 23: Interobserver error II^R.

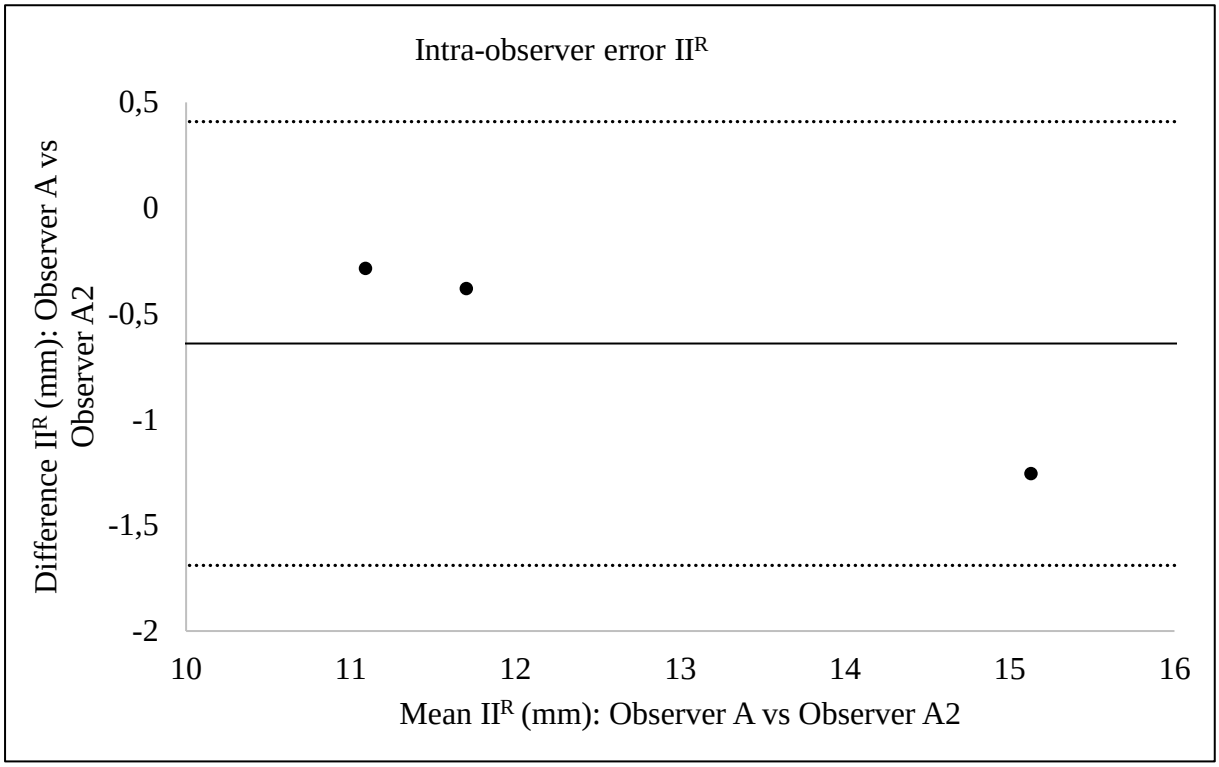

Figure 24: Intra-observer error II^R.

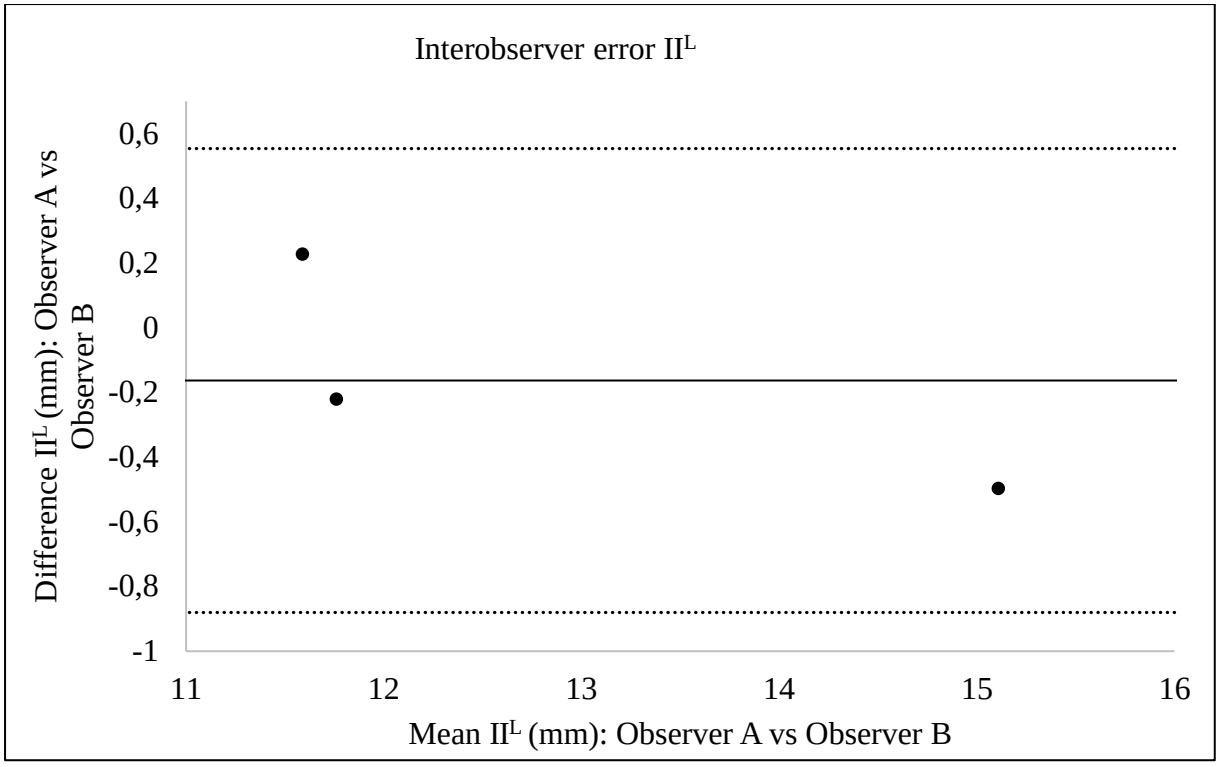

Figure 25: Interobserver error II^L.

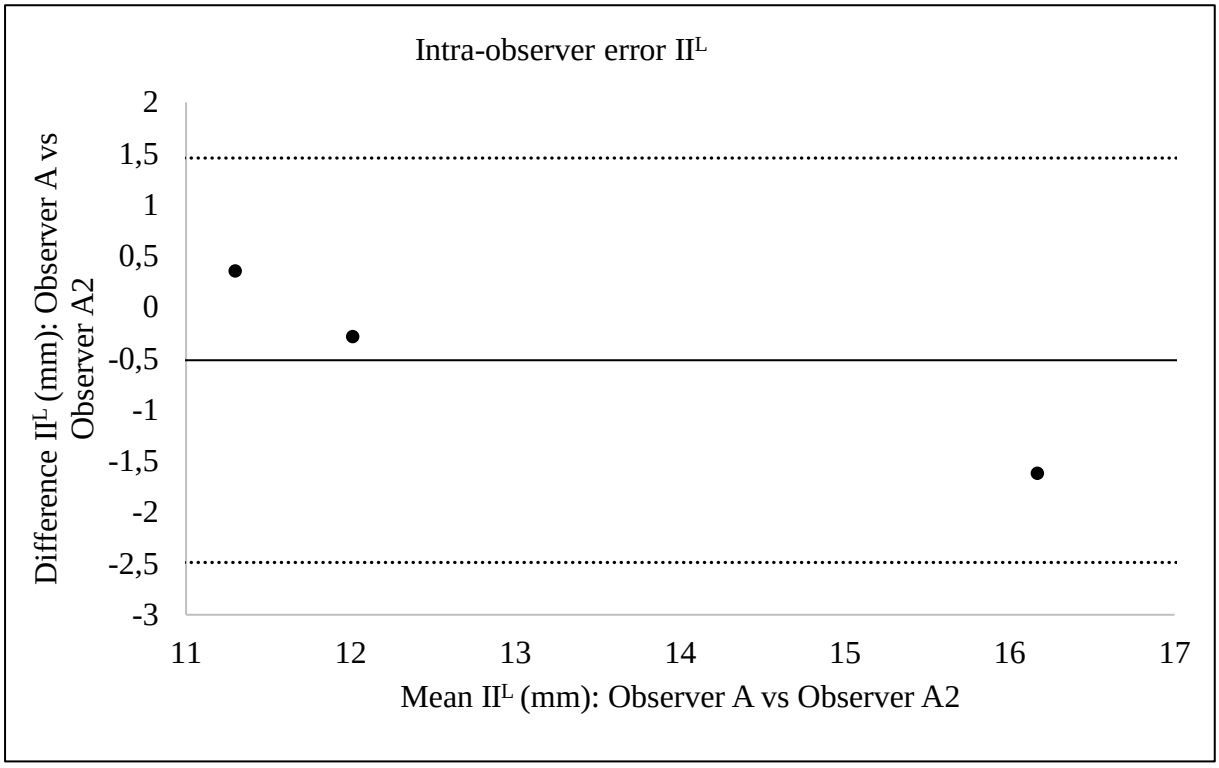

Figure 26: Intra-observer error II^L.

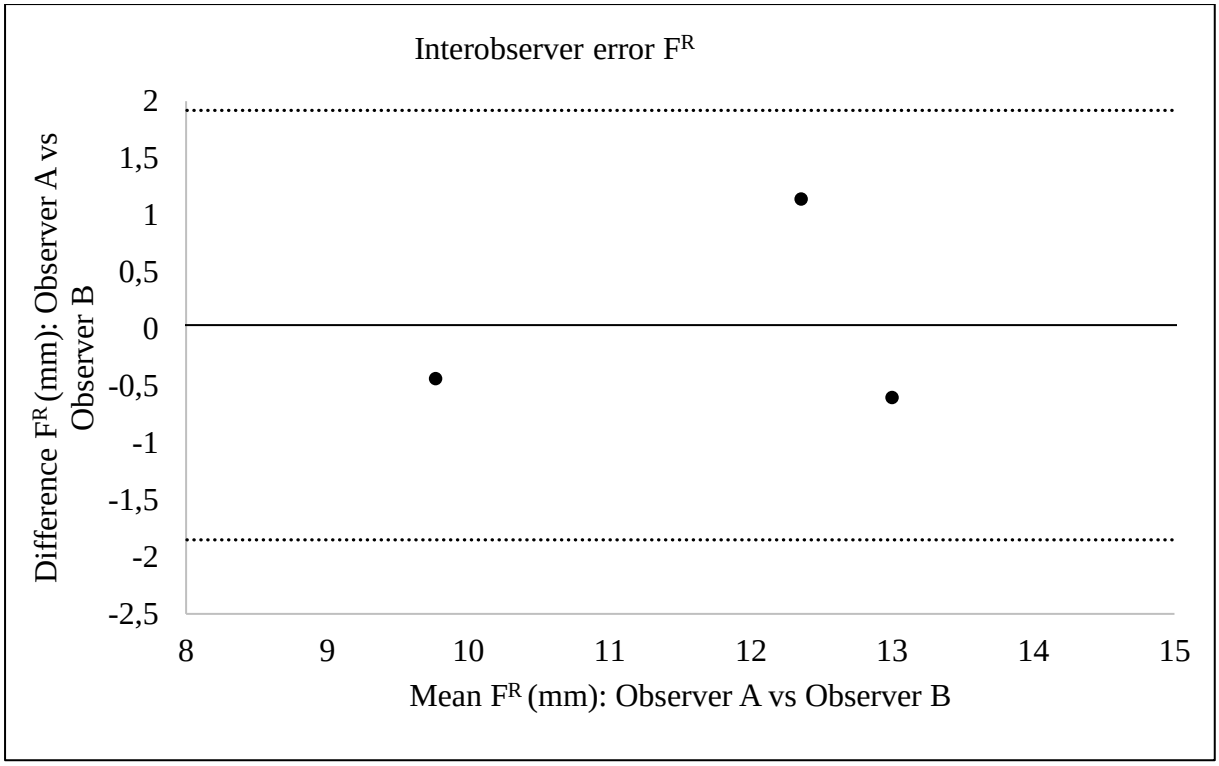

Figure 27: Interobserver error F^R.

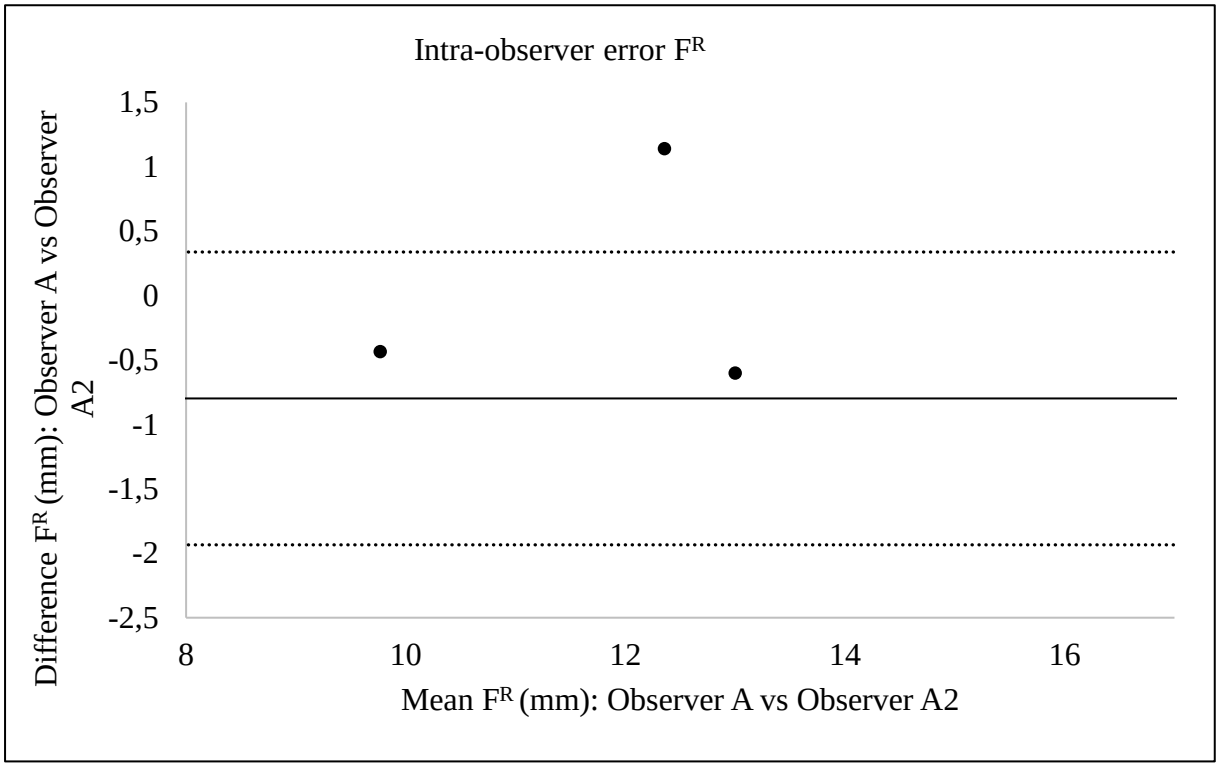

Figure 28: Intra-observer error F^R.

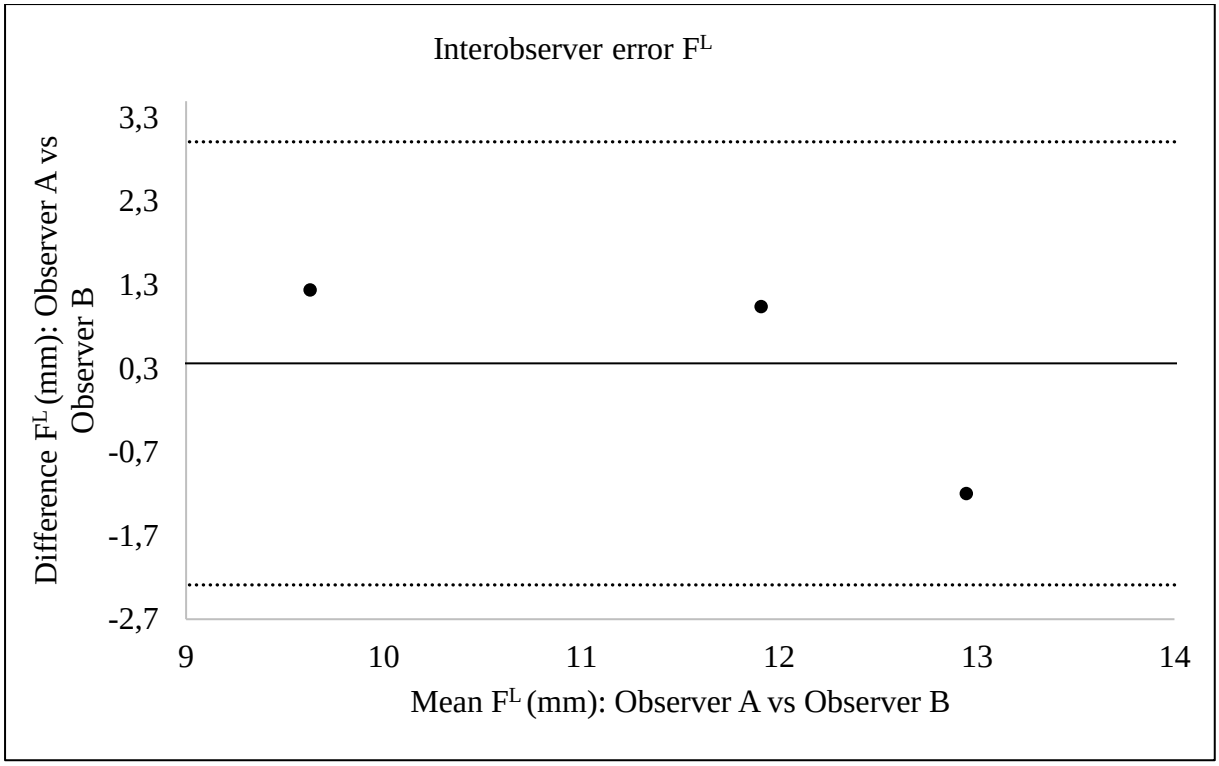

Figure 29: Interobserver error F^L.

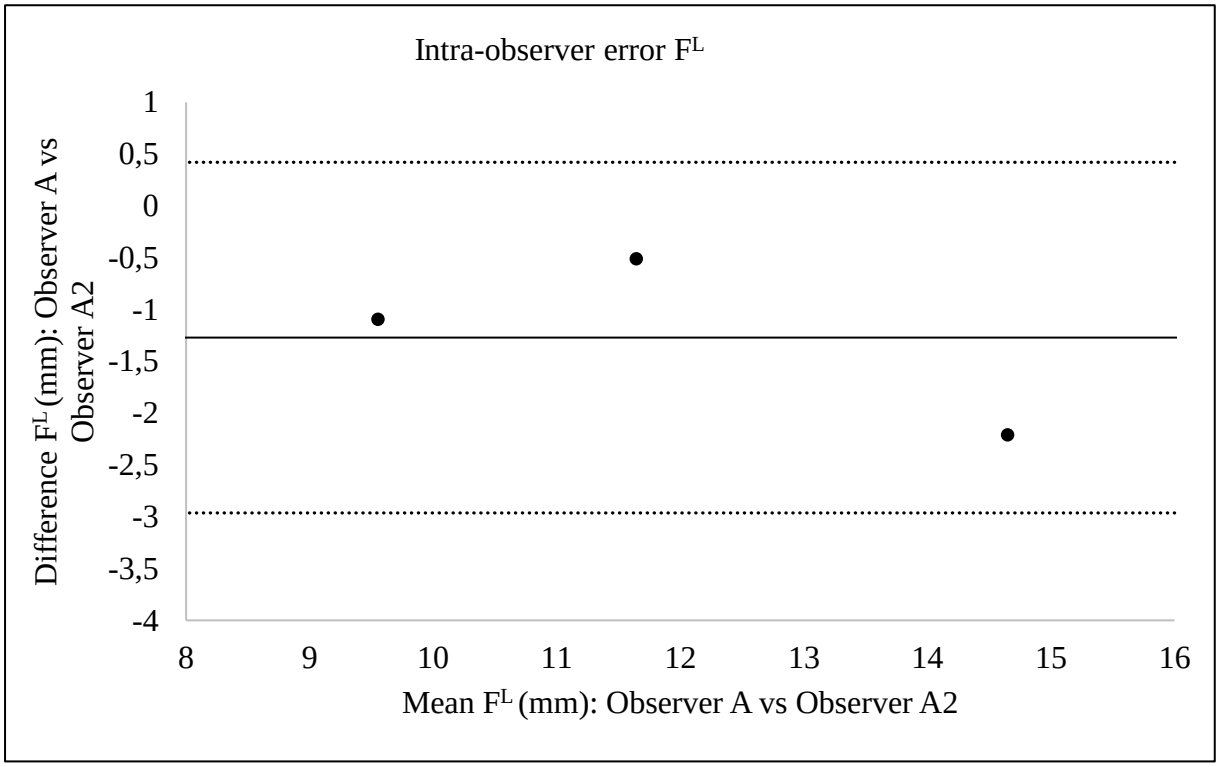

Figure 30: Intra-observer error F^L.